Experimental and numerical uncertain vibration analysis of multilayered timber structures assembled using compressed wood dowels

Tuan Anh Bui

DOCTORAL THESIS

UNIVERSITY OF LORRAINE

Specialized: Energy and Mechanics

Tuan Anh BUI

Experimental and numerical uncertain vibration analysis of multilayered timber structures assembled using compressed wood dowels

9/12/2020

Members of the jury:

President of the jury:

M. Tarak BEN-ZINEB	Professor, University of Lorraine – FRANCE

Rapporteurs:

Mme. Annette HARTE	Professor, National University of Ireland Galway - IRELAND
M. Thierry TISON	Professor, Université Polytechnique Hauts-de-France - FRANCE

Examiners:

Mme. Danièle WALDMANN	Professor, Université du Luxembourg – LUXEMBOURG
Mme. Pampa DEY	Professor, Laval University - CANADA
M. Marc OUDJENE	Maître de conférences HDR, University of Lorraine – FRANCE (Directeur de thèse)
M. Pascal LARDEUR	Professor, University of Technology of Compiègne – FRANCE (Co-directeur de thèse)

LERMAB, Université de Lorraine, Ecole Doctorale SIMPPé,

Epinal, France

Acknowledgments

This dissertation is the outcome of my research work carried out at LERMAB, University of Lorraine (from March 2017 to October 2018) and at Roberval Laboratory, University of Technology of Compiègne (from October 2018 to December 2020). It is only natural to express acknowledgments to those who played a vital role in the successful completion of this work.

First of all, I would like to express my heartfelt gratitude to Professor Marc OUDJENE and Professor Pascal LARDEUR, my research supervisors, for their patient guidance and continuous support during the whole span of my study. It is my great honor to carry out my research under their supervision.

I am also grateful to my committee members, Professor Tarak BEN-ZINEB, Professor Annette HARTE, Professor Thierry TISON, Professor Danièle WALDMANN and Professor Pampa DEY for the insightful comments that have improved the quality of my thesis and have been helpful in the development of my future career.

I would like to thank LERMAB and Roberval Laboratory for organizing professional working environments and facilitating good researching tools during my PhD period.

I would like to thank Mr. Jamal TAKHCHI for his support of coding in Matlab. Moreover, I would also like to thank Dr. Tan Nhu NGUYEN, Dr. Dang Phong BACH, Mr. Cong Uy NGUYEN, Mr. Duc Phong Nguyen and Dr. Van Diem THI for scientific discussion. In addition, I am thankful to my colleagues in Division of Engineering Mechanics, Thuyloi University, Vietnam for their valuable helps.

My thesis was supported by the scholarship from Vietnamese Ministry of Education and Training and funding of European Regional Development Fund (ERDF) via Interreg NWE grant 348 “Towards Adhesive Free Timber Buildings”. These financial supports are gratefully acknowledged.

To my family, especially my dear parents, who follow every step I walk with their wholehearted support, I simply cannot thank them enough. Their encouragement has given me more motivation to complete this journey.

Last but not least, I would like to give my special thanks to my wife, Duyen NGUYEN, for her understanding, sacrifice and unconditional love.

Table of Contents

Acknowledgments ..... **i**

Table of Contents ..... **iii**

List of Figures ..... **vii**

List of Tables ..... **xi**

List of Publications ..... **xiii**

Introduction en français ..... **xv**

Chapter 1: Introduction **1**

1.1 Background and motivations 1

1.1.1 Multilayered timber structures 1

1.1.2 Towards Adhesive-Free Timber Buildings (AFTB) project 1

1.1.3 History of using wood dowel in timber structure 2

1.1.4 Performance of timber structures assembled by compressed wood dowels 7

1.1.5 Vibration performance of timber structures 7

1.2 Objective of the thesis 8

1.3 Outline 8

Chapter 2: Experimental modal analysis **11**

2.1 Production of adhesive free laminated beams and adhesive free CLT panels 12

2.1.1 Compressed spruce dowels 12

2.1.2 Adhesive free laminated beams (AFLB) and adhesive free CLT (AFCLT) panels 14

2.2 Experimental set-up 16

2.2.1 Hammer impact excitation 16

2.2.2 Moisture content condition 18

2.2.3 Repeatability test 18

2.3 Characteristic of wood material 20
2.4 Single layer beams 20
2.5 Three-layer AFLBs 23
2.5.1 Effect of compressed wood dowels 24
2.5.2 Effect of the number of dowels 27
2.5.3 Effect of moisture content 28
2.6 AFCLT panels 32
2.7 Academic contribution 37
2.8 Conclusion 37
Chapter 3: Finite element models 39
3.1 Introduction 40
3.1.1 Existing finite element (FE) models 40
3.1.2 Verification and Validation methodology 42
3.2 FE model for single layer beam 43
3.2.1 Sensitivity analysis 44
3.2.2 Verification of the model 45
3.2.3 Validation of the model 48
3.2.4 Effect of homogeneous material assumption 49
3.3 FE model for three-layer AFLB 51
3.3.1 Sensitivity analysis 52
3.3.2 Verification of the model 53
3.3.3 Validation of the model 55
3.3.4 Effect of stiffness of CSD on frequencies of AFLB 56
3.4 FE model for AFCLT panel 57
3.4.1 Verification of the model 58
3.4.2 Validation of the model 59
3.5 FE model for full-size AFCLT panel 62
3.5.1 Prediction of frequencies and modal shapes 62
3.5.2 Comparison with EC5 requirements 64
3.5.3 Optimization for the first frequency 66

3.6 Simplified FE model 69
3.6.1 Simplifying dowels by beam elements 70
3.6.2 Simplifying layer by shell elements 74
3.6.3 Simplifying shape of dowel 76
3.6.4 Computational cost effect 79
3.7 Academic contribution 80
3.8 Conclusion 80
Chapter 4: Variability with MSP 83
4.1 Introduction 84
4.1.1 Short overview on non-deterministic methods 84
4.1.2 Presentation of the Modal Stability Procedure (MSP) 85
4.2 General MSP formulation 86
4.3 Development of MSP formulation for 20-node hexahedral solid element 88
4.3.1 MSP mesh convergence 91
4.3.2 Comparison between MSP and FE model in the nominal case 93
4.4 Uncertain parameters and distribution law 94
4.5 Assessment of the MSP to calculate variability 96
4.5.1 Error indicator 96
4.5.2 Comparison between MSP and direct MCS for single layer beam and AFLB 97
4.5.3 Error indicator for AFCLT panels 100
4.6 Influence of uncertain properties of compressed wood dowels 101
4.7 Comparison between MSP and experimental results 102
4.7.1 Comparison for single layer beam 102
4.7.2 Comparison for AFLB 103
4.7.3 Comparison for AFCLT panel 104
4.8 Prediction variability of full-size AFCLT panel 106
4.9 Computational cost 107
4.10 Academic contribution 108
4.11 Conclusion 108

Chapter 5: General conclusion and perspectives 111

5.1 General conclusion 111

5.2 Perspectives 112

Bibliography 114

List of Figures

Figure 1.1: Examples of multilayered Engineered Wood Products (EWPs) 1
Figure 1.2: Multilayered timber structures assembled using compressed wood dowels 2
Figure 1.3: Beam-column connection in traditional Chinese pagodas (Meng *et al.* (2019)) 3
Figure 1.4: Concept of adhesive free laminated timber beams ("Brettstapel"): 3
Figure 1.5: Concept of Dowellam by Structure Craft 4
Figure 1.6: Diagrams of the THOMA Holz 100 (Deutsches Institut für Bautechnik (2018)) 5
Figure 1.7: Nur Holz panel (Habitat Naturel (2009)) 6
Figure 1.8: Springback of compressed wood dowel 6
Figure 2.1: Production of compressed wood dowels: (a) Hot press machine and (b) Typical thicknesses of spruce blocks before and after densification 12
Figure 2.2: Pressure and temperature profiles during the compression process (El-Houjeyri *et al.* (2019)) 13
Figure 2.3: Typical produced compressed spruce dowels 13
Figure 2.4: Schematic illustration of the three-layer AFLB 14
Figure 2.5: Adhesive free laminated beams 15
Figure 2.6: Typical AFCLT manufactured panels 16
Figure 2.7: Experimental set-up of beam specimens under free – free conditions 17
Figure 2.8: Experimental set-up of AFCLT panels under free – free conditions 18
Figure 2.9: FRFs at point P11 of one AFLB - repeatability test 19
Figure 2.10: FRFs at point P5 of one AFCLT panel - repeatability test 19
Figure 2.11: Density distribution of a Douglas timber board 20
Figure 2.12: FRFs at point P4 for 16 single layer oak beams 21
Figure 2.13: FRFs at point P4 for 16 single layer spruce beams 21
Figure 2.14: Experimental modal shapes for the single layer beams 21
Figure 2.15: Average longitudinal elastic modulus and standard deviation (σ) for the first three vibration modes 23
Figure 2.16: FRFs at point P11 for the AFLB assembled using 27 dowels 24
Figure 2.17: Comparison of average frequency and corresponding standard deviation (σ) for the AFLBs and the glued beam 25
Figure 2.18: Comparison of average damping and corresponding standard deviation (σ) for the AFLBs and the glued beam 26

Figure 2.19: Comparison of average frequency and corresponding standard deviation (σ) for the AFLBs connected by 13 or 27 CSDs 27
Figure 2.20: Comparison of average damping and corresponding standard deviation (σ) for the AFLBs connected by 13 or 27 CSDs 27
Figure 2.21: Measurement of moisture content of a beam using the H-DI 3.10K moisture meter 29
Figure 2.22: Effect of moisture content on frequencies for the single layer beam 30
Figure 2.23: Effect of moisture content on frequencies for the glued beam 30
Figure 2.24: Effect of moisture content on the first three frequencies of the AFLB 31
Figure 2.25: FRFs at point P15 for the AFCLT panels 33
Figure 2.26: Comparison of average frequencies and standard deviation (σ) between normal panel and groove panel 35
Figure 2.27: Comparison of average viscous damping ratio and standard deviation (σ) between normal panel and groove panel 36
Figure 3.1: Cross-section and parameters of three-layer beam 40
Figure 3.2: Diagram of the dowellam floor (a) and the simplified FE model (b) in Filippoupolitis *et al.* (2017) 41
Figure 3.3: Description of the Verification and Validation methodology 42
Figure 3.4: Single layer beam FE model 43
Figure 3.5: The first five numerical mode shapes of single layer beam 46
Figure 3.6: Convergence study of frequencies of single layer beam FE model: 47
Figure 3.7: Comparison between numerical and experimental frequencies 49
Figure 3.8: Local elastic modulus (blue line), global elastic modulus (red line) and clear wood area ratios CWAR (dashed line) along the length of different oak boards (Tapia and Aicher (2019)) 50
Figure 3.9: CAD model of AFLB 51
Figure 3.10: Local coordinate system of dowel and layers 53
Figure 3.11: Convergence study of FE model of AFLB 54
Figure 3.12: Converged FE mesh of AFLB 54
Figure 3.13: The first seven numerical mode shapes of AFLB 56
Figure 3.14: Effect of stiffness of dowel on frequencies of AFLB 57
Figure 3.15: CAD model of AFCLT panel without groove 58
Figure 3.16: Convergence study of the first three frequencies 58
Figure 3.17: Converged mesh of AFCLT panel 59
Figure 3.18: Numerical mode shapes of AFCLT panel 60
Figure 3.19: CAD model of full-size AFCLT panel 62

Figure 3.20: Comparison of predicted frequencies between AFCLT panel and glued CLT panel 63
Figure 3.21: The first four numerical mode shapes of full-size AFCLT panel 63
Figure 3.22: Design parameters *a* and *b* recommended by the Eurocode 5 64
Figure 3.23: Vibration performance of the full-size AFCLT panel 65
Figure 3.24: Full-size AFCLT panel assembled by 4320 vertical dowels 66
Figure 3.25: AFCLT panel assembled by 30-degree dowels 67
Figure 3.26: First frequency of full-size AFCLT panel with 2 simply supported edges 67
Figure 3.27: First frequency of full-size AFCLT panel with 4 simply supported edges 68
Figure 3.28: Local coordinate system of dowel and global coordinate system of AFCLT panel 69
Figure 3.29: Deformation of layer and dowel of the AFLB for the 1st vibrational mode from the reference model 70
Figure 3.30: Local axes for beam element 70
Figure 3.31: Simplified FE model of AFLB using beam and shell elements 72
Figure 3.32: Connection detail between layers and dowel 73
Figure 3.33: Simplified FE model of AFLB using shell elements to model layers 74
Figure 3.34: Comparison between mode shape from simplified model and mode shape from reference model 76
Figure 3.35: Dimensions of original dowel (a) and square dowel (b) 77
Figure 3.36: 3D model of AFLB with square dowels 77
Figure 3.37: Proposed simplified FE model of AFLB 78
Figure 3.38: Proposed simplified FE model for full-size AFCLT panel 79
Figure 4.1: Flowchart of the MSP (Yin *et al.* (2018)) 86
Figure 4.2: Reference and physical coordinate systems of 20-node hexahedral element 90
Figure 4.3: Convergence study of MSP nominal frequencies using 4 different formulations 92
Figure 4.4: Gaussian distribution law 95
Figure 4.5: Flowchart of the error indicator (Yin *et al.* (2018)) 96
Figure 4.6: Distribution of frequencies of single layer beams 98
Figure 4.7: Distribution of frequencies of AFLB 99
Figure 4.8: Influence of the number of trials nt on the error between MSP and direct MCS in case of the 7th frequency of the AFLB 100
Figure 4.9: Comparison of mean value and CoV of frequencies of oak single layer beam between experiment (with 16 specimens), direct MCS and MSP (16 trials) 102
Figure 4.10: Comparison of mean value and CoV of frequencies of oak single layer beam between experiment (with 16 specimens), direct MCS and MSP (10,000 trials) 103

Figure 4.11: Comparison of experimental and numerical mean value and CoV of frequencies of AFLB..... 104
Figure 4.12: Distribution of the first six frequencies of AFCLT panel..... 105
Figure 4.13: Comparison of experimental and numerical mean value and CoV of frequencies of AFCLT panel..... 106
Figure 4.14: Mean and standard deviation of the fundamental frequency of eight full-size AFCLT panels..... 107

List of Tables

Table 2.1: Dynamic properties and corresponding variability for the oak and spruce single layer beams 22
Table 2.2: Longitudinal elastic modulus and density for single layer beams 23
Table 2.3: Quantity of three-layer beams 24
Table 2.4: Dynamic properties and corresponding variability for the AFLB assembled using CSDs 28
Table 2.5: Experimental modal shapes for the AFCLT panels 34
Table 2.6: Dynamic properties and corresponding variability for the AFCLT panels 36
Table 3.1: Sensitivity of frequencies to material properties of single layer beam 44
Table 3.2: The relationship between the mechanical properties and the density (unit: g/cm^3) of wood (Jodin (1994)) 45
Table 3.3: Number of finite elements along three directions for convergence 48
Table 3.4: The mean values of MAC of the single layer beams 48
Table 3.5: Comparison results from two FE models for the oak board 50
Table 3.6: Mechanical properties of oak layers and CSDs in FE model of AFLB 52
Table 3.7: Sensitivity of frequencies to material properties of layers of AFLB 52
Table 3.8: Sensitivity of frequencies to material properties of dowels of AFLB 52
Table 3.9: Number of elements in the converged mesh for layers and dowels of AFLB 54
Table 3.10: Comparison between numerical and experimental results for AFLB 55
Table 3.11: Comparison between numerical and experimental results for AFCLT panel 59
Table 3.12: Comparison of numerical frequencies of normal panel and groove panel 61
Table 3.13: Comparison between numerical and experimental deflection for AFCLT panel .. 61
Table 3.14: Vibrational characteristic values of full-size AFCLT panel according to the Eurocode 5 requirements 65
Table 3.15: Parameters for the design of AFCLT panel 66
Table 3.16: Effect of increase of moduli E_2, E_3 and G_{23} of dowel on frequencies of the AFLB 71
Table 3.17: Effect of increase of moduli E_2, E_3 and G_{23} of dowel on frequencies of the AFCLT panel 71
Table 3.18: Comparison between 3D solid model and simplified FE model uses beam and shell elements 73
Table 3.19: Comparison between results from the simplified model and the reference model for AFLB 75

Table 3.20: Comparison between results from the 3D square-dowel model and the reference model for AFLB 78
Table 3.21: Comparison between results from the proposed simplified FE model and the reference model for AFLB 79
Table 3.22: Comparison of computational cost between the proposed simplified FE model and the reference model for full-size AFCLT panel 80
Table 3.23: Comparison between results from the proposed simplified FE model and the reference model for full-size AFCLT panel 80
Table 4.1: Reference coordinates of the vertex nodes 90
Table 4.2: Reference coordinates of the nodes on the sides parallel to the axis ξ 91
Table 4.3: Reference coordinates of the nodes on the sides parallel to the axis η 91
Table 4.4: Reference coordinates of the nodes on the sides parallel to the axis ζ 91
Table 4.5: Comparison of frequencies of single layer beam between FE model and MSP formulations 93
Table 4.6: Comparison of frequencies of the AFLB between FE model and MSP formulation 4 93
Table 4.7: Comparison of frequencies of the AFCLT panel between FE model and MSP formulation 4 933
Table 4.8: Description of uncertain parameters of oak layer and compressed wood dowel .. 95
Table 4.9: Description of the random parameters of single layer beam, AFLB and AFCLT panel 95
Table 4.10: Comparison of mean value and standard deviation of frequencies of single layer beams from MSP and direct MCS 97
Table 4.11: Comparison of mean value and standard deviation of frequencies of AFLB from MSP and direct MCS 97
Table 4.12: Estimation error between MSP and MCS for 10,000 trials of AFCLT panel 100
Table 4.13: Estimation error between MSP and MCS for 10,000 trials of full-size AFCLT panel 101
Table 4.14: Variability of frequencies of AFLB caused by variability of properties of dowels 101
Table 4.15: Comparison of computational cost between MSP and 10,000 MCS trials 107

List of Publications

Journals

[1] Bui, T.A., Oudjene, M., Lardeur, P., Khelifa, M., Rogaume, Y. (2020). Towards experimental and numerical assessment of the vibrational serviceability comfort of adhesive free laminated timber beams and CLT panels assembled using compressed wood dowels. *Engineering Structures*, 216.

Conferences

[1] Bui, T.A., Oudjene, M., Lardeur, P., Khelifa, M., Rogaume, Y. (2017). Low amplitude vibration performance of multilayered timber beams assembled through compressed wood dowels. *6èmes journées du GDR 3544 « Sciences du bois »*, Nantes, France.

[2] Bui, T.A., Oudjene, M., Lardeur, P., Khelifa, M., Rogaume, Y. (2018). Vibration performance of adhesive free multi-layered timber beams assembled through compressed wood dowels. *2018 World Conference on Timber Engineering*, Seoul, Republic of Korea.

[3] Bui, T.A., Lardeur, P., Oudjene, M. (2018). Experimental analysis of vibration uncertainty of free adhesive laminated timber beams assembled using compressed wood dowels. *21st International Conference on Composite Structures*, Bologna, Italy.

[4] Bui, T.A., Lardeur, P., Oudjene, M. (2018). Experimental study of vibration uncertainty of multilayered timber beams assembled through wood dowels. *International Conference on Uncertainty in Structural Dynamics*, Leuven, Belgium.

[5] Bui, T.A., Lardeur, P., Oudjene, M. (2019). Vérification et validation d'un modèle éléments finis pour l'étude vibratoire des structures bois multicouches assemblées par des tourillons. *14ème Colloque National en Calcul des Structures*, Giens, France.

[6] Bui, T.A., Oudjene, M., Lardeur, P., Khelifa, M., Rogaume, Y. (2019). Vérification et validation de modèles éléments finis pour l'étude vibratoire des structures bois multicouches assemblées par des tourillons. *3DEXPERIENCE® Conference*, Paris, France.

Introduction en français

Contexte et motivations

Structures en bois multicouches

De nos jours, le bois est largement utilisé dans la construction car il s'agit d'un matériau respectueux de l'environnement (Adhikari et Ozarska (2018)). Cependant, les propriétés mécaniques du bois scié varient considérablement. Cela dépend fortement des espèces, des conditions de croissance et les propriétés varient même d'un arbre à l'autre. Par conséquent, les produits en bois d'ingénierie, y compris le bois lamellé-collé et le bois lamellé-croisé, sont préférés pour réduire l'anisotropie et améliorer la stabilité dimensionnelle par rapport au bois scié. Le lamellé-collé, qui peut être utilisé comme colonnes verticales ou poutres horizontales, est fabriqué en collant plusieurs couches de bois ensemble. Le lamellé-croisé est un panneau en bois massif obtenu par empilement et collage de plusieurs couches de bois. Les panneaux de type lamellé-croisé peuvent supporter à la fois des charges hors plan et dans le plan et ils sont utilisés comme systèmes de mur de cisaillement, de plancher et de toit. Ces produits en bois d'ingénierie présentent un potentiel de marché élevé et ils sont de plus en plus utilisés pour la construction massive en bois, en particulier pour les grands bâtiments en bois.

Le projet européen AFTB (Towards Adhesive-Free Timber Buildings)

Comme le lamellé-collé et le lamellé-croisé sont obtenus en collant plusieurs couches de bois, des adhésifs pétrochimiques importants sont utilisés et cela est souligné comme une préoccupation qui affecte leur durabilité, leur recyclabilité et leur impact environnemental plus large. Plus précisément, les adhésifs dans des conditions de haute température peuvent émettre des gaz toxiques, ce qui pourrait provoquer des cancers pour les personnes qui les inhalent (International Agency for Research on Cancer (2004)). De plus, une exposition constante aux adhésifs pourrait entraîner des réactions cutanées allergiques (Frihart et Hunt (2010)). D'une part, la quantité de panneaux de type lamellé-croisé produits en 2016 en Europe a été estimée à 680000 m^3 et devrait passer à 1250000 m^3 d'ici 2020 (Unece (2017)). D'autre part, la Commission européenne (2001) a une politique spécifique visant à développer une économie sobre en carbone en réduisant les émissions de gaz à effet de serre de 80% d'ici 2050. Il est donc nécessaire de développer des techniques d’assemblage plus «vertes» et durables pour répondre à tous les principes acceptables relatifs à l'approche d'analyse du cycle de vie (ACV) des bâtiments. Dans ce contexte, un consortium de six partenaires de six pays européens a été formé dans le cadre d'un projet de recherche conjoint financé par le programme Interreg de l'Europe du Nord-Ouest, appelé AFTB (Adhesive Free Timber

Buildings), pour développer des produits en bois d'ingénierie sans adhésif, y compris des poutres stratifiées sans adhésif et du lamellé-croisé sans adhésif utilisant des tourillons en bois densifié comme élément de jonction pour remplacer les adhésifs toxiques traditionnels. Ici, les produits en bois d'ingénierie sans adhésif utilisent le gonflement irréversible dépendant de l'humidité des chevilles en bois thermo-mécaniquement comprimées pour obtenir un ajustement serré des connexions.

Histoire de l'utilisation du tourillon en bois dans la structure en bois

L'utilisation de tourillons en bois comme matériau d'assemblage n'est pas nouvelle. Les tourillons en bois dur ont été utilisés avec succès pour relier les éléments de structure dans les cadres en bois pendant des milliers d'années.

Malheureusement, les tourillons en bois dur (non densifié) souffrent de fluage / relaxation et de perte de rigidité avec le temps. Certains travaux présentaient du bois lamellé sans adhésif, assemblé avec des tourillons ou des clous en bois dur (Ramage et al. (2017)) et dénommé «Brettstapel».

Selon Henderson et al. (2018), la conception la plus ancienne de la technologie Brettstapel a été développée dans les années 1970 et impliquait l'utilisation de fixations à clous ; cependant, environ deux décennies plus tard, les attaches métalliques ont été remplacées par l'utilisation de tourillons en bois dur. Ces produits en bois d'ingénierie fabriqués sans l'utilisation d'attaches métalliques ou d'adhésifs, sont plus durables et respectueux de l'environnement.

Ces dernières années, un autre concept de panneau en bois massif, appelé *dowellam* (Dowel Laminated Timber) a été conçu et développé par *Structure Craft* en Amérique du Nord (Vancouver, Canada) (Structure Craft (2018)).

Plus récemment, une évaluation technique européenne (ETA) a été obtenue et publiée par la société Thoma Holz100 (Deutsches Institut für Bautechnik (2018)) sur les performances mécaniques des panneaux de type lamellé-croisé sans adhésif assemblés à l'aide de tourillons en hêtre (non compressé). Dans ce document, seules les données concernant le comportement en flexion sous charge transversale ont été données, le confort de service vibratoire n'a pas été évalué.

En outre, Rombach a développé une conception pour les panneaux *Nur Holz* qui utilisent des vis en hêtre filetées pour relier les lamelles de bois. Plus de 300 bâtiments en panneaux *Nur Holz* ont été construits dans le monde (Habitat Naturel (2009)).

Des travaux de recherche ont été entrepris pour étudier le comportement structurel des poutres en bois lamellé assemblées à l'aide de tourillons en hêtre soudés par rotation (non

compressé) (O'Loinsigh et al. (2012a), (b)). Jin et coll. (2015) ont entrepris un programme expérimental pour étudier la faisabilité de structures en bois sandwich en treillis bidimensionnel utilisant des tourillons de bouleau collés.

Cependant, on pense que les assemblages réalisés avec des tourillons en bois dur normal pourraient souffrir d'une faible rigidité et résistance ainsi que d'un fluage / relaxation et d'une perte de rigidité avec le temps. L'utilisation de tourillons en bois compressé (ou densifié) pourrait surmonter ces faiblesses, car le bois comprimé a de meilleures propriétés mécaniques en augmentant sa densité pendant le processus de compression (Guan et al. (2010); Sotayo et al. (2020a)). En outre, l'effet de mémoire de forme du bois comprimé, également connu sous le nom de gonflement irréversible (retour élastique), permet un ajustement permanent des connexions.

Le bois comprimé a attiré l'attention des chercheurs en raison de ses propriétés mécaniques supérieures à celles du bois indigène (Morsing (1998); Peyer et al. (2000); Blomberg (2006); Yoshihara et Tsunematsu (2007) ; Cloutier et al. (2008); Jung et al. (2008); Skyba et al. (2009); Madhoushi et al. (2010); Anshari et al. (2011); Li et al. (2013); Riggio et al. (2016); Song et al. (2018)). Ces études se sont principalement concentrées sur l'effet du processus de compression sur les propriétés mécaniques du bois comprimé. Cependant, il existe très peu d'études publiées sur le comportement structurel des structures en bois assemblées par des tourillons en bois comprimé.

Performance des structures en bois assemblées par des tourillons en bois comprimé

Hassel et al. (2008) ont proposé un système de mur de cisaillement en blocs de bois qui utilise du bois comprimé comme éléments de liaison. Le retour élastique des éléments en bois comprimé provoque un ajustement plus serré des blocs de bois, améliorant ainsi la rigidité du système. De plus, les éléments en bois compressé absorbent la plupart des contraintes et des dommages, permettant à la structure d'être réajustée et réutilisée après des tremblements de terre.

Guan et al. (2010) ont étudié la performance structurelle de l'assemblage poutre-poteau à l'aide de tourillons et de plaques de bois compressé. On peut voir une haute performance de la connexion caractérisée par les courbes moment-rotation.

Mehra et al. (2018) ont évalué la performance structurelle du système de connexion poutre-poutre à l'aide de tourillon et de plaques en bois comprimé. La capacité de charge, la rigidité en flexion, la capacité de moment maximum et la rigidité en rotation du système de connexion ont été comparées à celles obtenues à partir d'un système de connexion similaire utilisant des tourillons et des plaques en acier. La charge de rupture moyenne pour le système de connexion en bois comprimé n'est que de 20,3% inférieure à celle obtenue pour le système

de connexion en acier car les propriétés mécaniques du bois comprimé sont inférieures à celles de l'acier.

Plus récemment, les performances mécaniques des poutres stratifiées sans adhésif et des panneaux en lamellé-croisé sans adhésif ont été évaluées dans El-Houjeyri et al. (2019); Sotayo et al. (2020b). Cependant, à notre connaissance, la performance vibratoire de la structure en bois assemblée par des tourillons en bois compressé n'a pas été publiée ailleurs.

Performances vibratoires des structures en bois

Des mesures des propriétés vibratoires des planchers en bois, y compris les planchers en lamellé-croisé, ont été réalisées par de nombreux chercheurs (Jarnerö et al. (2015); Chúláin et al. (2016); Rijal et al. (2016); Weckendorf et al. (2016); Ussher et al. (2017a); Ebadi et al. (2018); Suárez-Riestra et al. (2019); Zhang et al. (2019)), entre autres. Ces études comprennent les fréquences naturelles, les formes modales, les rapports d'amortissement ainsi que l'effet causé par le type de plancher et les conditions aux limites sur ces propriétés dynamiques.

De nombreuses études (Glisovic et Stevanovic (2010); Hu et Gagnon (2012); Negreira et al. (2015); Ussher et al. (2017b); Casagrande et al. (2018); Huang et al. (2020)) ont été effectuées pour mesurer les réponses au mouvement du sol en lamellé-croisé causées par les pas humains, améliorant ainsi la compréhension des performances de service vibratoire du sol en lamellé-croisé et obtenant de meilleures directives de conception pour les planchers en bois résidentiels.

Récemment, la dynamique structurelle dans la gamme des basses fréquences du plancher *Dowellam* a été évaluée par Filippoupolitis et al. (2017). Les résultats montrent que le sol *Dowellam* répond aux exigences d'aptitude au service des vibrations de l'Eurocode 5.

Cependant, d'une part, il n'y a jusqu'à présent aucun ouvrage publié traitant du confort de service vibratoire des produits en bois d'ingénierie sans adhésif assemblés au moyen de tourillons en bois compressé. D'autre part, le confort de service vibratoire des produits en bois d'ingénierie sans adhésif utilisant des tourillons en bois comprimé n'est couvert par aucune norme de construction. Il est donc nécessaire d'évaluer les caractéristiques dynamiques de ces nouveaux produits en vue de leur utilisation dans la construction.

Objectif de la thèse

Le programme de recherche AFTB (Adhesive Free Timber Buildings) comprend l'évaluation des performances structurelles, des performances au feu et des performances vibratoires de service des produits en bois d'ingénierie sans adhésif développés. Dans le cadre des travaux de recherche menés dans le cadre du projet AFTB, cette thèse porte sur

l'évaluation du confort de service vibratoire des panneaux en lamellé-croisé sans adhésif en tant que systèmes de revêtement de sol. Dans la construction en bois, le confort vibratoire des planchers à base de bois est un problème clé car ils sont légers et plus sujets aux vibrations gênantes causées par les activités humaines, telles que la marche normale et le saut des enfants (Zhang et al. (2013)). Dans l'Union européenne, les exigences de l'Eurocode 5 sont généralement adoptées pour la conception de confort de service vibratoire des planchers en bois de charpente à l'état limite de service (Comité européen de normalisation (2004)). Plusieurs études traitant des performances vibratoires au service des planchers à base de bois sont disponibles dans la littérature (Zhang et al. (2013), (2019) ; Jarnerö et al. (2015); Chúláin et al. (2016); Rijal et al. (2016); Weckendorf et al. (2016); Ussher et al. (2017a); Ebadi et al. (2018); Suárez-Riestra et al. (2019)).

L'évaluation de l'aptitude au service vibratoire est plus pertinente pour les panneaux en lamellé-croisé sans adhésif développés car ils sont susceptibles de présenter une rigidité inférieure par rapport aux planchers en lamellé-croisé collés conventionnels et donc une valeur de fréquence fondamentale réduite.

Contenu de la thèse

Les grandes lignes de cette thèse sont les suivantes :

Dans le chapitre 2, nous présentons tout d'abord la production des tourillons en bois compressé et des produits en bois d'ingénierie sans adhésif, y compris des poutres stratifiées sans adhésif et des panneaux en lamellé-croisé sans adhésif. Le dispositif d'analyse modale expérimentale est décrit. Ensuite, les caractéristiques de vibration expérimentales des poutres monocouche, des poutres stratifiées sans adhésif à trois couches et des panneaux en lamellé-croisé sans adhésif sont données. La comparaison des caractéristiques vibratoires des poutres stratifiées sans adhésif par rapport à une poutre collée similaire est présentée.

Au chapitre 3, un modèle éléments finis (EF) pour simuler le comportement vibratoire des poutres stratifiées sans adhésif et des panneaux en lamellé-croisé sans adhésif est développé. La méthodologie de vérification et de validation est appliquée pour évaluer et améliorer la capacité prédictive du modèle EF. Ensuite, les caractéristiques vibratoires prédites d'un système de revêtement de sol réaliste fabriqué avec un panneau en lamellé-croisé sans adhésif sont discutées en ce qui concerne les exigences de conception d'aptitude au service vibratoire de l'Eurocode 5. Pour terminer le chapitre, un modèle EF simplifié pour les poutres stratifiées sans adhésif ***et*** les panneaux en lamellé-croisé sans adhésif est discuté.

Dans le chapitre 4, la variabilité numérique de la fréquence naturelle des poutres stratifiées sans adhésif et des panneaux en lamellé-croisé sans adhésif est étudiée par la procédure de stabilité modale (MSP). Un bref aperçu des méthodes non déterministes est

d'abord présenté. Nous présentons ensuite l'hypothèse et la formulation générale de la méthode MSP. La méthode MSP est ensuite développée pour le modèle EF de poutre monocouche, les poutres stratifiées sans adhésif et les panneaux en lamellé-croisé sans adhésif. Les résultats obtenus avec la méthode MSP sont comparés à ceux obtenus par la méthode de référence (Simulation Monte Carlo directe) et par des expériences. Un indicateur d'erreur est également développé. Pour terminer le chapitre, le coût de calcul de la méthode MSP est discuté.

Enfin, des conclusions et des perspectives sont données au chapitre 5.

Chapter 1: Introduction

1.1 Background and motivations

1.1.1 Multilayered timber structures

Nowadays, timber is widely used in construction because it is an environmentally friendly material (Adhikari and Ozarska (2018)). However, mechanical properties of sawn timber vary greatly. It strongly depends on species, growing conditions, and it even varies from tree to tree. Therefore, engineered wood products (EWPs), including glued laminated timber (Glulam) and Cross Laminated Timber (CLT) (Figure 1.1), are preferred to reduce anisotropy and to enhance dimensional stability as compared to the sawn timber. Glulam, what can be used as vertical columns or horizontal beams, is manufactured by gluing several layers of timber together. CLT is a massive timber panel obtained by crosswise stacking and gluing several timber layers. CLT panels can bear both out-of-plane and in-plane loadings and they are being used as shear wall, floor and roof systems. These engineered wood products show high market potential and they are increasingly being used for massive timber construction, especially for tall timber buildings.

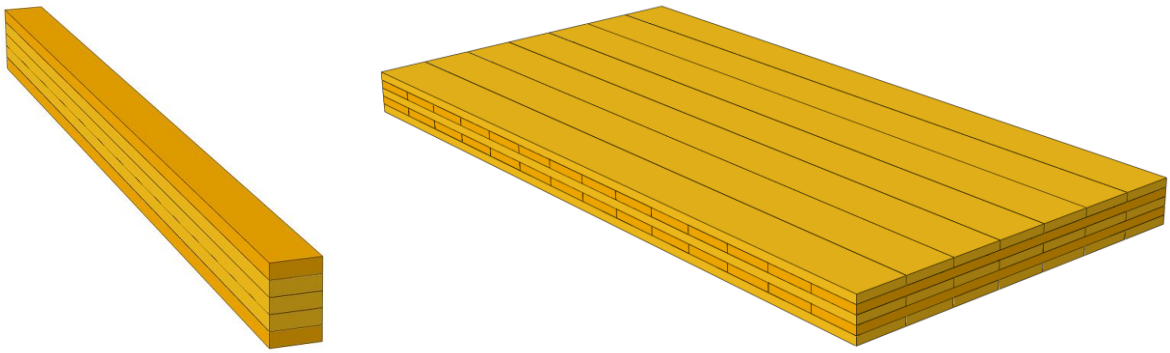

a) Glued laminated timber beam b) Cross laminated timber panel

Figure 1.1: Examples of multilayered Engineered Wood Products (EWPs)

1.1.2 Towards Adhesive-Free Timber Buildings (AFTB) project

As Glulam and CLT are obtained by gluing several timber layers, significant petrochemical adhesives are used and this is pointed out as a concern that affects their sustainability, recyclability and broader environmental impact. More specifically, the adhesives under high-temperature conditions can emit toxic gas, which could cause cancer for people who inhale it (International Agency for Research on Cancer (2004)). In addition,

constant exposure with the adhesives could lead to allergic skin reactions (Frihart and Hunt (2010)). On the one hand, the amount of CLT panels produced in 2016 in Europe was estimated to 680,000 m^3 and expected to increase to 1,250,000 m^3 by 2020 (Unece (2017)). On the other hand, the European Commission (2001) has a specific policy aiming to develop a low-carbon economy by reducing greenhouse gas emissions to 80% by 2050. There is, therefore, a need to develop more "green" and sustainable joining techniques to meet all acceptable principles related to life cycle assessment (LCA) approach of buildings. In this context, a consortium with six partners from six European countries was formed through a joint research project funded by the North-West European Interreg Programme, called AFTB, to develop adhesive free engineered wood products (AFEWPs), including adhesive free laminated beam (AFLB) and adhesive free CLT (AFCLT) using densified wooden dowels as a joining element to substitute the traditional toxic adhesives (Figure 1.2) . Here, the AFEWPs make use of irreversible moisture-dependent swelling of thermo-mechanically compressed wood dowels to achieve tight fitting of connections.

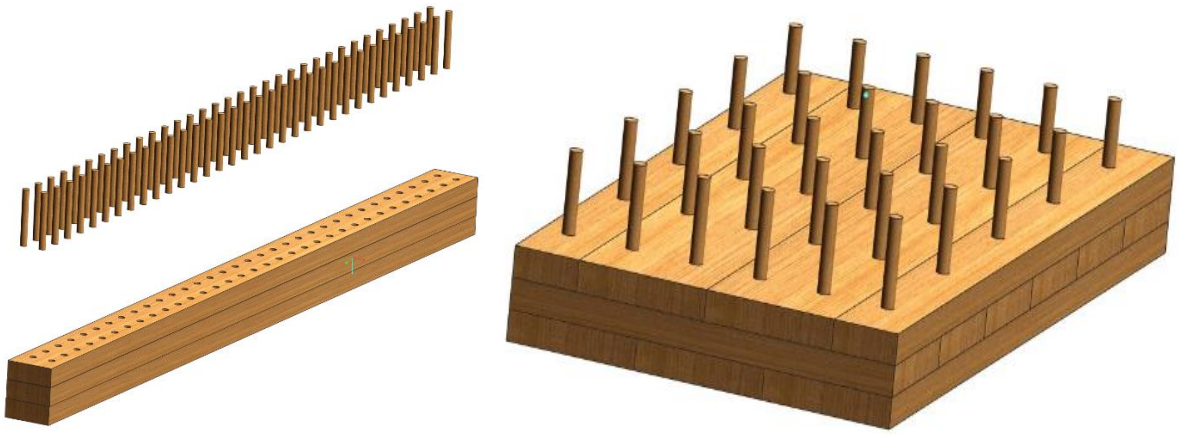

a) Adhesive free laminated timber beam b) Adhesive free cross laminated timber panel

Figure 1.2: Multilayered timber structures assembled using compressed wood dowels

1.1.3 History of using wood dowel in timber structure

The use of wood dowels as joint material is not new. Hardwood dowels have been successfully used to connect structural members in timber frames for thousands of years (Figure 1.3).

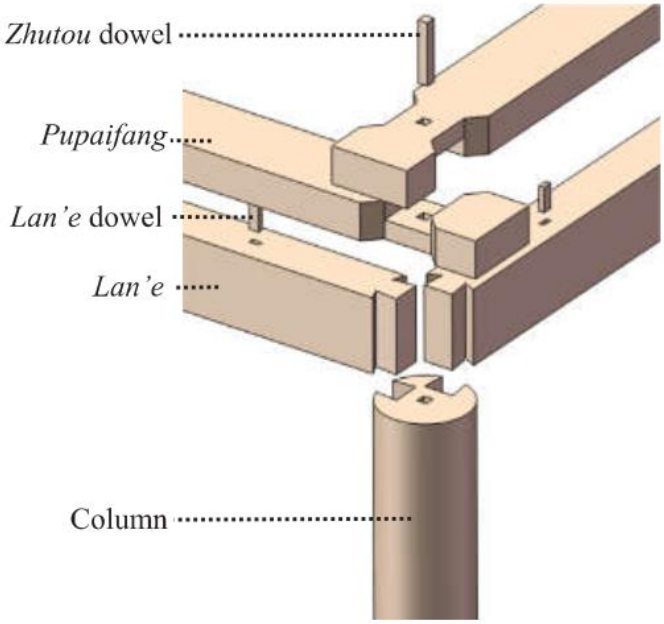

Figure 1.3: Beam-column connection in traditional Chinese pagodas (Meng *et al.* (2019))

Unfortunately, hardwood dowels (not densified) suffer from creep/relaxation and loss of stiffness over time. Some works presented adhesive free laminated timber assembled with hardwood dowels or nails (Ramage *et al.* (2017); Structure Craft (2018)) and referred to as "Brettstapel".

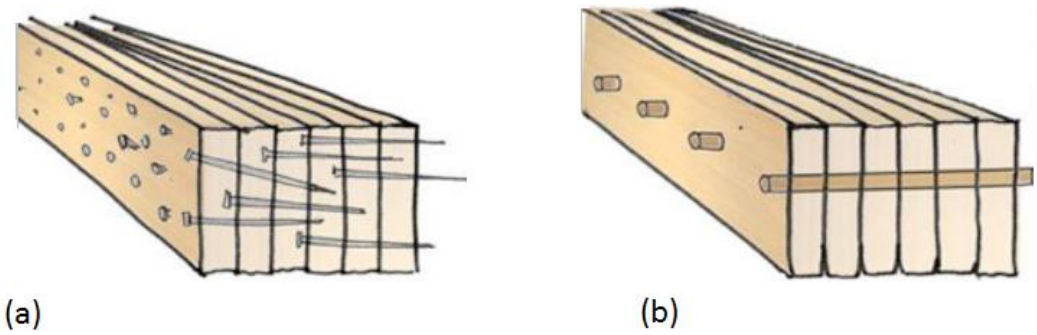

Figure 1.4: Concept of adhesive free laminated timber beams ("Brettstapel"): (a) assembled using nails and (b) assembled through hardwood dowels

According to Henderson *et al.* (2018), the earliest design of the Brettstapel technology was developed in the 1970s and involved the use of nail fasteners; however, about two decades later, metallic fasteners were replaced with the use of hardwood dowels (Figure 1.4b), since 1999. These EWPs fabricated without the use of metal fasteners or adhesives, are more sustainable and environmentally-friendly.

In recent years, another concept of wood mass timber panel (Figure 1.5), called dowellam (Dowel Laminated Timber) was designed and developed by Structure Craft in North-America (Vancouver Canada) (Structure Craft (2018)).

Figure 1.5: Concept of Dowellam by Structure Craft

More recently an European Technical Assessment (ETA) was obtained and published by the Thoma Holz100 company (Deutsches Institut für Bautechnik (2018)) on the mechanical performance of AFCLT panels assembled using beech dowels (uncompressed) (Figure 1.6). In that document only data regarding the flexural behavior under transverse loading was given, the vibrational serviceability comfort was not assessed.

Furthermore, Rombach developed a design for Nur Holz panels that use threaded beech screws to connect the timber laminae, as shown in Figure 1.7. There are more than 300 buildings made of Nur Holz panels have been built worldwide (Habitat Naturel (2009)).

Some research works have been undertaken to investigate the structural behaviour of laminated timber beams assembled using rotationally-welded beech dowels (uncompressed) (O'Loinsigh *et al.* (2012a), (b)). Jin *et al.* (2015) undertook an experimental program to investigate the feasibility of wood-based two-dimensional lattice truss core sandwich timber structures using glued birch dowels.

However, it is believed that connections made with normal hardwood dowels could suffer from low stiffness and strength as well as from creep/relaxation and a loss of stiffness over time. The use of compressed (or densified) wood dowels could overcome these weaknesses as compressed wood has greater mechanical properties by increasing its density during the compression process (Guan *et al.* (2010); Sotayo *et al.* (2020a)). Also, the shape-memory effect of compressed wood, also known as irreversible swelling (springback) makes permanent tight-fitting of connections (Figure 1.8).

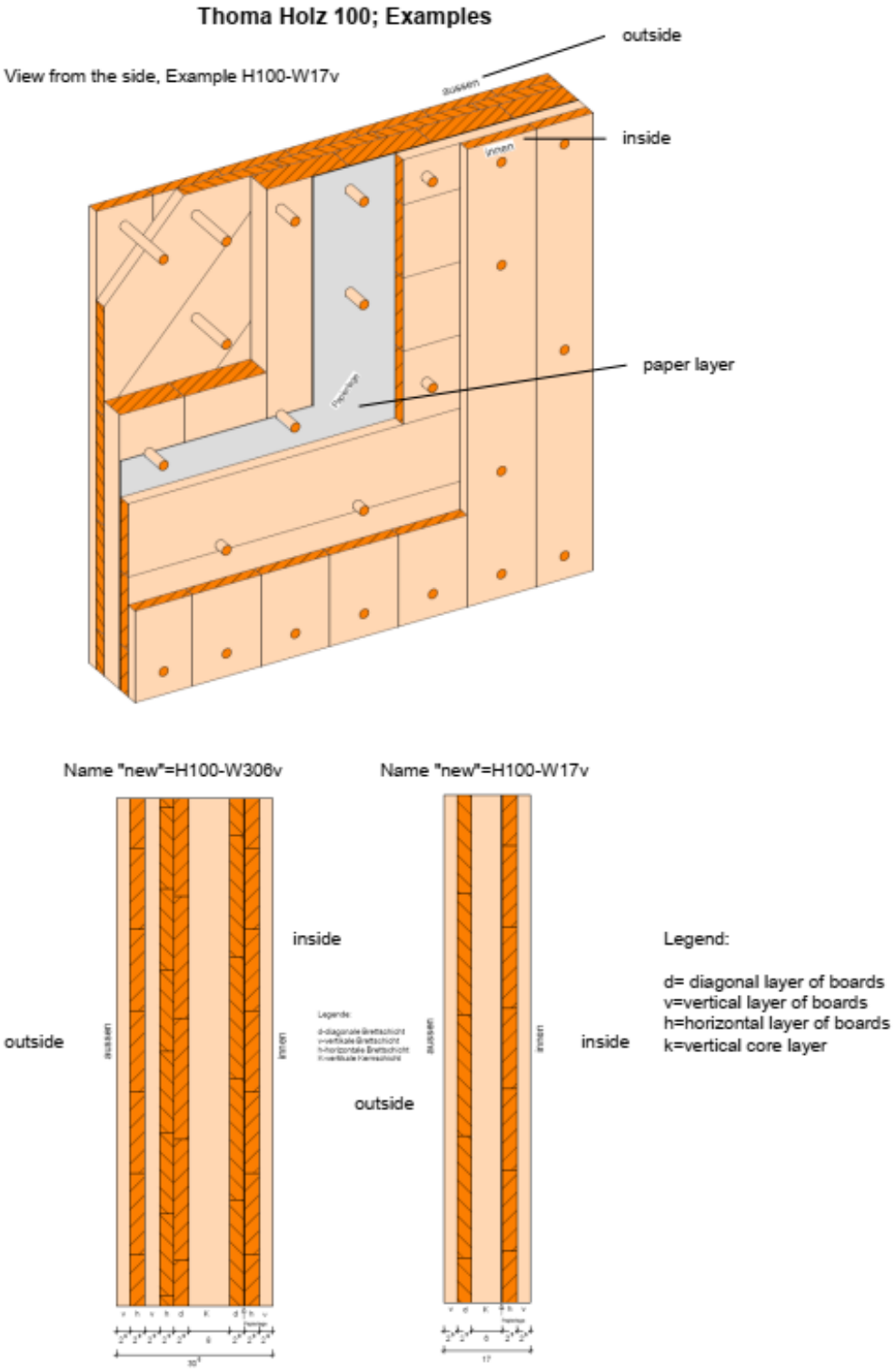

Figure 1.6: Diagrams of the THOMA Holz 100 (Deutsches Institut für Bautechnik (2018))

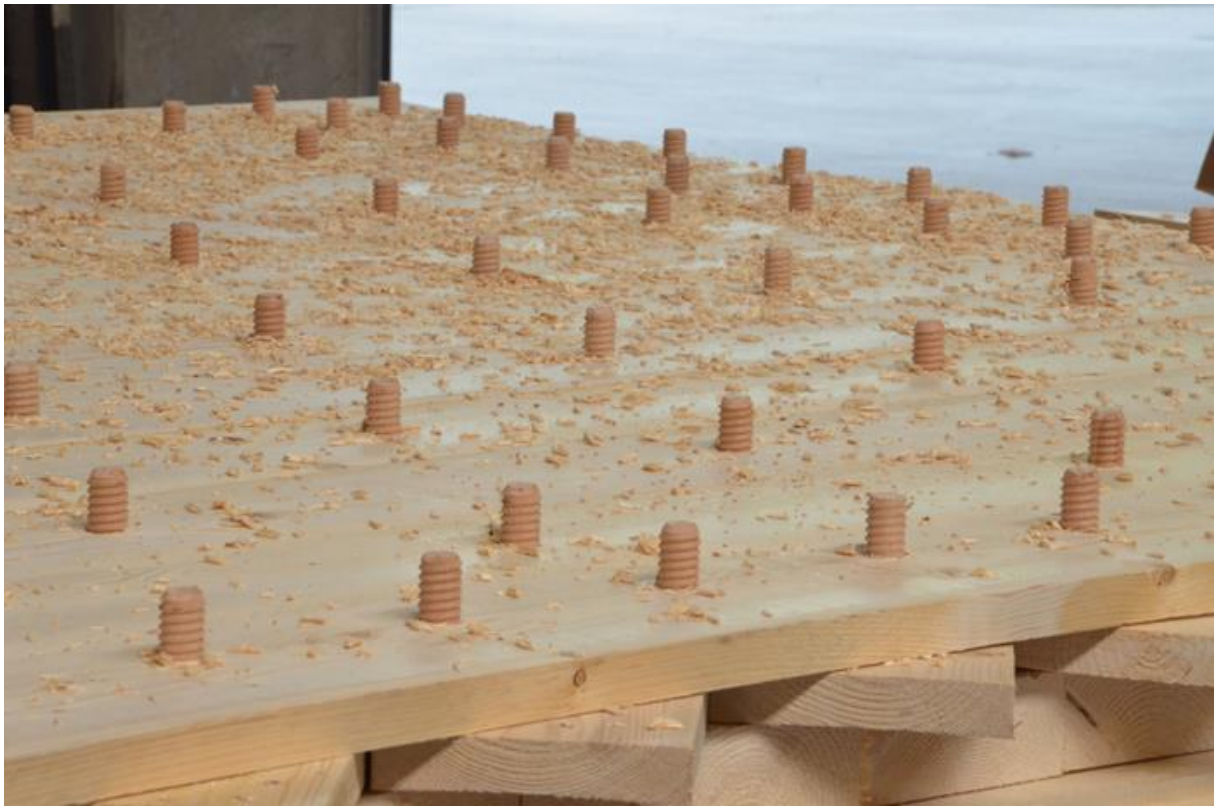

Figure 1.7: Nur Holz panel (Habitat Naturel (2009))

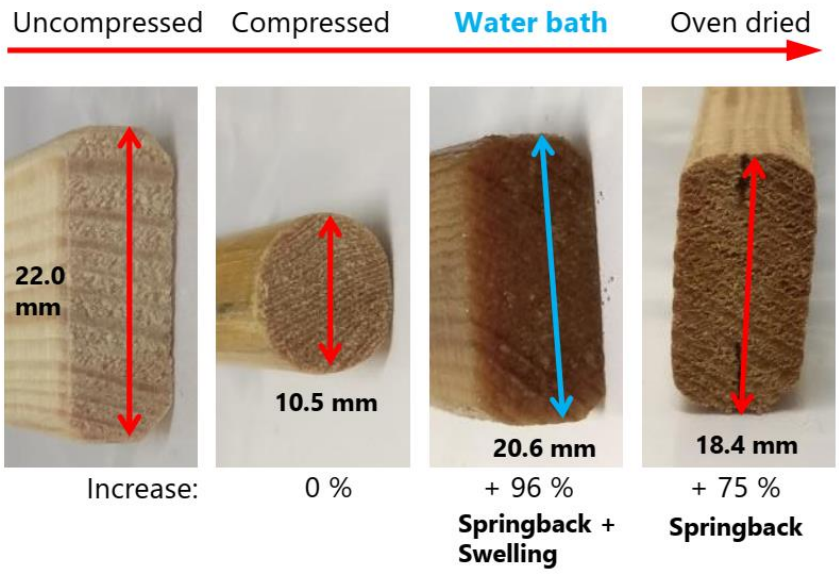

Figure 1.8: Springback of compressed wood dowel (see the website: https://www.nweurope.eu/media/10253/tech-brief-03-properties-of-compressed-wood.pdf)

Compressed wood has attracted the attention of researchers due to its mechanical properties superior to that of the native wood (Morsing (1998); Peyer *et al.* (2000); Blomberg (2006); Yoshihara and Tsunematsu (2007); Cloutier *et al.* (2008); Jung *et al.* (2008); Skyba *et al.* (2009); Madhoushi *et al.* (2010); Anshari *et al.* (2011); Li *et al.* (2013); Riggio *et al.* (2016); Song *et al.* (2018)). These studies have focused mainly on the effect of the compression

process on the mechanical properties of compressed wood. However, there is very few published studies related to the structural behavior of timber structures assembled by compressed wood dowels.

1.1.4 Performance of timber structures assembled by compressed wood dowels

Hassel *et al.* (2008) proposed a wooden block shear wall system which uses compressed wood as connecting elements. The springback of the compressed wood elements causes a tighter fit of the wooden blocks, thereby improving the system stiffness. Moreover, compressed wood elements absorb most of the stress and damage, allowing the structure to be readjusted and reused after earthquakes.

Guan *et al.* (2010) studied the structural performance of beam-to-column connection using compressed wood dowels and plates. It can be seen a high performance of the connection from the moment-rotation relationship.

Mehra *et al.* (2018) assessed the structural performance of beam-to-beam connection system using compressed wood dowels and plates. The load carrying capacity, bending stiffness, maximum moment capacity and rotational stiffness of the connection system were compared to that obtained from a similar connection system using steel dowels and plates. The mean failure load for the compressed wood connection system is only 20.3% less than that achieved for the steel connection system because the mechanical properties of compressed wood are smaller than that of steel.

More recently, the mechanical performance of AFLB and AFCLT panel was evaluated in El-Houjeyri *et al.* (2019); Sotayo *et al.* (2020b). However, at our best knowledge the vibrational performance of timber structure assembled by compressed wood dowels has not been published elsewhere.

1.1.5 Vibration performance of timber structures

Measurements of vibration properties of timber floors, including CLT floors, have been performed by many researchers (Jarnerö *et al.* (2015); Chúláin *et al.* (2016); Rijal *et al.* (2016); Weckendorf *et al.* (2016); Ussher *et al.* (2017a); Ebadi *et al.* (2018); Suárez-Riestra *et al.* (2019); Zhang *et al.* (2019)), among others. These studies include natural frequencies, modal shapes, damping ratios as well as the effect caused by type of floors and boundary conditions on those dynamic properties.

Many studies (Glisovic and Stevanovic (2010); Hu and Gagnon (2012); Negreira *et al.* (2015); Ussher *et al.* (2017b); Casagrande *et al.* (2018); Huang *et al.* (2020)) have been performed to measure motion responses of CLT floor caused by human footsteps, thereby

improving the understanding of vibration serviceability performance of CLT floor and getting better design guidelines for residential timber floors.

Recently, the structural dynamics in low-frequency range of dowellam floor was assessed by Filippoupolitis *et al.* (2017). The results show that the dowellam floor meets the vibration serviceability requirements of Eurocode 5.

However, on the one hand, up to now there is no published works dealing with the vibrational serviceability comfort of adhesive free engineering wood products (AFEWPs) assembled through compressed wood dowels. On the other hand, the vibrational serviceability comfort of AFEWPs using compressed wood dowels is not covered by any building standards. There is, therefore, a need to assess the dynamic characteristics of such new products towards their utilization in construction.

1.2 Objective of the thesis

The AFTB research programme includes assessment of structural performance, fire performance and serviceability vibrational performance of the developed AFEWPs. As part of the research work carried out in the framework of the AFTB project, this thesis focusses on the vibrational serviceability comfort assessment of AFCLT panels as flooring systems. In timber construction, the vibrational comfort of timber-based floors is a key issue as they are light-weight and more prone to the annoying vibrations caused by human activities, such footfall from normal walking and children's jumping (Zhang *et al.* (2013)). In the European Union, the Eurocode 5 requirements are generally adopted for the vibrational serviceability comfort design of structural timber floors in the serviceability limit state (European Committee for Standardization (2004)). Several studies dealing with vibratory performance in service of timber-based floors are available in the literature (Zhang *et al.* (2013); Jarnerö *et al.* (2015); Chúláin *et al.* (2016); Rijal *et al.* (2016); Weckendorf *et al.* (2016); Ussher *et al.* (2017a); Ebadi *et al.* (2018); Suárez-Riestra *et al.* (2019); Zhang *et al.* (2019)).

The vibrational serviceability assessment is more relevant for the developed AFCLT panels because they are likely to exhibit lower stiffness as compared to the conventional glued CLT floors and thus reduced fundamental frequency value.

1.3 Outline

The outline of this thesis is as follows:

In Chapter 2, we first introduce the production of the compressed wood dowels and AFEWP, including AFLB and AFCLT panel. Next, the experimental modal analysis device is described. Then, the experimental vibration characteristics of single layer beams, three-layer

AFLBs and AFCLT panels are given. The comparison of the vibrational characteristics of AFLB against similar glued beam is presented.

In Chapter 3, a finite element (FE) model to simulate vibrational behavior of AFLB and AFCLT panel is developed. Verification and Validation methodology is applied to evaluate and improve the predictive capability of the FE model. Then, the predicted vibrational characteristics of a realistic flooring system made with AFCLT panel are discussed with regard to the vibrational serviceability design requirements of Eurocode 5. To end the chapter, a simplified FE model for AFLB and AFCLT panel is discussed.

In Chapter 4, the numerical variability of natural frequency of AFLB and AFCLT panel is investigated by the Modal Stability Procedure (MSP). A short overview on non-deterministic methods is first introduced. We present then the assumption and the general formulation of the MSP. The MSP is then developed for the FE model of single layer beam, AFLB and AFCLT panel. The results of the MSP are compared with those obtained by the reference method (Monte Carlo Simulation) and by experiments. An error indicator is also developed. To end the chapter, the computational cost of the MSP is discussed.

Finally, conclusions and perspectives are drawn in chapter 5.

Chapter 2:
Experimental modal analysis

This chapter presents an experimental investigation of the vibration performance of adhesive free laminated beams (AFLB) and adhesive free cross-laminated timber panels, assembled by either compressed spruce dowels or normal oak dowels (not compressed). The compressed dowels were cut from compressed spruce block which was compressed under high pressure and temperature up to 68% compression ratio. The experimental modal analyses were carried out under free-free conditions using a hammer impact. Frequency response functions, natural frequencies, mode shapes, and damping ratios were assessed experimentally. In addition, similar glued beams have been manufactured and tested for comparison purpose. The effect of moisture content on the frequencies of AFLB is also presented in this chapter.

2.1 Production of adhesive free laminated beams and adhesive free CLT panels

2.1.1 Compressed spruce dowels

In adhesive free laminated beams and CLT panels, dowels are important parts. They connect all laminae and resist the separation of laminae vertically and horizontally by bending (O'Loinsigh *et al.* (2012a)). They are subjected to greater equivalent stress compared with laminae when the laminated beam is bent. When the mechanical properties of dowels are improved, the stiffness of the beam and panel may be improved (O'Loinsigh *et al.* (2012b)). Therefore, compressed spruce with higher mechanical properties compared with normal timber is the most suitable material for dowels.

Spruce timber blocks with average density value of 437 kg/m^3, with 10±2% moisture content, were used to manufacture compressed spruce dowels. The compression of the spruce blocks was done, in the radial direction, using a hot-pressing machine (Figure 2.1a) with a maximum pressure force of 1500kN.

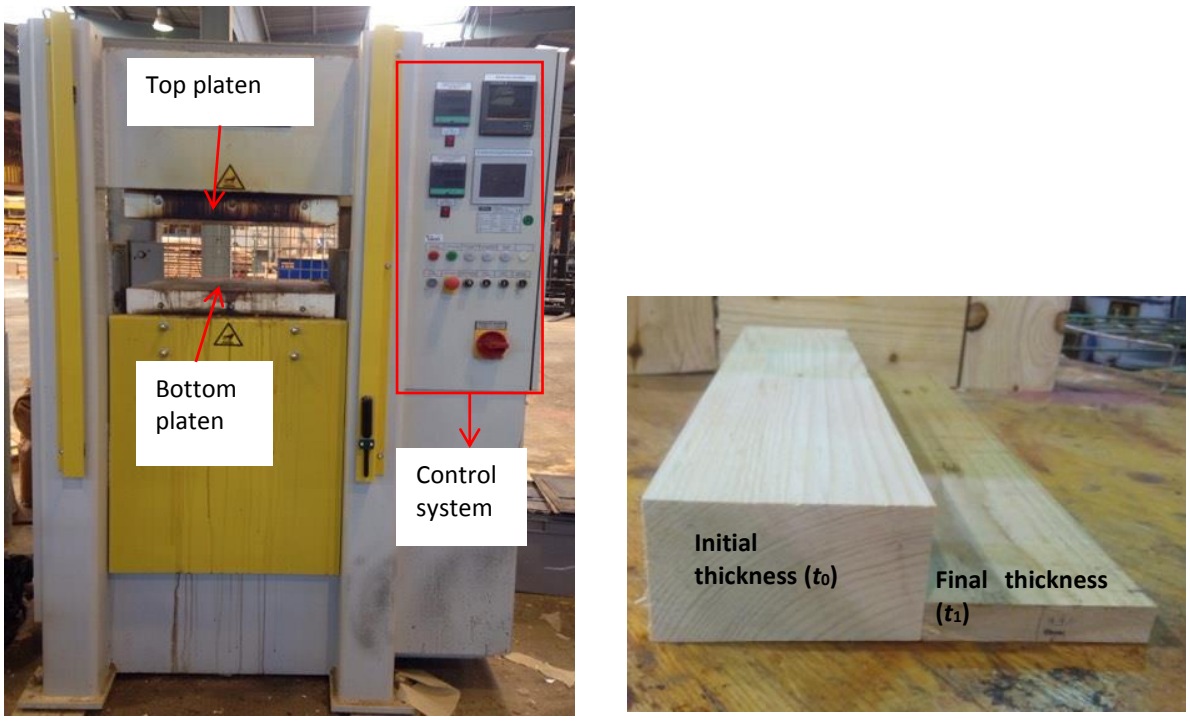

(a) (b)

Figure 2.1: Production of compressed wood dowels: (a) Hot press machine and (b) Typical thicknesses of spruce blocks before and after densification

During the five-hour compression process, the pressure was kept to approximate 18 MPa and the temperature reduced linearly from 130°C to 60°C (Figure 2.2).

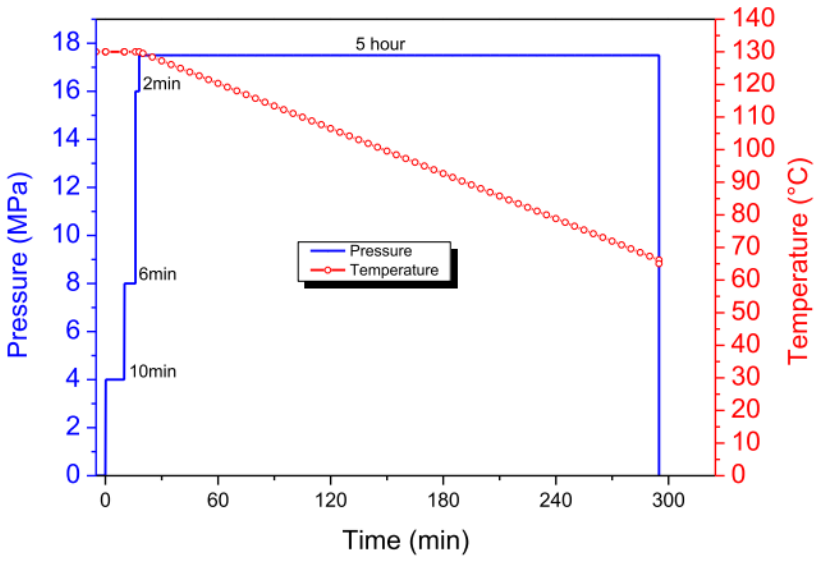

Figure 2.2: Pressure and temperature profiles during the compression process (El-Houjeyri *et al.* (2019))

The typical shape of spruce blocks before and after compression process in the radial direction can be seen in Figure 2.1b. Once the spruce timber blocks were compressed in the radial direction at a level of compression of 68% (*CR*=68%), they were cut and planned to obtain plates with a desired thickness of 16 mm. The Compression Ratio (*CR*) was calculated, based on the initial thickness t_0 and the final thickness t_1, by the following equation (Anshari *et al.* (2010)):

$$CR(\%) = \frac{t_0 - t_1}{t_0} \times 100 \qquad (2.1)$$

From the compressed plates, rounded compressed wood dowels with 16 mm diameter were produced (Figure 2.3).

Figure 2.3: Typical produced compressed spruce dowels

2.1.2 Adhesive free laminated beams (AFLB) and adhesive free CLT (AFCLT) panels

The manufacture and testing of AFLB is necessary as a first stage to access the vibrational characteristics of the adhesive free multilayered timber structures. On one hand, the study of AFLB gives us a good understanding before working on the adhesive free timber floor. Indeed, the deflection of AFLB is mainly by bending in the long direction while the flooring system may be bent in both long and wide directions. On the other hand, AFLB can be produced in large numbers to compare the influence of parameters such as the number of dowels, material of dowels and layers. The smaller scale of AFLB compared with the floor can help us save material and manufacture time.

The AFLB were manufactured by stacking three timber layers having the following dimensions: 70 mm x 22.5 mm x 1450 mm (Figure 2.4). Two timber species have been considered for the laminates, namely spruce timber and oak timber. All the laminae were weighed and moisture content measured prior to testing to obtain information about the density. The dowels were either made of 68% compressed spruce or normal oak timber with 16 mm diameter (d =16 mm). Two different dowel spacings were considered, namely 7 times and 3 times the dowel diameter (7d and 3d), involving 13 dowels and 27 dowels per beam, respectively. In addition, several three-oak-layer and three-spruce-layer glued beams with similar dimensions compared with AFLB were manufactured and tested for comparison.

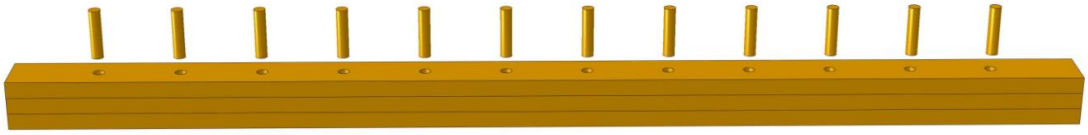

Figure 2.4: Schematic illustration of the three-layer AFLB

First, the laminae were drilled to obtain one row holes with 16 mm diameter. After that, they were stacked, pressed using clamping devices (Figure 2.5) and assembled by insertion of the dowels using wood hammer.

a) Assembly of beams

b) Typical manufactured beams

Figure 2.5: Adhesive free laminated beams

Similarly to the construction method of the beams, three-ply AFCLT panels with dimensions of 75 mm x 1050 mm x 2100 mm, assembled through 196 compressed spruce dowels each, were manufactured (Figure 2.6a). The laminae are 25 mm thick, 150 mm wide and respectively, 2100 mm and 1050 mm long for longitudinal and transverse laminae. Then adhesive free CLT panels have been manufactured and include five panels with grooves and five panels without grooves (Figure 2.6b). The tongues and grooves may improve the connection on the side of laminae, thereby increase the stiffness of AFCLT panels. By comparing the dynamic property of the two types of panels in section 2.6, we can see the role of tongues and grooves.

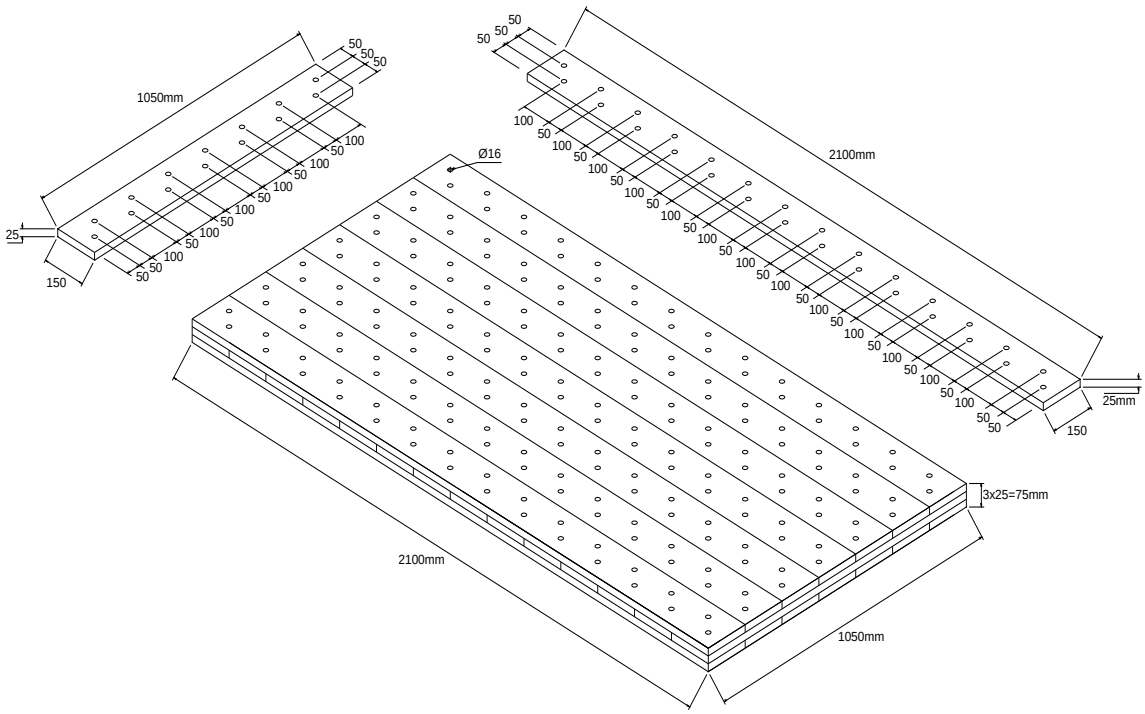

a) Geometrical definitions of AFCLT panels

b) Produced AFCLT panels

Figure 2.6: Typical AFCLT manufactured panels

2.2 Experimental set-up

2.2.1 Hammer impact excitation

From Cetrangolo *et al.* (2015); Zhang *et al.* (2019), it can be concluded that the vibration characteristic of timber structures is highly sensitive to boundary conditions. Therefore, in this study all beams and panels were tested under free-free conditions to minimize the effect of

boundary condition. Moreover, in numerical point of view, it is not easy to simulate the real boundary condition of the beams and panels. The free–free conditions were achieved thanks to the mineral wool system placed at the two beam ends and by vertical suspension for the AFCLT panels as shown in Figures 2.7 and 2.8, respectively. The AFCLT panel was supported at one location near the width by a mini crane as shown in Figure 2.8. The stiffness of the mineral wool is very low, which ensures free–free conditions (Bui *et al.* (2018)). The mineral wool system can keep beam's equilibrium better than the suspension; therefore, it can reduce the preparation time for each test given the large number of beams tested. However, the AFCLT panel is too heavy to be supported by mineral wool system. Therefore, a suspension was found better for the panel.

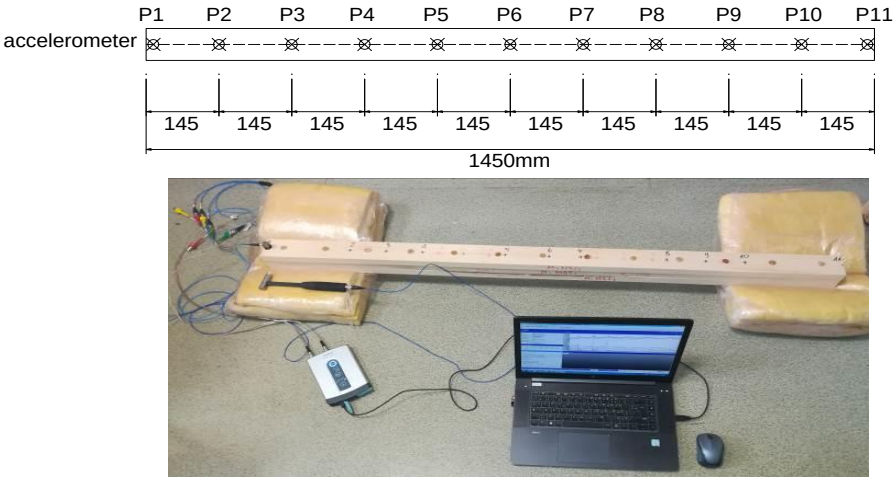

Figure 2.7: Experimental set-up of beam specimens under free – free conditions

One triaxial accelerometer (model 356A15) was fixed at position P1. The beams and panels were excited by hammer impact at 11 and 15 points, respectively, regularly spaced (Figures 2.7 and 2.8). Responses at these points were obtained using the reciprocity theorem. The vibration signals of the accelerometer were recorded by LMS SCADAS XS hardware and the frequency response functions (FRFs) were calculated by LMS Test Lab software (LMS International (2017)). A calibration step has been done before each test and the parameters of vibration measurement were automatically calculated and suggested by the software based on the frequency range of interest.

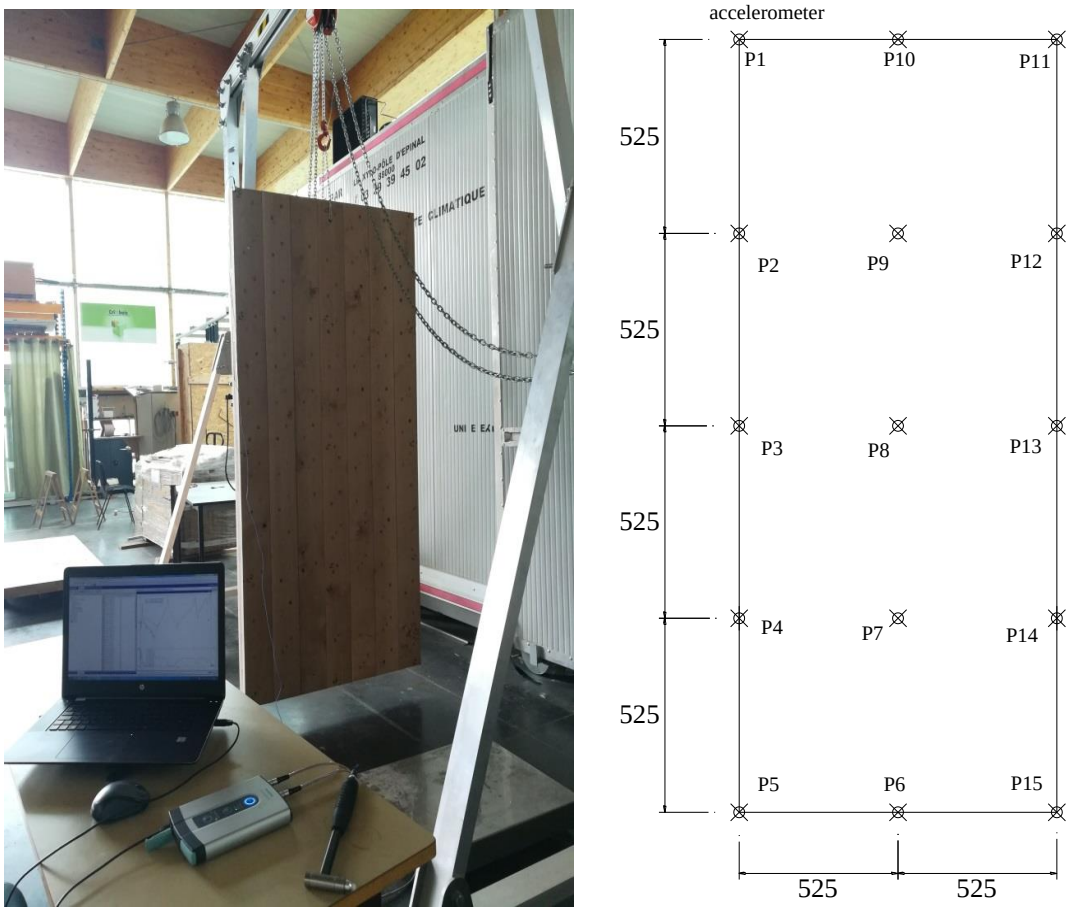

Figure 2.8: Experimental set-up of AFCLT panels under free – free conditions

2.2.2 Moisture content condition

Moisture content has significant effect on mechanical behavior of wood (Gülzow *et al.* (2011); Ido *et al.* (2013); Silva *et al.* (2012)). Therefore, all single layer beams, AFLB and AFCLT panels were tested at 9% moisture content corresponding to the ambient environment (temperature and relative humidity) at the LERMAB laboratory at time of testing. However, taking into account the effect of moisture content on vibrational characteristic of AFLB seems relevant and necessary. The influence of moisture content on frequencies of a single layer beam, a glued beam and an AFLB is presented in Section 2.5.3.

2.2.3 Repeatability test

Repeatability tests were conducted on beams and AFCLT panel systems prior to the modal analysis in order to check the measurement uncertainty. Figures 2.9 and 2.10 show examples of FRF for both AFLB and AFCLT panel which were subjected to two series of hammer impacts. Each series of test contains five hammer impacts for which a mean FRF is calculated.

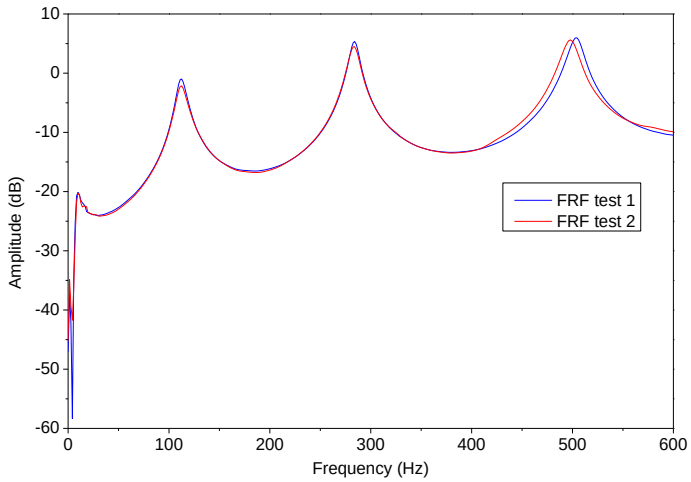

Figure 2.9: FRFs at point P11 of one AFLB - repeatability test

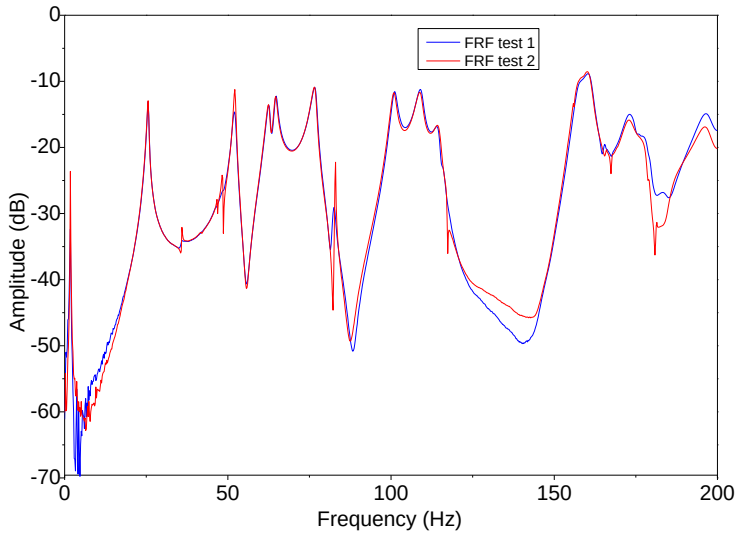

Figure 2.10: FRFs at point P5 of one AFCLT panel - repeatability test

Each curve displayed in Figures 2.9 and 2.10 represents the mean FRFs for both the AFLB and AFCLT panel respectively. It can be seen that the mean FRFs for the two series of impacts are close to each other in both cases. Therefore it can be concluded that the measurement uncertainty is negligible. It proves that results obtained from experiments are stable and reliable.

2.3 Characteristic of wood material

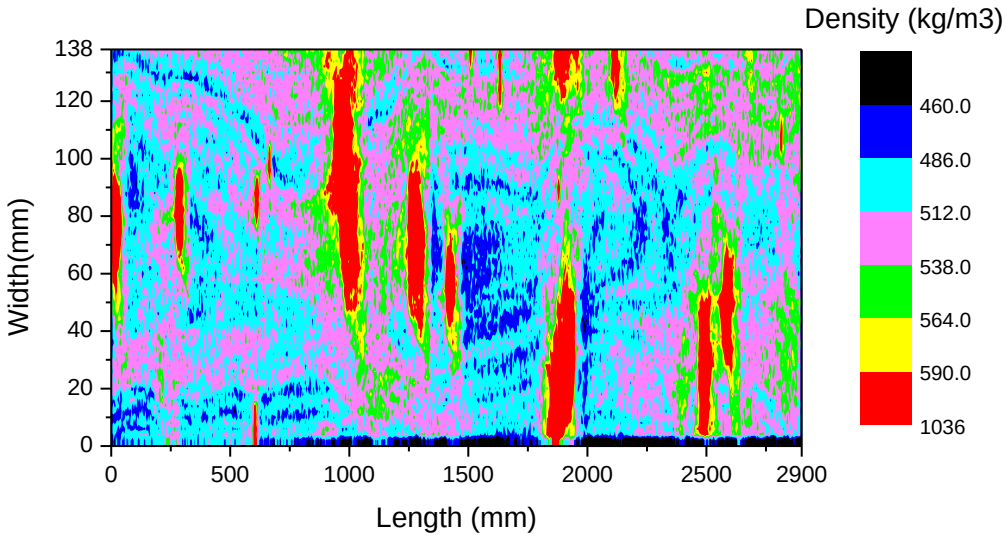

Figure 2.11: Density distribution of a Douglas timber board

Figure 2.11 shows the density distribution of a Douglas timber board, with dimensions: 2900 mm x 138 mm x 30 mm, obtained by X-ray (Viguier *et al.* (2017)). It can be observed that the density distribution of wood is not uniform but like a random field. In particular, the density at the knots is very high, indicated by red colour. However, in the first step, the mechanical properties of wood are assumed to be homogeneous. The effect of this assumption on natural frequencies of the timber board is discussed in Chapter 3.

2.4 Single layer beams

Sixteen oak and sixteen spruce single layer beams were analyzed to evaluate the mechanical properties as well as their variability level. The results were used for numerical study of dynamic properties as well as variability of the AFLB and the AFCLT panel (Chapters 3 and 4). All single layer beams were tested at 9% moisture content using the hammer impact excitation system. Their dimensions are 70 mm width, 22.5 mm thickness and 1450 mm length.

The FRFs at an edge point of the oak and spruce single layer beams are depicted in Figures 2.12 and 2.13 respectively, where variability is clearly visible.

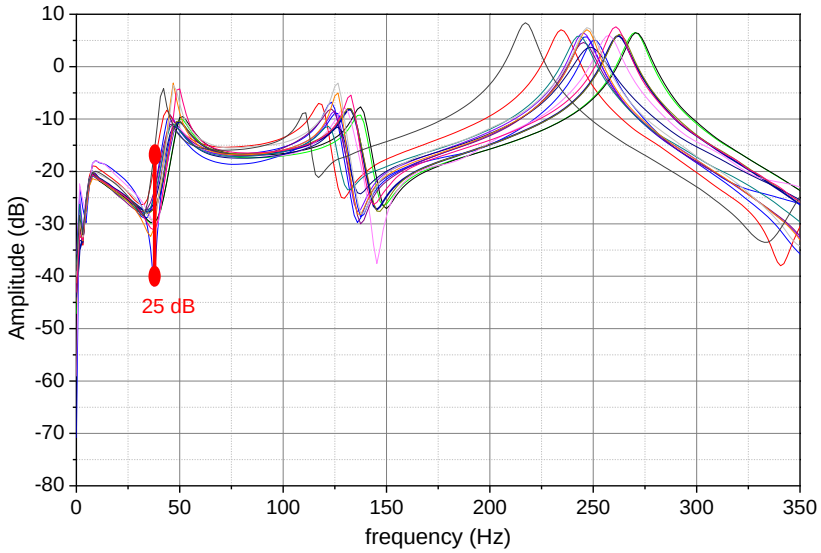

Figure 2.12: FRFs at point P4 for 16 single layer oak beams

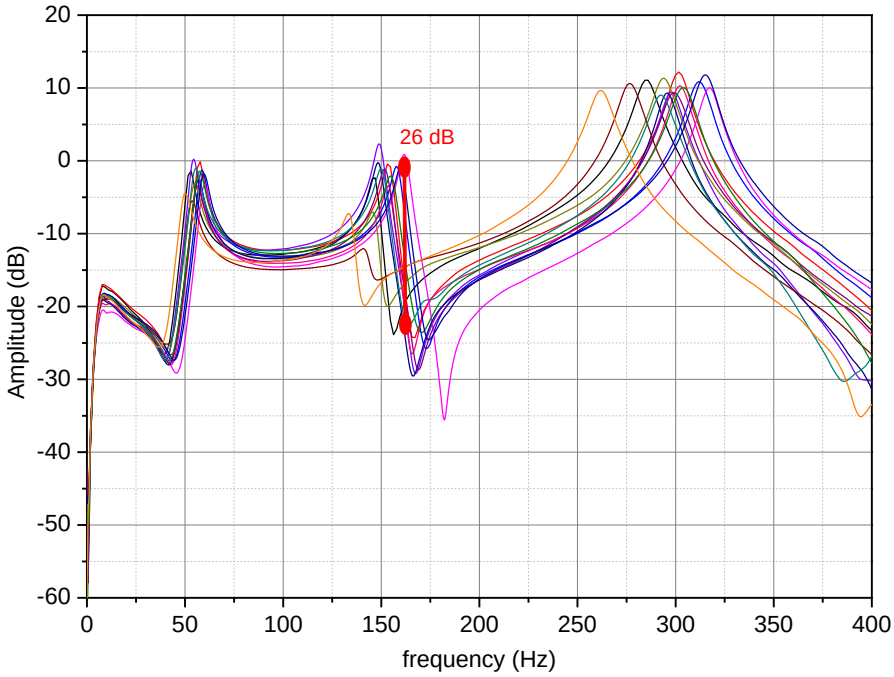

Figure 2.13: FRFs at point P4 for 16 single layer spruce beams

The recorded experimental modal shapes obtained for the first three frequencies are displayed in Figure 2.14.

Figure 2.14: Experimental modal shapes for the single layer beams

The frequency values as well as their corresponding variability for the oak and spruce single layer beams are summarized in Table 2.1. The mean values of frequencies and damping of the spruce beams are higher than that of the oak beams. However, the variability of dynamic property of the spruce beams is high while the variability of the oak beams is relatively moderate.

		Spruce		Oak	
		Mean	CoV	Mean	CoV
Mode 1	frequency (Hz)	54.2	7.9%	46.5	4.8%
	damping (%)	4.3	11.3%	3.7	8.1%
Mode 2	frequency (Hz)	147.4	8.4%	127.8	5.2%
	damping (%)	2.0	12.8%	1.9	7.2%
Mode 3	frequency (Hz)	288.6	8.8%	250.4	5.1%
	damping (%)	2.1	13.3%	1.8	10.3%

Table 2.1: Dynamic properties and corresponding variability for the oak and spruce single layer beams

Single layer beams obey to the thin beam theory because the ratio of their thickness to length is less than 1/20. They were weighed to calculate the density. It was assumed that the mechanical properties of beams are homogeneous. Therefore, the longitudinal Young modulus of each single layer beam was extracted from the analytical expression of the frequencies according to the classical thin beam theory:

$$f_n = \frac{a_n}{2\pi L^2}\sqrt{\frac{EI}{A\rho}} \tag{2.2}$$

where: $a_1 = \left(\frac{3\pi}{2}\right)^2 ; a_2 = \left(\frac{5\pi}{2}\right)^2 ; a_3 = \left(\frac{7\pi}{2}\right)^2$

I is the second moment of inertia, ρ is the mass density, A and L are the section area and the length of the specimen, respectively. Theoretically the elastic modulus can be calculated from the frequency and the corresponding a_n for the mode of interest. Figure 2.15 shows that the three values of the mean elastic modulus calculated based on the first three vibration modes are close, this is a hopeful and consistent result.

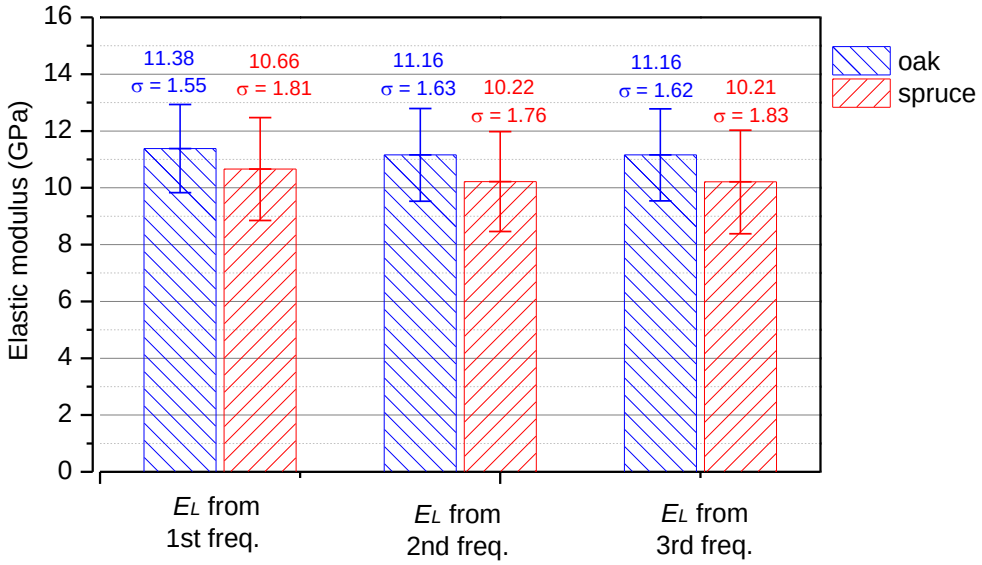

Figure 2.15: Average longitudinal elastic modulus and standard deviation (σ) for the first three vibration modes

The density and the longitudinal elastic modulus calculated from the first frequency as well as the corresponding variability level for the oak and spruce single layer beams, are summarized in Table 2.2. Although the elastic modulus of spruce is smaller than that of oak, the frequency values for the spruce beams are slightly higher as compared to those for oak beams (Table 2.1). The main reason is the ratio E_L/ρ which is smaller in the case of the oak beams. It can be seen also from the Table 2.2 that the variability level of the density of oak and spruce layers is moderate, while that of the elastic modulus of layers is high.

Species		Min	Max	**Mean**	CoV
Oak	E_L (GPa)	7.94	13.97	**11.38**	13.6%
	ρ (kg/m^3)	543.8	671.3	**623.9**	6.5%
Spruce	E_L (GPa)	7.23	14.59	**10.66**	17.0%
	ρ (kg/m^3)	379.2	490.4	**429.9**	6.9%

Table 2.2: Longitudinal elastic modulus and density for single layer beams

2.5 Three-layer AFLBs

This section presents an experiment campaign with 6 three-layer glued beams and 28 three-layer AFLBs including different types for comparison purpose. Table 2.3 summarizes the different constructed and tested beams. The comparison of frequencies and damping ratio among different AFLB types shows the role of parameters such as material of layers, material and number of dowels in dynamic characteristics of AFLB. It is useful to optimize the design of adhesive free timber structures and thus reduce the number of AFCLT panel specimens for experiment.

	Number and type of dowels	Quantity
Material of layer: oak	13 normal oak dowels (NODs)	3 beams
	13 compressed spruce dowels (CSDs)	3 beams
	27 NODs	5 beams
	27 CSDs	5 beams
	Glued beam (for comparison)	3 beams
Material of layer: spruce	13 NODs	3 beams
	13 CSDs	3 beams
	27 NODs	3 beams
	27 CSDs	3 beams
	Glued beam (for comparison)	3 beams

Table 2.3: Quantity of three-layer beams

2.5.1 Effect of compressed wood dowels

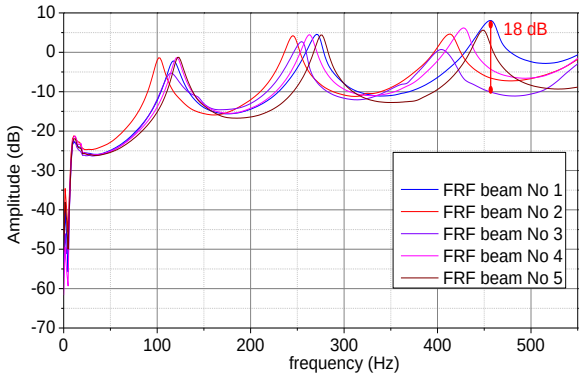

(a) Oak AFLB assembled by 27 NODs

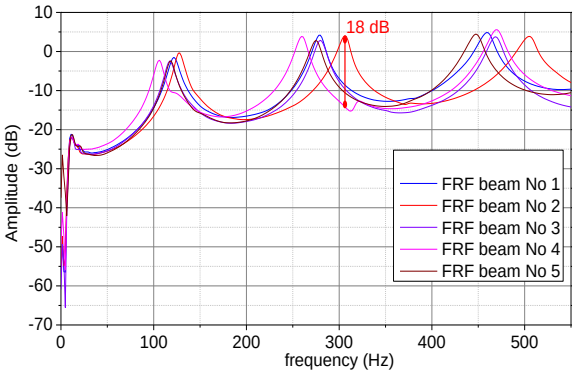

(b) Oak AFLB assembled by 27 CSDs

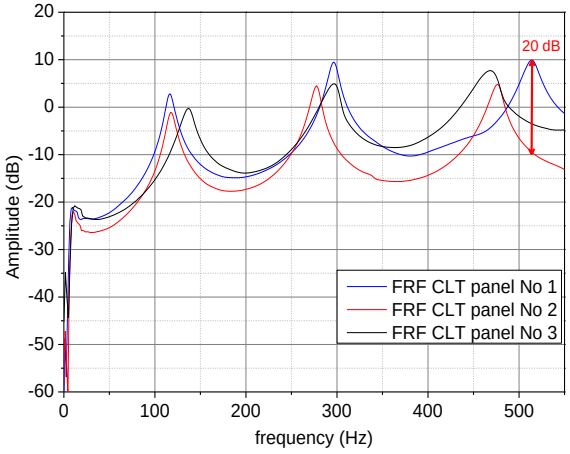

(c) Spruce AFLB assembled by 27 NODs

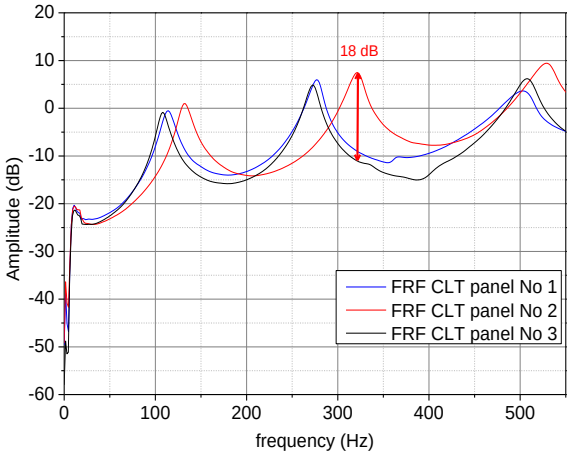

(d) Spruce AFLB assembled by 27 CSDs

Figure 2.16: FRFs at point P11 for the AFLB assembled using 27 dowels

Figure 2.16 shows FRFs at an end point for four different types of three-layer AFLBs assembled using 27 dowels. All beams were tested at 9% moisture content. As for the single layer beams, the variability level of the vibrational response of all AFLB types is significant. The

recorded experimental modal shapes obtained for the first three frequencies of the AFLBs are similar with the modal shapes of the single layer beams, which are displayed in Figure 2.14.

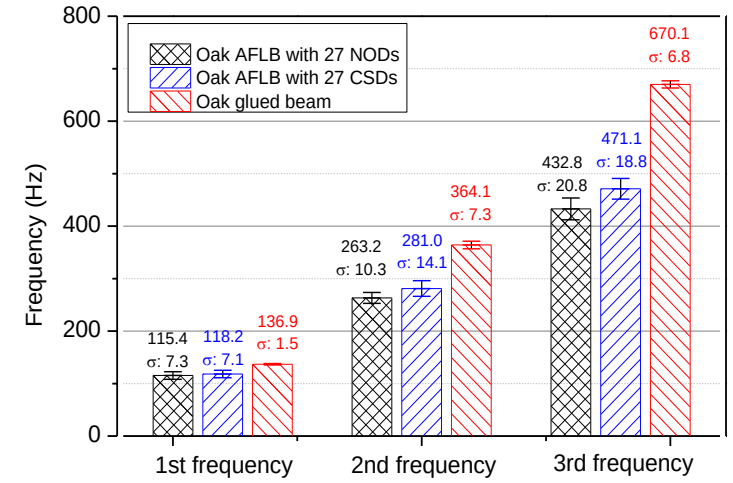

(a) Oak three-layer beams

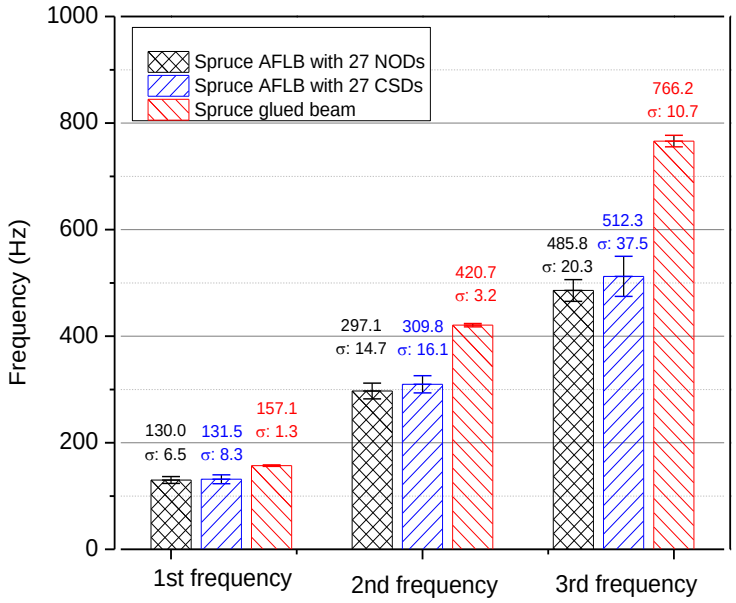

(b) Spruce three-layer beams

Figure 2.17: Comparison of average frequency and corresponding standard deviation (σ) for the AFLBs and the glued beam

Figure 2.17 compares the average vibration frequencies and corresponding standard deviation for the glued three-layer beams and the three-layer AFLBs connected by either 27 NODs or 27 CSDs. Three layers of the beams are either made of oak or spruce timber. It can be observed in both beam groups that CSDs improve the frequencies of the AFLB. It is logical because mechanical properties of CSD are higher than the values of NOD and in turn then lead to better interlayer stiffness. Moreover, the first frequency value exhibited by the AFLB connected by 27 CSDs is nearly the same as that of the glued beam. However, the difference seems to increase for higher frequencies. This phenomenon can be explained by the fact that

the shear stiffness of the AFLB is smaller than that of the glued beam. The shear stiffness of beam has a small effect on the first frequency but significant effects on the high frequencies. This phenomenon will be discussed in subsection 3.3.4. It is worth noting that the Eurocode 5 (European Committee for Standardization (2004)) requirement only concerns the first frequency of vibration.

On the other hand, the variability of both types of the AFLB is quite similar and it is higher than the variability of the glued beam. It means that dowel connection increases the variability of the AFLB.

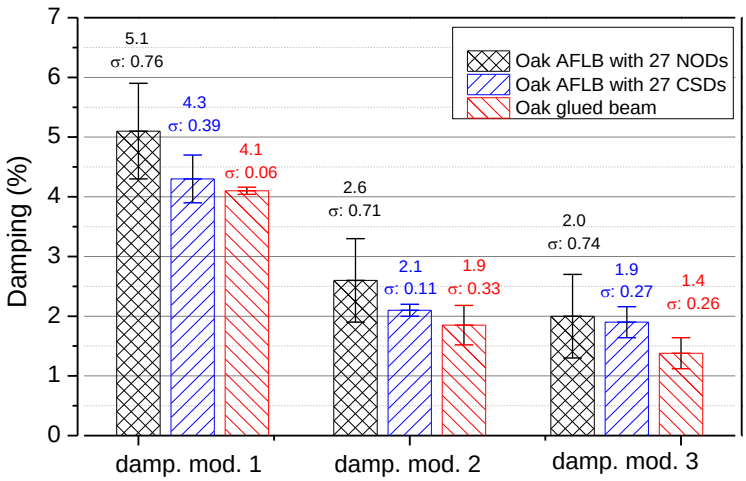

a) Oak three-layer beams

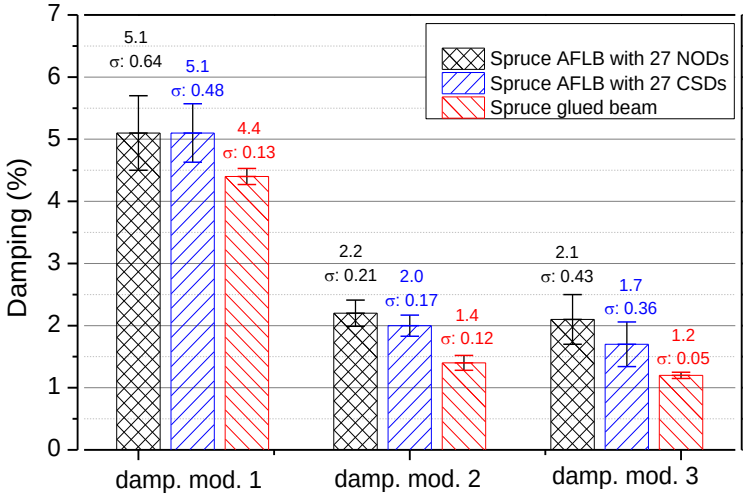

b) Spruce three-layer beams

Figure 2.18: Comparison of average damping and corresponding standard deviation (σ) for the AFLBs and the glued beam

The damping and corresponding standard deviation of the AFLBs and the glued beams are shown in the Figure 2.18. The mean value of damping ratio of the AFLBs is higher than the

value of the glued beam. However, the variability of the AFLBs is also higher than the variability of the glued beam.

2.5.2 Effect of the number of dowels

Figure 2.19 compares the mean value of frequencies and corresponding standard deviation between the AFLB connected by 13 CSDs and the AFLB connected by 27 CSDs. All the AFLBs were tested at 9% moisture content. For both oak and spruce AFLBs, the frequencies of the AFLB increase when the number of dowels increases.

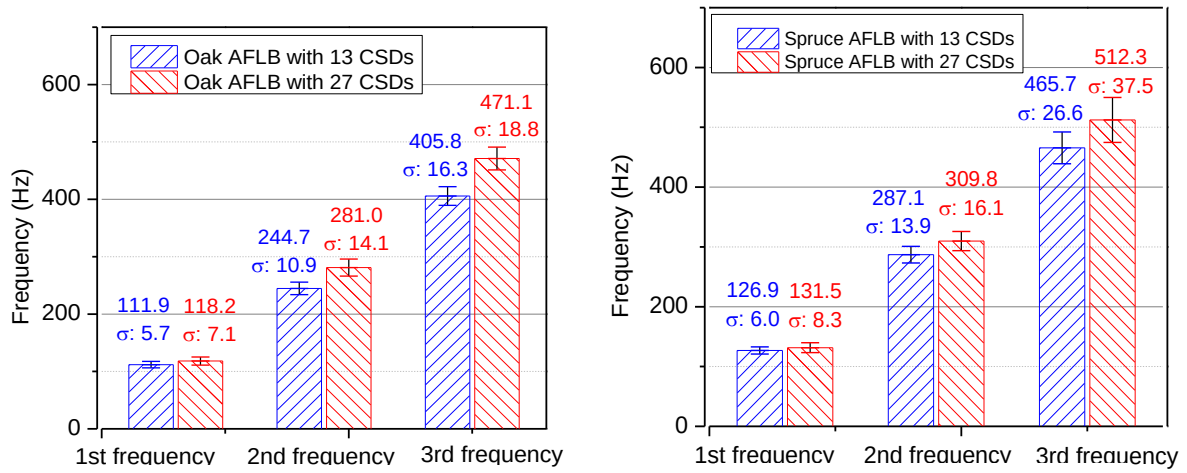

a) Oak three-layer AFLBs b) Spruce three-layer AFLBs

Figure 2.19: Comparison of average frequency and corresponding standard deviation (σ) for the AFLBs connected by 13 or 27 CSDs

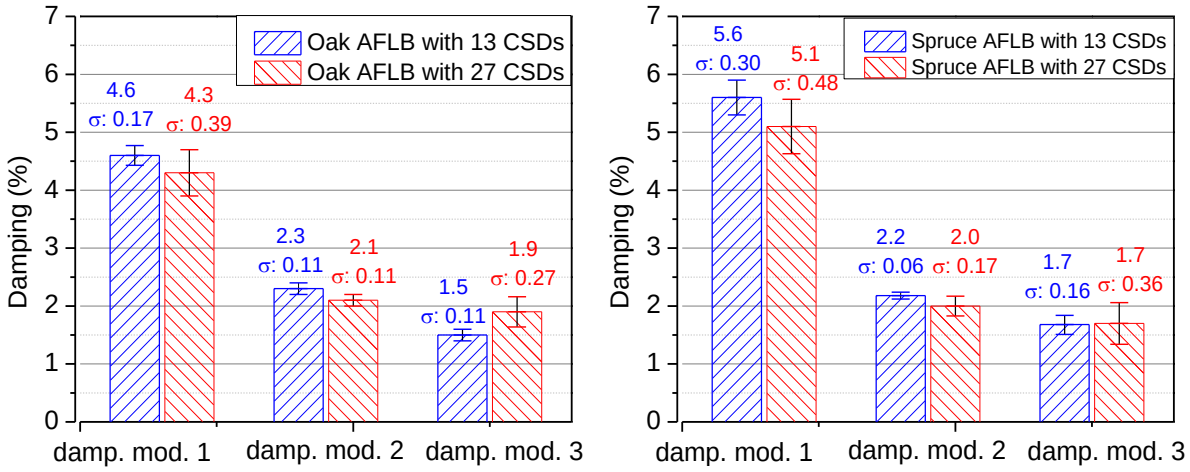

a) Oak three-layer AFLBs b) Spruce three-layer AFLBs

Figure 2.20: Comparison of average damping and corresponding standard deviation (σ) for the AFLBs connected by 13 or 27 CSDs

Figure 2.20 shows that the damping ratio of the AFLB connected by 13 CSDs is slightly higher than the value of the AFLB connected by 27 CSDs. However, this difference is not

significant because of the high variability level of the AFLBs, and therefore, it is not easy to draw a clear conclusion.

Table 2.4 summarizes the dynamic characteristics and their corresponding variability for the AFLB specimens. The variability of frequencies of four different AFLB types are quite similar. However, the variability of damping ratio of the AFLB assembled by 27 CSDs is higher than that of the AFLB assembled by 13 CSDs.

		Oak three-layer AFLB				Spruce three-layer AFLB			
		13 dowels		27 dowels		13 dowels		27 dowels	
		Mean	CoV(%)	Mean	CoV(%)	Mean	CoV(%)	Mean	CoV(%)
Mass (kg)		4.6	**9.0**	4.6	**6.7**	3.2	**8.1**	3.1	**2.4**
Mode 1	frequency (Hz)	111.9	**5.1**	118.2	**6.0**	126.9	**4.7**	131.5	**6.3**
	damping (%)	4.6	**3.7**	4.3	**9.0**	5.6	**5.4**	5.1	**9.4**
Mode 2	frequency (Hz)	244.7	**4.5**	281.0	**5.3**	287.1	**4.8**	309.8	**5.2**
	damping (%)	2.3	**4.8**	2.1	**4.6**	2.2	**2.7**	2.0	**8.5**
Mode 3	frequency (Hz)	405.8	**4.0**	471.1	**4.2**	465.7	**5.7**	512.3	**7.3**
	damping (%)	1.5	**7.3**	1.9	**13.7**	1.7	**9.4**	1.7	**21.2**

Table 2.4: Dynamic properties and corresponding variability for the AFLB assembled using CSDs

2.5.3 Effect of moisture content

From the sections 2.5.1 and 2.5.2, we can see that the variability of the AFLBs is significant. It derives from high variability level of the elasticity properties and the density of timber material. On the other hand, the environmental conditions (in particular the moisture content) can also greatly affect the elastic properties of the timber layer as well their density values (Silva *et al.* (2012)), which in turn may induce large variability. This is referred to as "intra variability". In this section, we therefore measured the frequencies of a single layer beam, a glued beam as well as one specimen beam for each type of AFLB at several moisture contents.

To study the effect of the moisture variation on the vibration frequencies of beams, several moisture contents were considered: 9%, 12%, 15% and 18%, which are the possible limits of moisture content of timber structure in reality (Fragiacomo *et al.* (2011)). The beams were stored in a humidity control room for one week. Then they were weighed, and their moisture content was tested by a moisture meter (Figure 2.21).

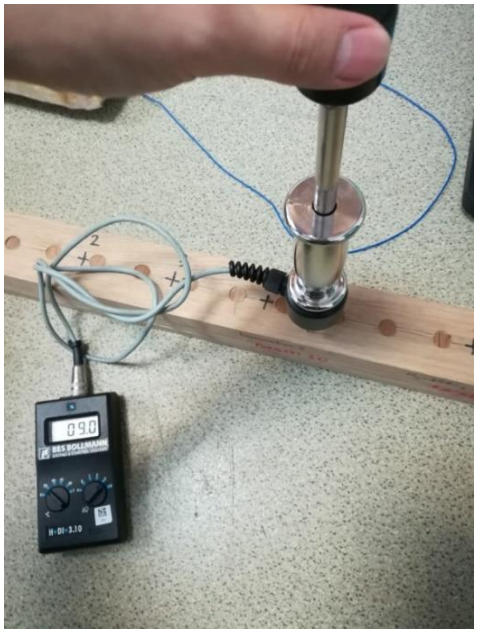

Figure 2.21: Measurement of moisture content of a beam using the H-DI 3.10K moisture meter

To understand the effect of moisture content on wood material, the frequencies of a single layer beam were first measured for each moisture content level; results are displayed in Figure 2.22. In addition to experimental measurements, the theoretical relation (equation 2.2) was used to calculate the frequencies as a function of the moisture content, where the elastic modulus and the mass were updated using equations 2.3 and 2.4, respectively.

$$\frac{E_{12}}{E_H} = \left(1 + \frac{1.5(H-12)}{100}\right) \tag{2.3}$$

$$M_H = M_{12}\frac{1+H}{1+12\%} \tag{2.4}$$

where E_{12} and M_{12} are the values of the modulus of elasticity and the mass at 12% moisture content, respectively. E_H and M_H are the values of the modulus of elasticity and the mass at moisture content level *H*%, respectively. It can be observed a fairly good agreement between the experimental measurements and the theoretically predicted frequencies. All the first three frequencies decrease linearly when the moisture content increases due to the decrease of the ratio *E*/*M*, which is the main source of variability (see equation 2.2). It is worth noting that identical results were obtained in the case of similar conventional glued three-layer beams (Figure 2.23).

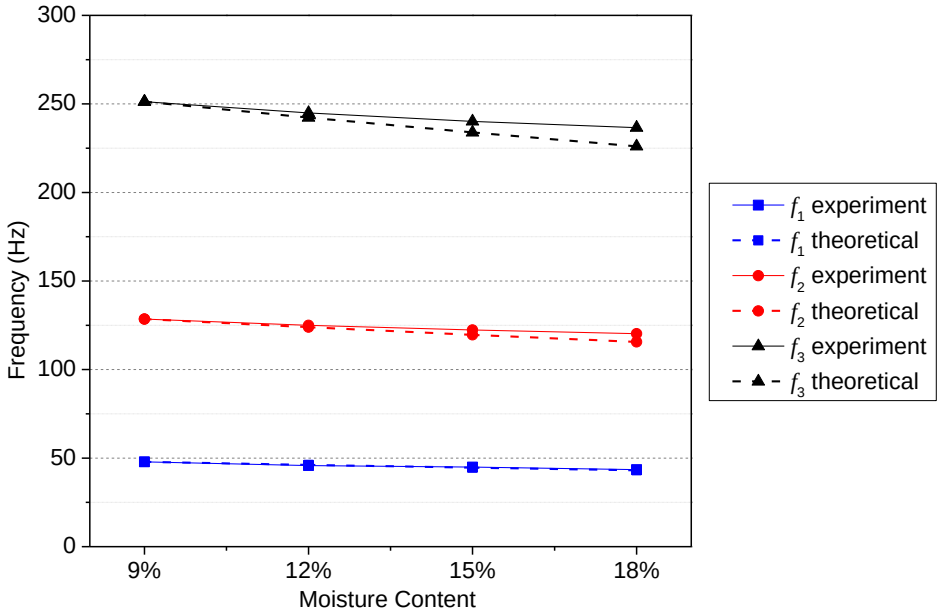

Figure 2.22: Effect of moisture content on frequencies for the single layer beam

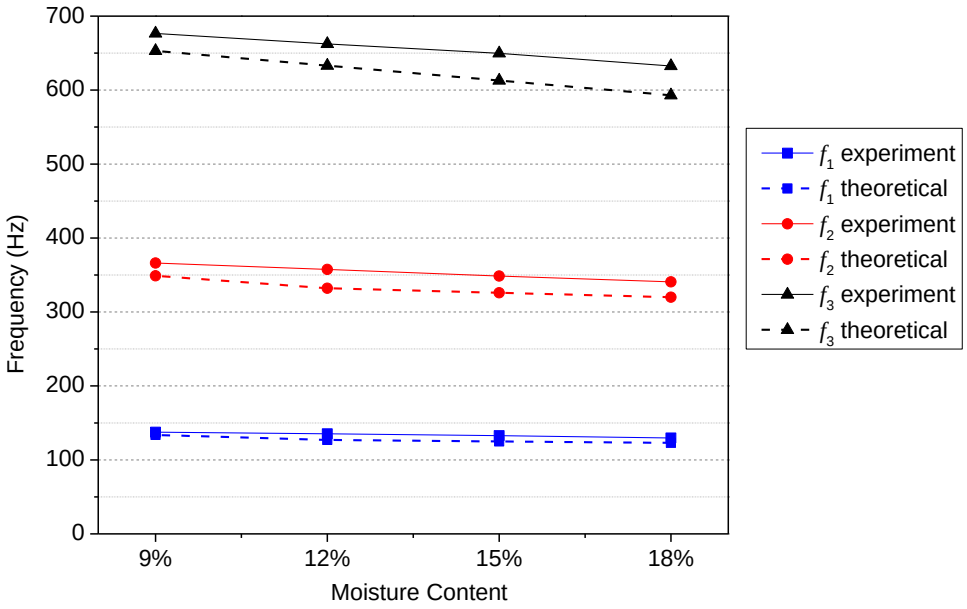

Figure 2.23: Effect of moisture content on frequencies for the glued beam

Figure 2.24 shows the evolution of the first three frequencies of the three-layer AFLB assembled either using NODs or CSDs, as a function of moisture content. The beams were subjected to two cycles of humidity variation. As in the case of the single layer beam, the moisture content varies between 9% and 18% for each cycle. A first observation is that intra variability of the dowelled three-layer beams is relatively high by comparison to that observed in the case of the single layer beam. Both dowelled three-layer beams show nonlinear variation of the frequencies when subjected to an increase of the moisture content. The first three frequencies of three-layer AFLBs, assembled using NOD or CSD, exhibit an increase up to about 15% moisture content followed by a decrease between 15% and 18% moisture

content. This phenomenon can be explained by the fact that in the case of AFLB there are two main sources of variability acting concurrently during the moisture increase. The first source is the ratio *E*/*M* and the former one is the moisture-dependent swelling of compressed wood dowels which improves the tight fitting of the connections when moisture content increases.

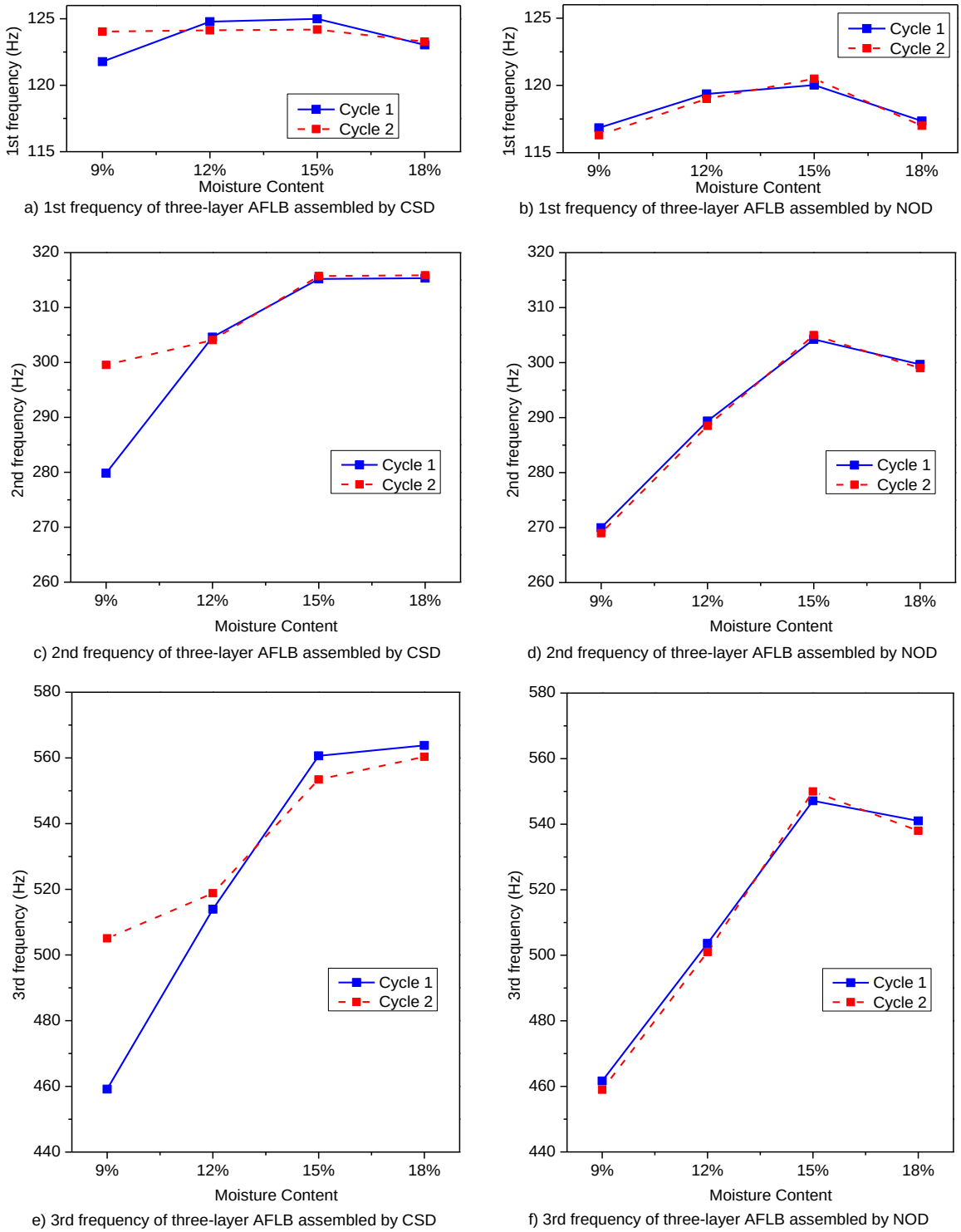

Figure 2.24: Effect of moisture content on the first three frequencies of the AFLB

Moreover, another phenomenon is observed. The results for the three-layer AFLBs assembled using NOD seem to be independent on the number of humidity cycles, while for the three-layer AFLBs assembled using CSD the first frequency significantly increases during the second cycle of humidity. In fact, in the case of virgin wood (uncompressed), the moisture-dependent swelling is reversible during the dry process, while in the case of compressed wood the moisture-dependent swelling presents reversible and irreversible parts (Blomberg (2006)), leading to a permanent swelling (also known as shape memory effect) which in turn leads to a better and permanent tight fitting of the assemblies. CSD improves the performance of connections but also reduce the intra variability.

2.6 AFCLT panels

To assess the vibrational performance of adhesive free timber floor system, ten AFCLT panels were manufactured and tested. The AFCLT panel includes three plies with dimensions of 75 mm x 1050 mm x 2100 mm, assembled through 196 CSDs (Figure 2.6a). There are five panels with grooves (namely groove panel) and five panels without grooves (namely normal panel) (Figure 2.6b). Comparison the dynamic property of the two types of panels shows the effect of grooves and it is useful for design optimization of AFCLT panel. The AFCLT panels are smaller than real timber floor to save material and manufacture time. Therefore, the experimental results of AFCLT panels cannot confirm that the vibrational characteristics of the adhesive free timber floor meet the requirements of Eurocode 5. However, it is useful to validate the finite element model of AFCLT panel. The finite element model then can be used to predict the vibrational performance of AFCLT floor with real dimensions.

The FRFs at an end point of two types of AFCLT panels are depicted in Figure 2.25, showing high variability level of the vibrational response. All panels were tested at 9% moisture content.

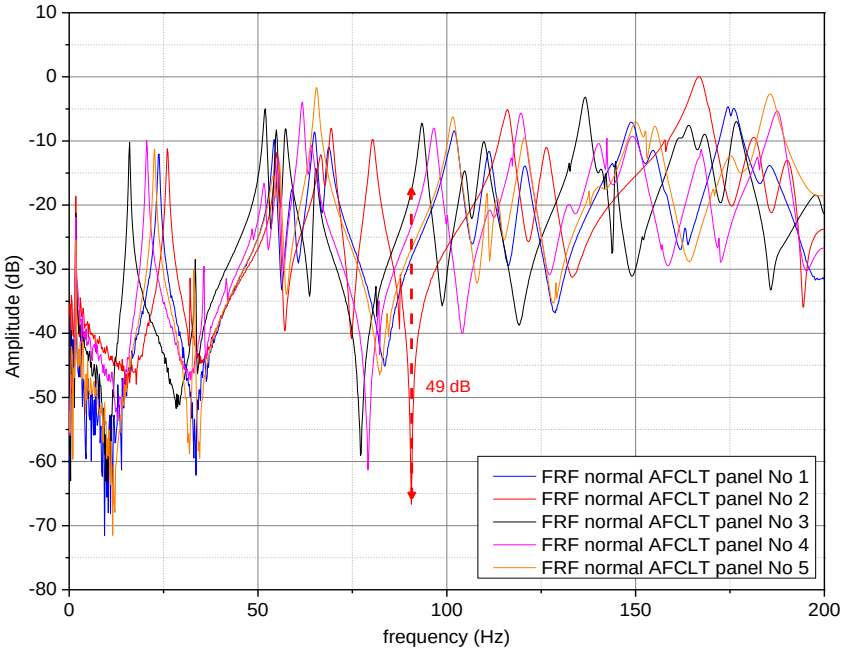

(a) Normal panels

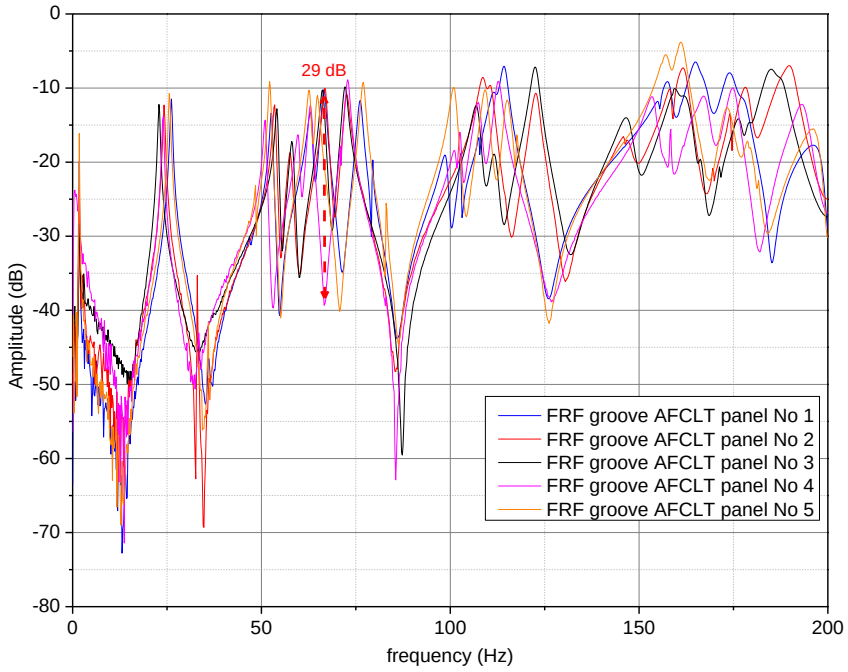

(b) Groove panels

Figure 2.25: FRFs at point P15 for the AFCLT panels

Mode	3D view	Longitudinal view	Width view
(1,1)	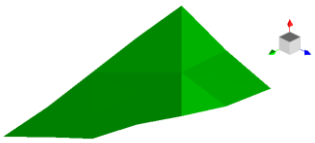		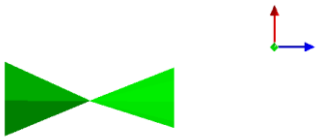
(2,0)	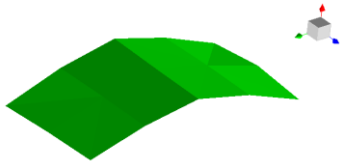	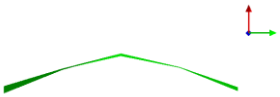	
(0,2)	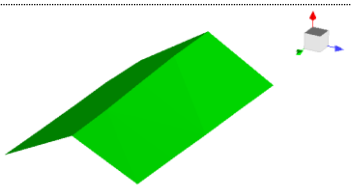		
(2,1)	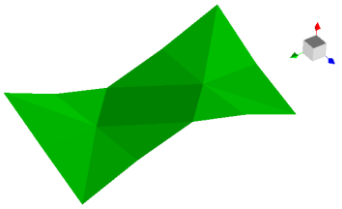		
(1,2)	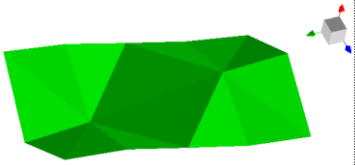		
(2,2)			
(3,0)	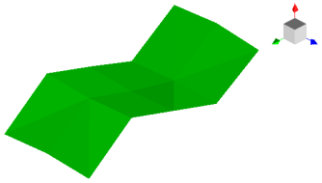	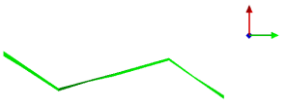	
(3,1)	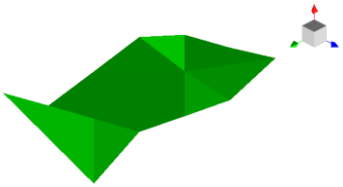	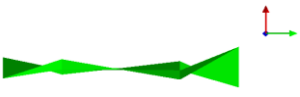	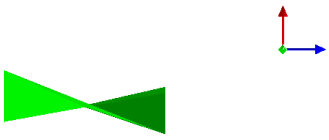
(3,2)	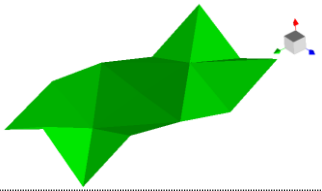	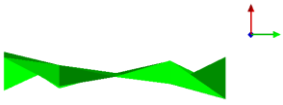	

Table 2.5: Experimental modal shapes for the AFCLT panels

Table 2.5 summarizes the first nine experimental modal shapes of the AFCLT panels. The modes are named Mode (*m*,*n*) where *m* and *n* are the number of node line according to the length and width directions. It is worth noting that the first mode is the twisting mode, instead of bending mode. This is due to the free-free vibration conditions.

Figure 2.26 displays the vibration frequency values for the two types of panels. It can be seen that the frequency values measured for the normal panels are almost identical to those measured for the groove panels. It is worth noting that the first fundamental frequency value is about 22 Hz and corresponds to the twisting mode. In the case of real floor system supported, at least, on two sides, the serviceability vibrational performance of the panels should be assessed with regard to the bending vibration mode. In free-free conditions, the first bending mode corresponds to the second mode (mode (2,0)).

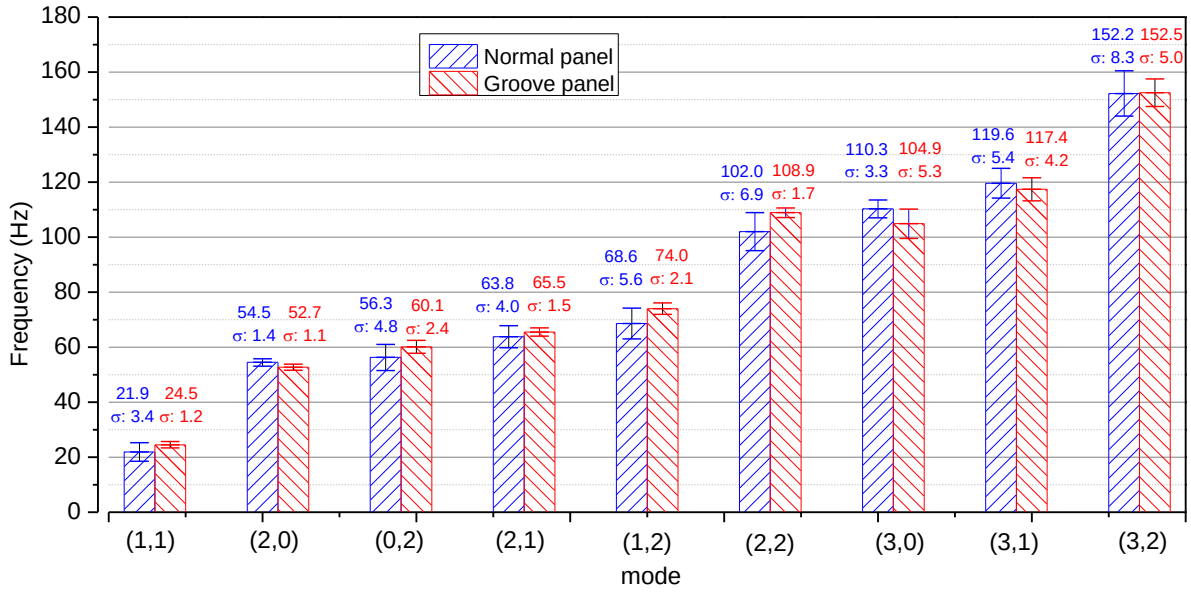

Figure 2.26: Comparison of average frequencies and standard deviation (σ) between normal panel and groove panel

As for the frequencies, Figure 2.27 shows that damping ratio values measured for the normal panels are almost identical to those measured for the groove panels. The damping ratios of AFCLT panels are significantly lower than the values of AFLBs (section 2.5) because of the supporting condition (Figure 2.7). However, this difference is not relevant since the aim of this study is not focused on the comparison between the AFLB and the AFCLT panel.

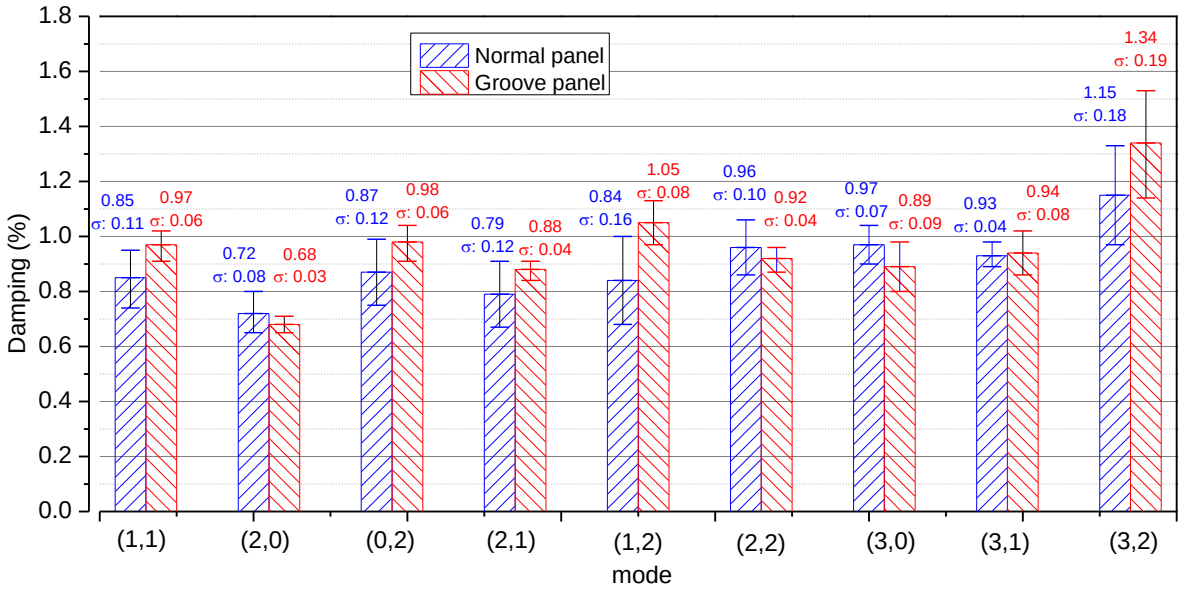

Figure 2.27: Comparison of average viscous damping ratio and standard deviation (σ) between normal panel and groove panel

		Normal panel		Groove panel	
		Mean	CoV(%)	Mean	CoV(%)
Mass (kg)		119.6	**2.2**	117.4	**0.7**
Mode (1,1)	frequency (Hz)	21.9	**15.6**	24.5	**4.8**
	damping (%)	0.85	**12.5**	0.97	**5.8**
Mode (2,0)	frequency (Hz)	54.5	**2.5**	52.7	**2.0**
	damping (%)	0.72	**10.8**	0.68	**4.5**
Mode (0,2)	frequency (Hz)	56.3	**8.5**	60.1	**4.0**
	damping (%)	0.87	**13.7**	0.98	**6.5**
Mode (2,1)	frequency (Hz)	63.8	**6.3**	65.5	**2.2**
	damping (%)	0.79	**14.6**	0.88	**4.2**
Mode (1,2)	frequency (Hz)	68.6	**8.2**	74.0	**2.8**
	damping (%)	0.84	**19.3**	1.05	**7.6**
Mode (2,2)	frequency (Hz)	102.0	**6.8**	108.9	**1.6**
	damping (%)	0.96	**10.9**	0.92	**4.7**
Mode (3,0)	frequency (Hz)	110.3	**3.0**	104.9	**5.1**
	damping (%)	0.97	**6.9**	0.89	**10.2**
Mode (3,1)	frequency (Hz)	119.6	**4.5**	117.4	**3.6**
	damping (%)	0.93	**4.6**	0.94	**8.5**
Mode (3,2)	frequency (Hz)	152.2	**5.4**	152.5	**3.3**
	damping (%)	1.15	**15.5**	1.34	**14.5**

Table 2.6: Dynamic properties and corresponding variability for the AFCLT panels

Table 2.6 summarizes the dynamic characteristics and their corresponding variability for two types of the panels. The variability of frequencies of the groove panels is moderate but the variability of the normal panels is higher. The cause may be the smaller mass variability of the groove panels as compared to that of the normal panels. On the other hand, the variability of damping ratio of both types of panels is high.

2.7 Academic contribution

It is the first time the vibration performance of multilayer timber structures assembled by CSDs has been evaluated by experiment. The experimental results help to increase understanding of the mechanical behaviour of these structures and is necessary for validating finite element model dedicated to these structures. The level of inter and intra variability is investigated, providing a preliminary assessment of the characteristic of these types of structures.

2.8 Conclusion

The vibrational serviceability performance of AFCLT panels and AFLB was experimentally assessed in this chapter. The vibrational characteristics of the single laminations composing the beams and CLT panels were first investigated. The vibrational serviceability performance of AFLB was demonstrated by comparison to their glued counterparts. It was shown that the first vibrational frequency value of the AFLB assembled through 27 CSDs is nearly the same as compared to that exhibited by the glued beams, while the difference seems to increase with the higher frequencies. However, the damping ratio was found to be higher in the case of AFLB. As far as AFCLT panels are concerned, close frequency and damping ratio values were observed for panels with or without grooves.

Variability of natural frequencies and damping ratio has been quantified. The variability level of frequencies is moderate, and the variability level of damping ratios is globally high for the AFLB and AFCLT.

The effect of moisture content on the frequencies of the timber beams (intra-variability) was also assessed. The frequencies of the single layer beams decrease monotonically as the moisture content increases. However, the tendency is significantly different in the case of three-layer beams assembled using wood dowels (NOD or CSD). In this case evolution of frequencies according to the moisture content is much more complicated and leads to high intra variability levels.

In the next chapter, the vibration performance of a realistic flooring system made with AFCLT panel is predicted by finite element method. The predicted results will be discussed with regard to the Eurocode 5 vibrational serviceability design requirements.

Chapter 3:
Finite element models

This chapter develops finite element (FE) models to simulate the vibrational behaviour of single layer beams, adhesive free laminated beams (AFLB) and adhesive free cross-laminated timber panels (AFCLT). Verification and Validation methodology is applied to evaluate and improve the predictive capability of the FE model. After validation with experimental data, the model is used to predict the vibrational behaviour of a realistic flooring system made with AFCLT panel. The predicted results are discussed with regard to the vibrational serviceability design requirements of Eurocode 5. A parametric study is also performed to optimise the design of AFCLT floor and increase its stiffness. Finally, a simplified model is developed to reduce the computational cost.

3.1 Introduction

3.1.1 Existing finite element (FE) models

Mechanical behavior of multilayer timber structures assembled by dowels has been recently a topic of great interest. Models dedicated to those structures have been analyzed and presented in many publications. First, it can be found a simple model in Eurocode 5, called "Gamma-method". According to this model, the effective bending stiffness of three-layer doweled beam can be approximated by the following equation:

$$(EI)_{ef} = \sum_{i=1}^{3} (E_i I_i + \gamma E_i A_i a_i^2) \tag{3.1}$$

where I_i, A_i and E_i are the second moment of inertia, cross-section area and longitudinal elastic modulus of i-layer; a_i is the distance from the center of gravity of the whole cross-section to the center of gravity of i-layer (Figure 3.1). γ_i presents the shear coefficient of the semi-rigid connection and it is given by:

$$\gamma_2 = 1 \tag{3.2}$$

$$\gamma_i = \left(1 + \frac{\pi^2 E_i A_i s}{L^2 K}\right)^{-1} \text{ for } i = 1 \text{ and } i = 3 \tag{3.3}$$

where *s* is the dowel spacing, *L* is the span of beam and *K* is the slip modulus of the semi-rigid connection.

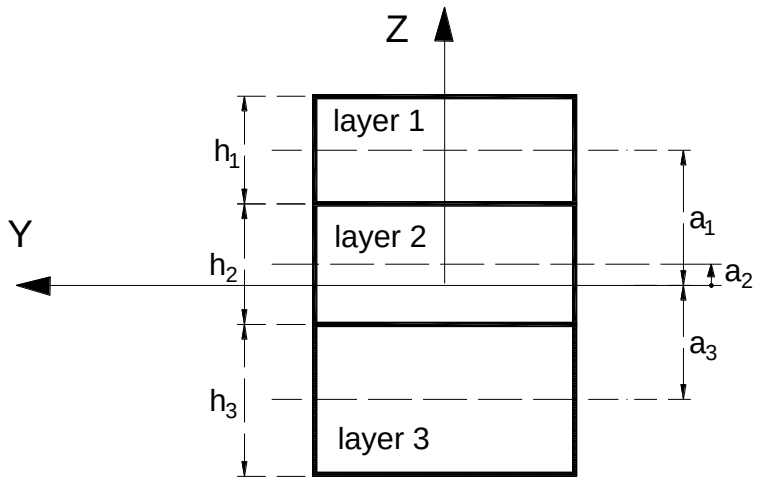

Figure 3.1: Cross-section and parameters of three-layer beam

From the practical point of view, this method is very simple for structural design and requires no major computational costs. Many researchers use this method to study and design the connection system of timber-concrete composite structures (Mascia and Soriano (2004); Premrov and Dobrila (2012); Rijal *et al.* (2015); Jelusic and Kravanja (2017)). However, this

method has some weaknesses. Grosse *et al.* (2003) recommended the maximum distance between two connectors (*s*-parameter) is 3% of the beam's span to ensure the accuracy of this method. Moreover, the slip modulus of dowel (*K*-parameter) can be only obtained from experiments (Van der Linden (1999); Oudjene *et al.* (2017); Dias *et al.* (2018)). When one wants to change a characteristic of dowel such as material, diameter or inclination, one needs the new experimental slip modulus.

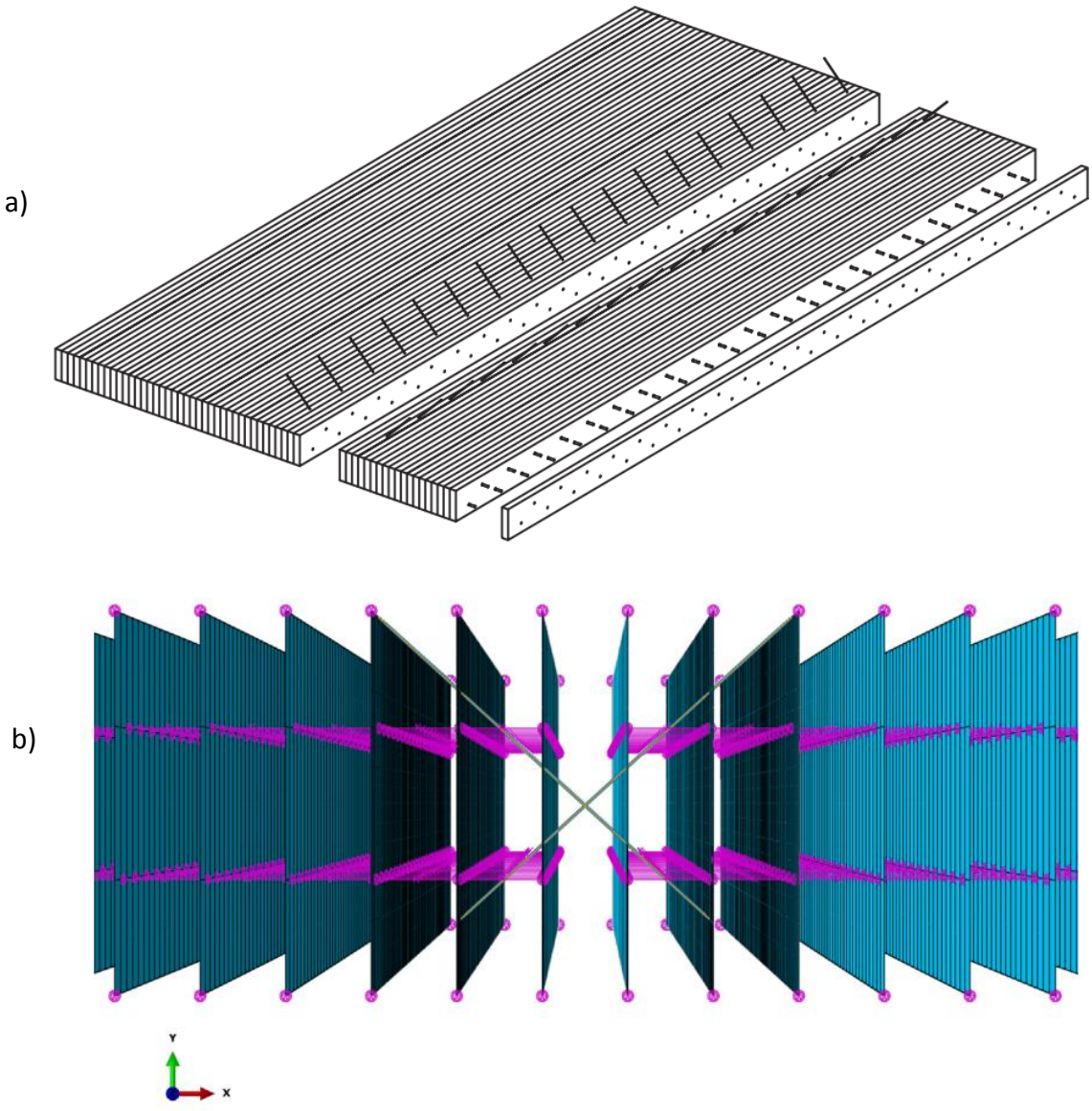

Figure 3.2: Diagram of the dowellam floor (a) and the simplified FE model (b) in Filippoupolitis *et al.* (2017)

Another approach is the FE method with simplified modeling of the dowels. Figure 3.2 shows the diagram of a dowellam timber floor and its FE model to simulate the vibrational behavior of the floor, which was developed in Filippoupolitis *et al.* (2017). In the FE model, timber boards are modeled using shell elements while dowels are modeled using spring

elements, thus significantly reducing the number of degrees of freedom (DOFs) of the model. However, the disadvantage of this method is that the stiffness of the spring element must be determined experimentally. It does not meet our expectations for the FE model, which must be able to predict the mechanical behavior of the structure without requiring too much experimental data.

A 3D FE model was proposed to study bending stress of doweled multilayer timber beam by O'Loinsigh *et al.* (2012b). The advantage of using solid brick elements for dowels and timber layers is the ability to describe more close-to-reality the physical phenomenon. On the other hand, the weakness of the 3D FE model is the high computational cost, in particular in the case of nonlinear analysis. However, the cost is cheaper for linear analysis that is often used to investigate the natural frequencies. Therefore, a 3D FE model is proposed to study the natural frequencies of the AFLB as well as the AFCLT panels.

3.1.2 Verification and Validation methodology

Verification and Validation (V&V) methodology (Scigliano *et al.* (2011); Lardeur *et al.* (2012b)) is applied to evaluate and improve the predictive capability of the FE model. V&V includes two steps as presented in Figure 3.3. Starting from the physical reality observed by experiments, two types of models are identified: a reference mechanical model and finite element models. The reference mechanical model is constructed from mechanical assumptions to properly describe the physical reality. It includes the partial differential equations related to the equilibrium equations, from the constitutive laws and from all the initial or boundary conditions. Appropriate numerical choices lead to the finite element models that will provide the numerical solutions of the given mechanical model.

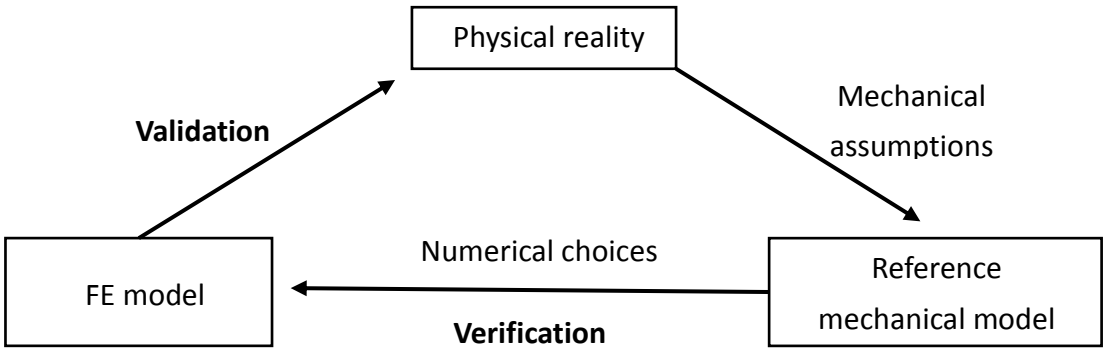

Figure 3.3: Description of the Verification and Validation methodology

The verification stage deals with only numerical aspects. The objective of the verification stage is to compare the highly accurate solution of the reference mechanical model with the numerical solutions determined by FE models. In the best case, the highly accurate solution is exact and comes from analytical developments. In the case of multilayer timber structures

assembled by compressed dowels, analytical solution is not available; therefore, the highly accurate solution is numerically obtained with a fine FE model. The verification process is completed when a satisfactory convergence of the FE model results to the accurate results of the reference mechanical model is achieved.

The validation stage deals with the comparison between the numerical results obtained with the verified FE model and the physical reality. The validation test is satisfactory if the difference between the experimental results and the verified FE model result is considered as acceptable. The verification stage must be the first step of the V&V process, because the numerical and mechanical errors can sometimes compensate each other, giving the impression of correctness.

3.2 FE model for single layer beam

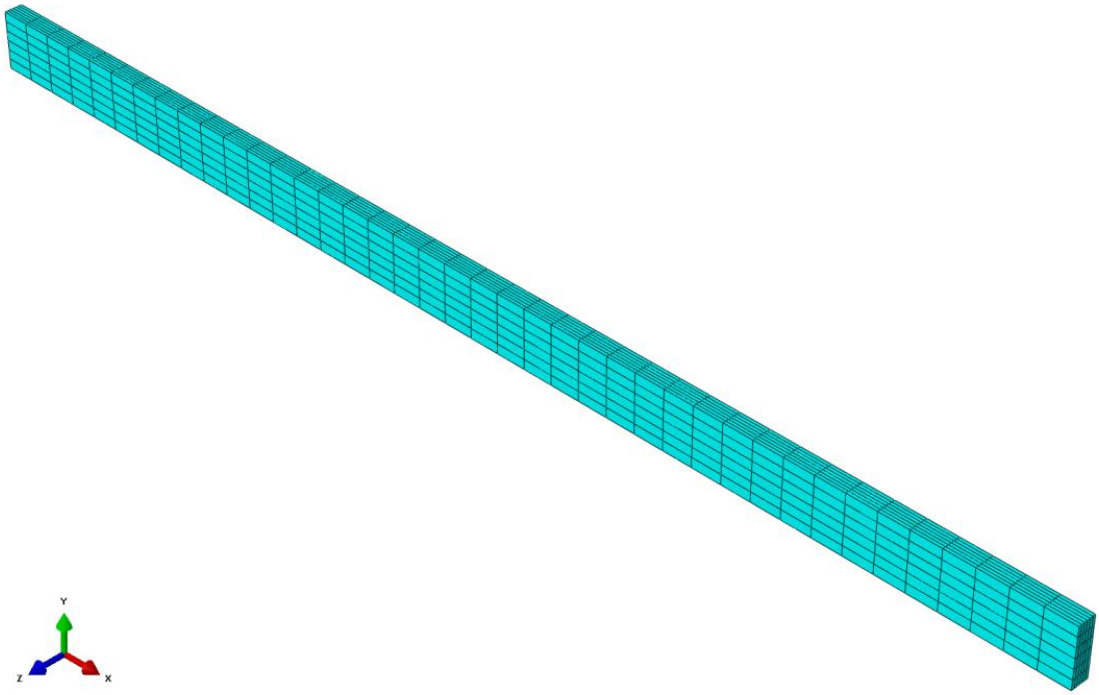

Figure 3.4: Single layer beam FE model

In our study, the FE models are built using Abaqus Standard that provides several formulations for solid elements (Dassault Systèmes Simulia Corp (2014)). Therefore, a FE model for single layer beam is first studied to choose the most appropriate solid element for the timber structures simulation. On the other hand, the mechanical properties of the timber are often considered homogeneous in an industrial or research context, even if this assumption is not exactly met in reality. Therefore, the effect of this assumption on the natural frequencies is assessed here by the FE model of single layer beam. Figure 3.4 shows the FE

model of single layer beam with dimensions: 1.45 m x 0.07 m x 0.0225 m. The L/h ratio is equal to 64, which is the characteristic of a thin beam.

3.2.1 Sensitivity analysis

Due to the uncertainty in mechanical properties of wood, a sensitivity analysis is necessary to know whether the different parameters have a significant influence on the result obtained from the FE model. The sensitivity of the wood properties to natural frequencies for the single layer beam is calculated by the Equation 3.4 and the results are reported in Table 3.1.

$$Sensitivity = \frac{\Delta output(\%)}{\Delta input(\%)} \tag{3.4}$$

	ρ	E_1	E_2	E_3	ν_{12}	ν_{13}	ν_{23}	G_{12}	G_{13}	G_{23}
f_1	-0.495	0.497	0	0	0	0	0	0	0.002	0
f_2	-0.499	0.491	0	0	0	0	0	0	0.008	0
f_3	-0.492	0.478	0	0	0	0	0	0.021	0	0
f_4	-0.496	0.005	0	0	0	0	0	0.431	0.07	0.005
f_5	-0.495	0.482	0	0	0	0	0	0	0.02	0

Table 3.1: Sensitivity of frequencies to material properties of single layer beam

It can be seen in Table 3.1 that E_2, E_3 and Poisson's ratios do not affect frequencies of single layer beam. The effect of G_{12} on torsional vibration mode (4^{th} mode) is significant. However, the role of the shear moduli is negligible compared to the role of E_1 and ρ in the case of bending modes (f_1, f_2, f_3 and f_5) because the single layer beam is thin. The FE model inputs: E_2, E_3, shear moduli and Poisson's ratios are calculated according Jodin (1994) as a function of the density (Table 3.2). The longitudinal elastic modulus and density of material are taken from experimental vibration tests (Section 2.4).

	Oak (hardwood)	Spruce (softwood)
E_2 (MPa)	$1810\left(\frac{\rho}{0.65}\right)^{1.3}$	$1000 + 2370(\rho - 0.45)$
E_3 (MPa)	$1030\left(\frac{\rho}{0.65}\right)^{1.74}$	$636 + 1910(\rho - 0.45)$
v_{12}	$E_1 / 37300\left(\frac{\rho}{0.65}\right)^{0.91}$	$E_1 / 34200 + 117000(\rho - 0.45)$
v_{13}	$E_1 / 31200\left(\frac{\rho}{0.65}\right)^{1.09}$	$E_1 / 30800 + 101000(\rho - 0.45)$
v_{23}	$E_2 / 2680\left(\frac{\rho}{0.65}\right)^{1.41}$	$E_2 / 2050 + 5280(\rho - 0.45)$
G_{12} (MPa)	$1260\left(\frac{\rho}{0.65}\right)^{1.14}$	$861 + 2080(\rho - 0.45)$
G_{13} (MPa)	$971\left(\frac{\rho}{0.65}\right)^{1.26}$	$745 + 989(\rho - 0.45)$
G_{23} (MPa)	$366\left(\frac{\rho}{0.65}\right)^{1.74}$	$83.6 + 228(\rho - 0.45)$

Table 3.2: The relationship between the mechanical properties and the density (unit: g/cm^3) of wood (Jodin (1994))

3.2.2 Verification of the model

Three types of solid element: a eight-node hexahedral solid element with reduced integration (C3D8R), a twenty-node hexahedron solid element with reduced integration (C3D20R) and a twenty-node hexahedral solid element with complete integration (C3D20), which are all suitable for modelling bending effect, are used for the convergence study. The converged frequencies and mode shapes obtained with the three finite element types are similar. Figure 3.5 shows the first five mode shapes.

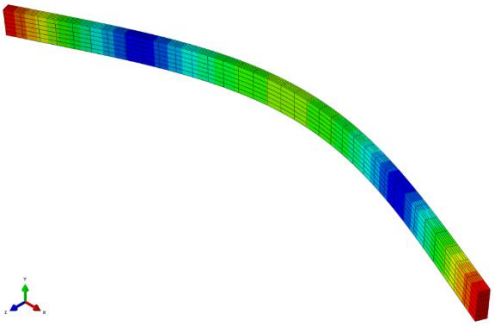

1st mode

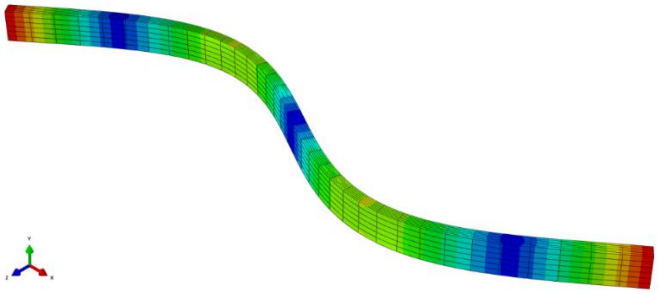

2nd mode

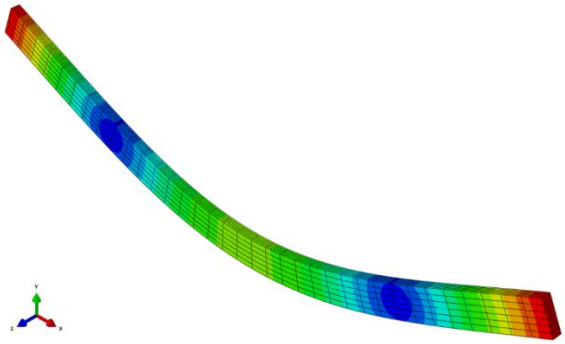

3rd mode

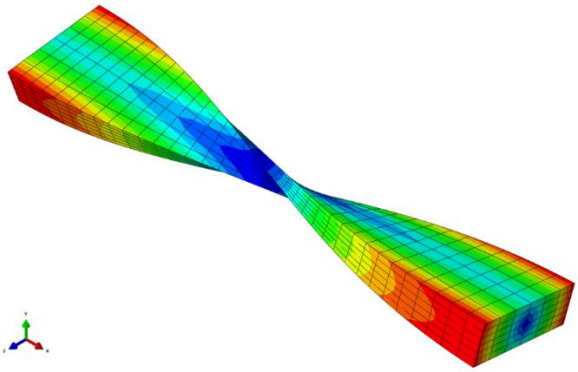

4th mode

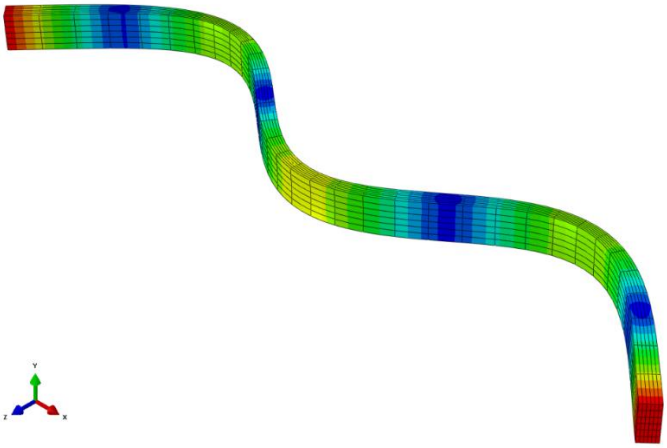

5th mode

Figure 3.5: The first five numerical mode shapes of single layer beam

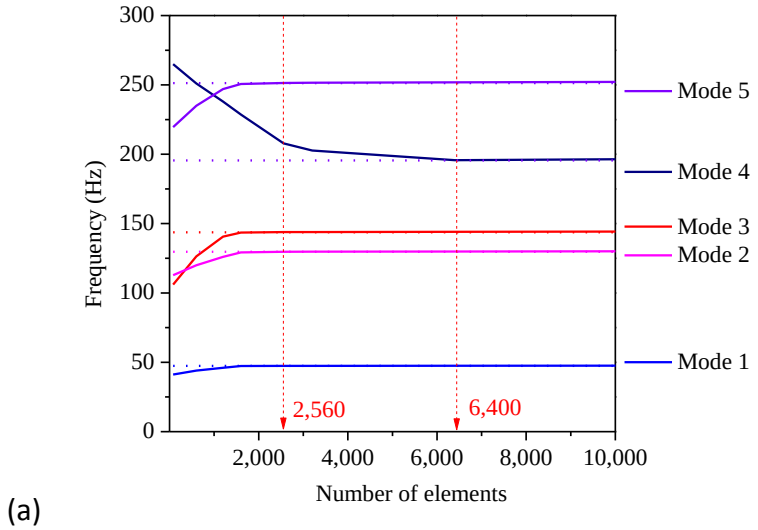

(a)

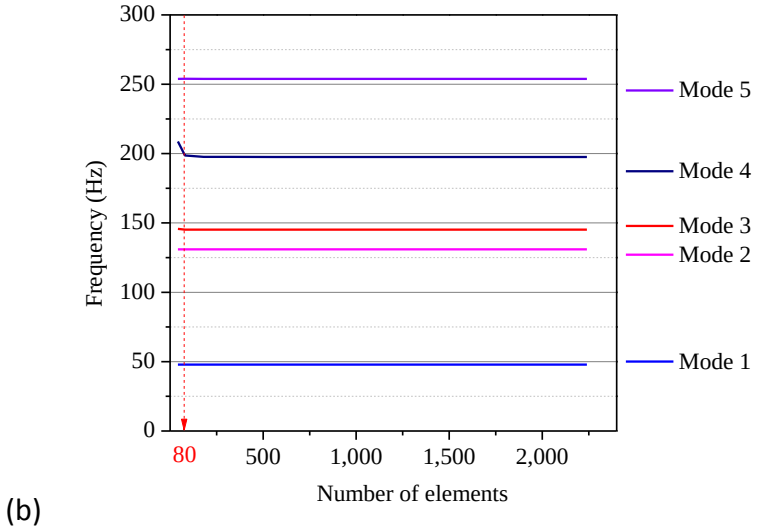

(b)

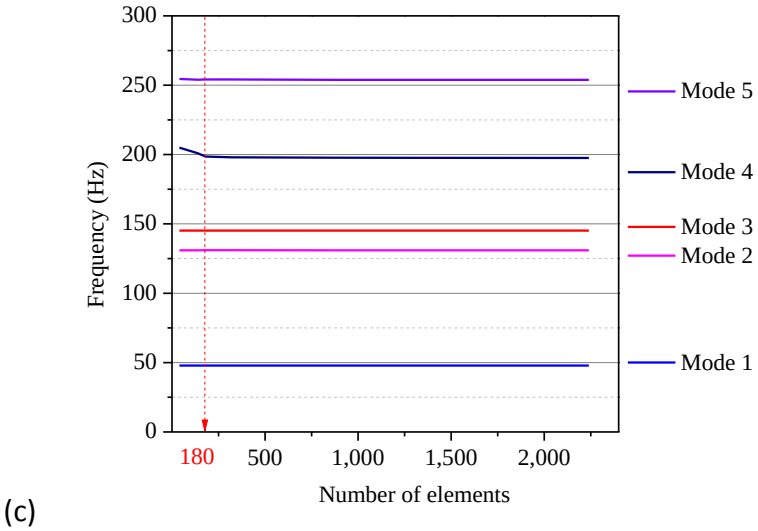

(c)

Figure 3.6: Convergence study of frequencies of single layer beam FE model:

(a) C3D8R element, (b) C3D20R element and (c) C3D20 element

However, the convergence performances are different for these three types of elements. We assume here that convergence is achieved when the error on frequencies,

compared with reference results obtained with a very fine mesh, are less than 1%. Eight-node solid element with reduced integration (C3D8R) requires the highest number of elements for convergence (Figure 3.6). The 1st, 2nd and 5th modes require 2560 elements to converge. However, the 3rd and 4th modes become stable with 6400 elements at least. On the other hand, FE model using 20-node solid elements (C3D20 or C3D20R) converge very quickly. The number of finite elements along the three directions for convergence is reported in Table 3.3. Finally, C3D20R element is chosen because it is the most efficient for convergence.

	Number of elements (Length x Width x Thickness)	Number of nodes
C3D8R	100 x 8 x 8 = 6400	8181
C3D20R	20 x 2 x 2 = 80	621
C3D20	20 x 3 x 3 = 180	1160

Table 3.3: Number of finite elements along three directions for convergence

3.2.3 Validation of the model

Figure 3.7 compares experimental frequencies and numerical frequencies obtained by the FE model with 80 C3D20R elements, for each single layer beam. Overall, the good correlation between numerical and experimental results shows the high performance of the FE model.

The numerical mode shapes are compared with the experimental one by the modal assurance criterion (MAC) values, which is calculated as follows:

$$MAC\left(\vec{\varphi}_{\exp},\vec{\varphi}_{num}\right)=\frac{\left|\vec{\varphi}_{\exp}\cdot\vec{\varphi}_{num}\right|}{\left|\vec{\varphi}_{\exp}\right|\cdot\left|\vec{\varphi}_{num}\right|} \tag{3.5}$$

where $\vec{\varphi}_{num}$ and $\vec{\varphi}_{\exp}$ are the eigenvectors of mode shapes obtained by the FE model and experiment, respectively. The comparison between the numerical and the experimental mode shapes is performed for each single layer beam. All the MAC values are very close to 1, showing that the numerical and the experimental mode shapes are very similar. The mean values of MAC are given in Table 3.4.

	Mode 1	Mode 2	Mode 5
Oak single layer beams	0.998	0.996	0.993
Spruce single layer beams	0.997	0.992	0.994

Table 3.4: The mean values of MAC of the single layer beams

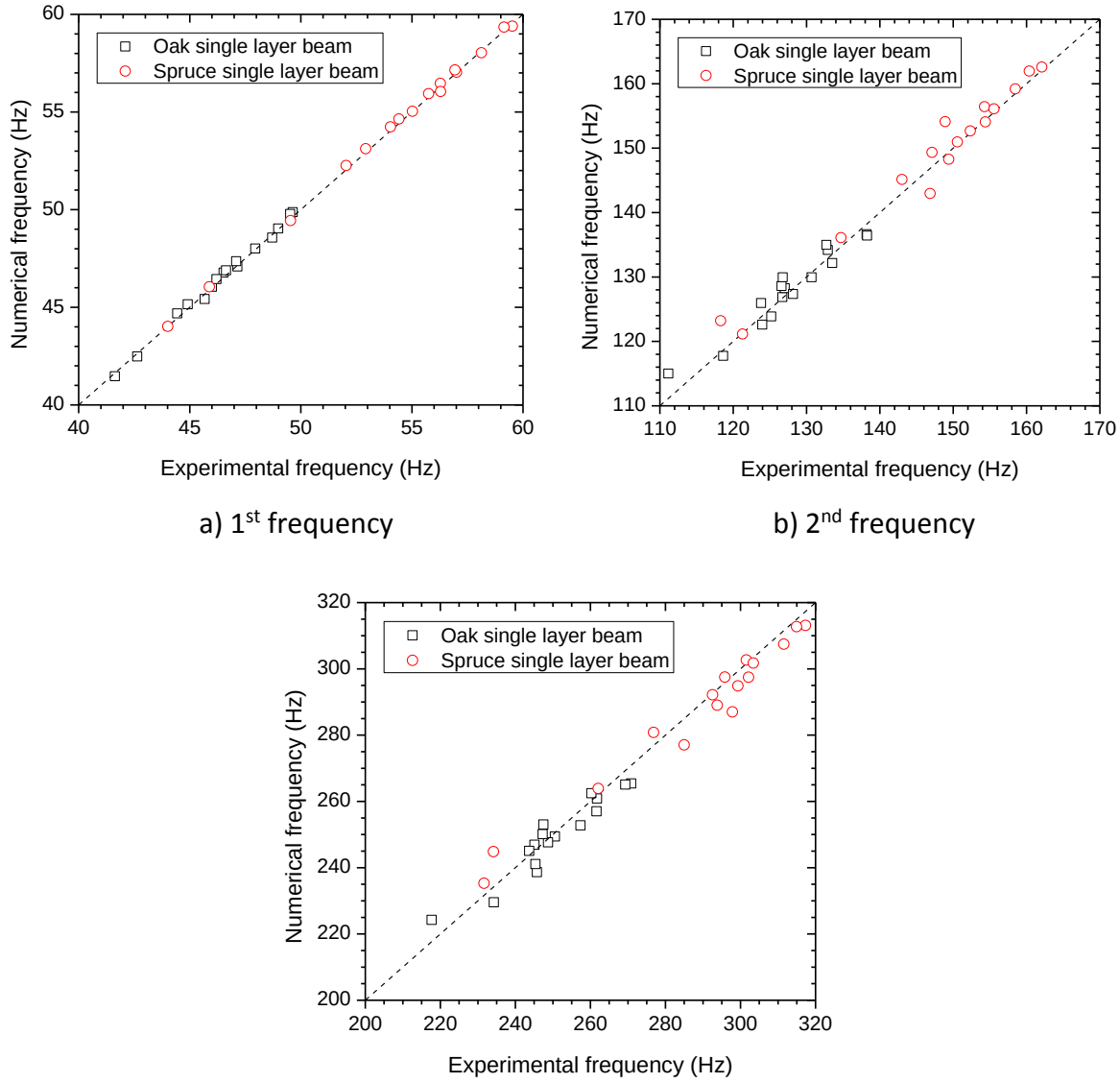

a) 1st frequency

b) 2nd frequency

c) 5th frequency

Figure 3.7: Comparison between numerical and experimental frequencies

3.2.4 Effect of homogeneous material assumption

The FE model considers that timber properties are homogeneous, but this is not true in reality. In particular, timber beams may have knots and other defects like cracks. The density and elastic properties of wood are not homogeneous, in particular in the vicinity and within the knots (see Section 2.3). The mechanical properties of wood could be described by random fields rather than homogeneous values. Several studies (Baño *et al.* (2013); Cao *et al.* (2019); Lukacevic *et al.* (2019)) showed that knot is the weakest point in a timber beam and the damage often occurs close to the location of knot in a static bending test.

Tapia and Aicher (2019) investigated local density and elastic modulus of 47 French oak boards by tension test. The results for the three typical boards are shown in Figure 3.8. The variability of local density along the length of each board is small but the variability of local

elastic modulus is high. The mean CoV of local density and local elastic modulus is 2.8% and 12.1%, respectively. However, the maximum values of CoV are 8.4% and 22.2% for local density and elastic modulus, respectively. To our knowledge the effect of variability of local density and elastic modulus on natural frequencies of timber beam has not been presented in any study. Therefore, the effect of knots on vibration is assessed below.

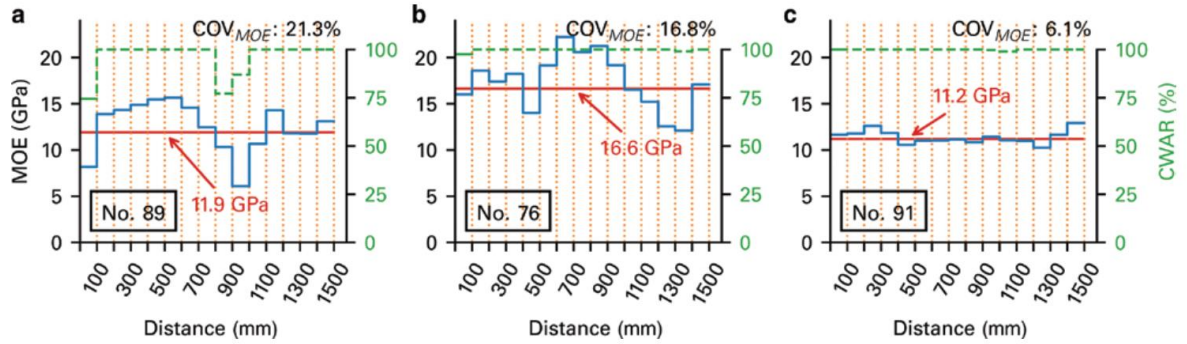

Figure 3.8: Local elastic modulus (blue line), global elastic modulus (red line) and clear wood area ratios CWAR (dashed line) along the length of different oak boards (Tapia and Aicher (2019))

In order to assess the effect of the homogeneous material assumption, two FE models to simulate timber board No.89, which has the highest variation of local properties, are built for comparison. In the first model, the board is divided into 15 parts along the length with different material properties from experiment (Tapia and Aicher (2019)). In the second model, the material of the whole board is homogeneous. The density and elastic modulus of the whole board equals the mean values of all parts of the first model.

	1st FE model	2nd FE model (homogeneous material)	Difference	MAC
f_1	43.94 Hz	45.33 Hz	3.2%	0.999
f_3	126.98 Hz	124.31 Hz	-2.1%	0.999
f_5	252.20 Hz	241.74 Hz	-4.1%	0.998

Table 3.5: Comparison results from two FE models for the oak board

The frequency of bending modes obtained with the two FE models are shown in Table 3.5. The differences are small or moderate for frequencies because the frequencies of beam are rather global quantities. The MAC values given in Table 3.5 are very close to 1, showing that the mode shapes from the two FE models are very similar.

In summary, vibration results obtained with the two models are close. Therefore, the assumption of homogeneous mechanical properties is acceptable in the context of the study about natural frequencies and modal shapes of timber structures.

3.3 FE model for three-layer AFLB

A FE model is developed to predict the vibrational behavior of the AFLB in this section. The FE model is validated by comparison numerical frequencies and modal shapes with the experimental ones obtained by a three-oak-layer AFLB. The longitudinal elastic modulus and density of the three layers of the AFLB are measured before assembly.

Figure 3.9 shows a CAD model of the three-oak-layer AFLB assembled by 27 CSDs. C3D20R element is used for both the timber layers and dowels. The longitudinal elastic modulus and density of the three oak layers are taken from experimental modal analysis, these properties are defined individually for each layer. The other elastic properties of layers are calculated according to the empirical relations given by Jodin (1994) as a function of the density while the properties of CSDs are taken from the literature (Bouhala *et al.* (2020)). The properties of three layers and CSDs are summarized in Table 3.6.

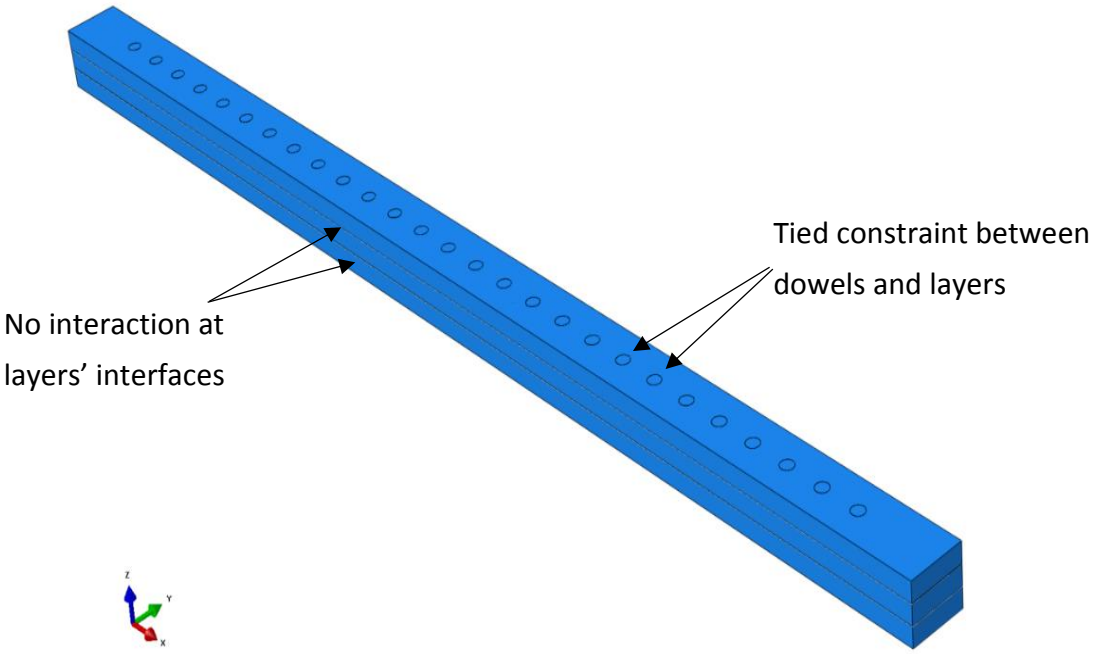

Figure 3.9: CAD model of AFLB

In the FE model, the dowel-to-layer and layer-to-layer interactions are chosen based on realistic conditions of the AFLB in vibration test. These conditions are:

- Vibration amplitude is very small,
- A small gap generally exists between layers after assembly.

Therefore, in the FE model:

- There is no direct interaction between interfaces of layers,

- The connections between dowels and layers are assumed to be sticky.

The sticky constraint ("tied" in Abaqus) for all degrees of freedom is defined between the cylindrical surface of dowels and the surface of the corresponding hole of the layers.

		Elastic moduli (MPa)			Poisson's ratios			Shear moduli (MPa)		
	ρ (kg/m^3)	E_1	E_2	E_3	v_{12}	v_{13}	v_{23}	G_{12}	G_{13}	G_{23}
Layer 1	628	12120	1731	970	0.34	0.40	0.68	1211	930	345
Layer 2	629	11740	1734	973	0.32	0.39	0.68	1214	932	346
Layer 3	612	12320	1674	927	0.35	0.42	0.68	1176	900	330
CSDs	1150	26000	1033	1082	0.41	0.41	0.37	800	800	100

Table 3.6: Mechanical properties of oak layers and CSDs in FE model of AFLB

3.3.1 Sensitivity analysis

The sensitivity of natural frequencies to the mechanical properties of timber layers and compressed wood dowels is studied and the results are summarized in Tables 3.7 and 3.8.

	ρ	E_1	E_2	E_3	v_{12}	v_{13}	v_{23}	G_{12}	G_{13}	G_{23}
f_1	-0.461	0.412	0	0	0	0	0	0.016	0.025	0
f_2	-0.461	0.468	0	0	0	0	0	0.022	0	0
f_3	-0.478	0.019	0	0	0	0	0	0.352	0.069	0
f_4	-0.459	0.329	0	0	0	0	0	0.039	0.067	0
f_5	-0.475	0.055	0	0	0	0	0	0.322	0.067	0
f_6	-0.459	0.411	0	0	0	0	0	0.070	0	0
f_7	-0.458	0.278	0	0	0	0	0	0.047	0.091	0

Table 3.7: Sensitivity of frequencies to material properties of layers of AFLB

	ρ	E_1	E_2	E_3	v_{12}	v_{13}	v_{23}	G_{12}	G_{13}	G_{23}
f_1	-0.03	0	0	0.03	0	0	0	0	0.01	0
f_2	-0.04	0	0	0	0	0	0	0	0	0
f_3	-0.02	0	0	0.01	0	0	0	0.006	0.02	0.01
f_4	-0.04	0	0	0.03	0	0	0	0	0.03	0
f_5	-0.02	0	0	0	0	0	0	0.003	0.02	0.02
f_6	-0.04	0	0	0	0	0	0	0	0	0.01
f_7	-0.04	0	0	0.03	0	0	0	0	0.04	0

Table 3.8: Sensitivity of frequencies to material properties of dowels of AFLB

In general, the effect of dowel properties on frequencies of AFLB is much smaller than that of layer properties because the volume of dowels is very small compared to the volume

of layers. In contrast to the layer, E_1 of dowel has no effect on the frequencies of AFLB because the dowel is not extended (or compressed) lengthwise when the AFLB vibrates. Indeed, direction 1 of dowel corresponds to the thickness of the beam (Figure 3.10). Finally, E_1 and ρ of the layer, which have been measured experimentally, have the highest influence on the AFLB frequencies. The variation of other properties of layer and dowel has only a small effect on the results of the FE model. Hence the assumption of mechanical properties of dowels and layers is acceptable.

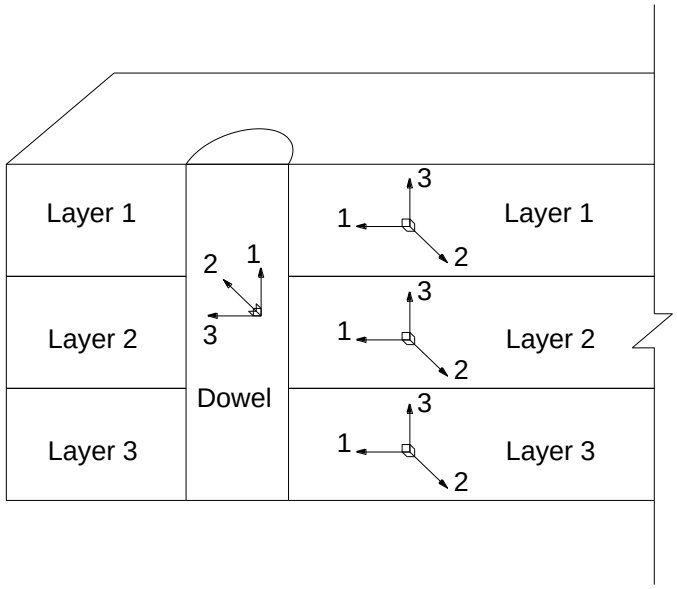

Figure 3.10: Local coordinate system of dowel and layers

3.3.2 Verification of the model

Figure 3.11 shows the mesh size dependency of frequencies of AFLB. It can be observed that the higher order frequencies require much more elements for the convergence by comparison to the first frequency. By using about 13500 elements, the first seven frequencies become stable. The number of elements in the FE model of a given layer in the AFLB where holes and dowels are involved is much higher than that of a single layer beam FE model. The geometry of the assembly leads to some difficulties to create meshes. It requires a very small mesh size for dowel because of small dimensions and circular shape of this part. The mesh which meets convergence conditions for the AFLB is displayed in Figure 3.12. The number of elements in layers and dowels is reported in Table 3.9.

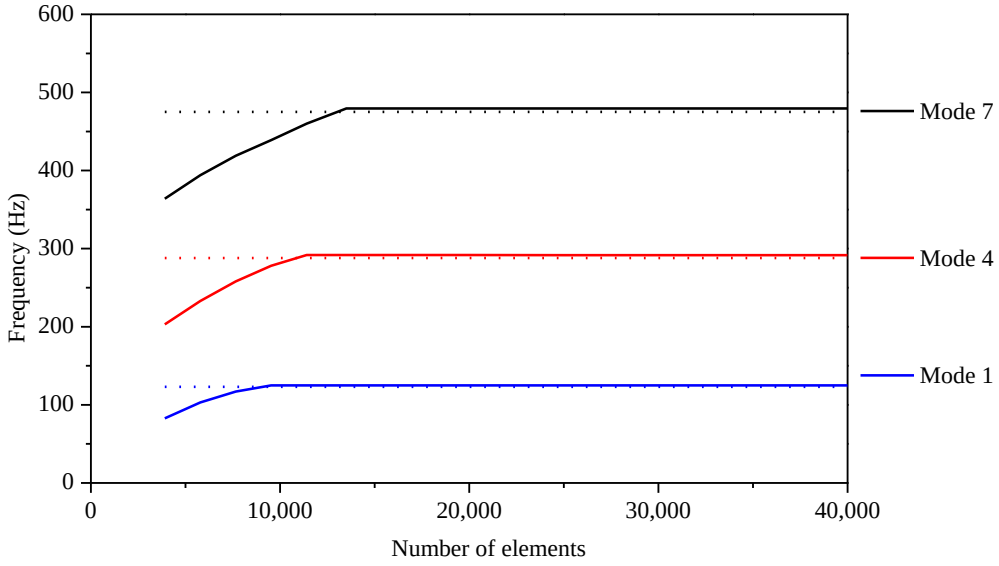

Figure 3.11: Convergence study of FE model of AFLB

	Number of elements
1 layer	2238 elements (140 along length, 5 in width, 3 through thickness)
3 layers	6714 elements
1 dowel	252 elements (14 through thickness)
27 dowels	6804 elements

Table 3.9: Number of elements in the converged mesh for layers and dowels of AFLB

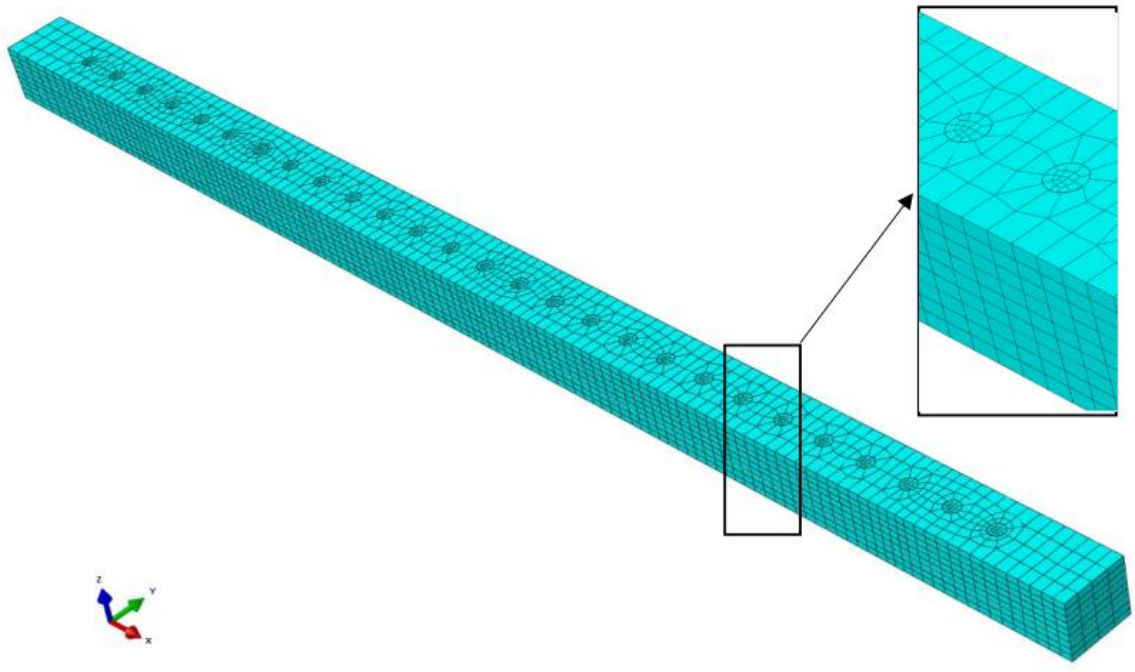

Figure 3.12: Converged FE mesh of AFLB

3.3.3 Validation of the model

For one given three-oak-layer AFLB the comparison between the experimental measurements and the numerically predicted results is presented hereafter. Table 3.10 depicts the error values on the vibration frequency from the FE model when compared to the corresponding experimental values. One major source of error is the complex connection between layers and dowels. Indeed the interaction assumptions lead to good results but they are certainly not perfectly respected in reality. Therefore, taking into account the complexity of the structure, it can be seen a fairly good agreement.

	Numerical	Experimental	Difference	MAC
f_1	124.9 Hz	121.8 Hz	2.6%	0.997
f_2	142.8 Hz	_	_	_
f_3	159.5 Hz	_	_	_
f_4	291.8 Hz	279.8 Hz	4.3%	0.986
f_5	328.3 Hz	_	_	_
f_6	364.2 Hz	_	_	_
f_7	480.3 Hz	459.2 Hz	4.6%	0.963

Table 3.10: Comparison between numerical and experimental results for AFLB

The mode shapes predicted numerically are displayed in Figure 3.13. It can be observed that the MAC values given in Table 3.10 are close to 1, so a very good agreement exists between numerical and experimental mode shapes.

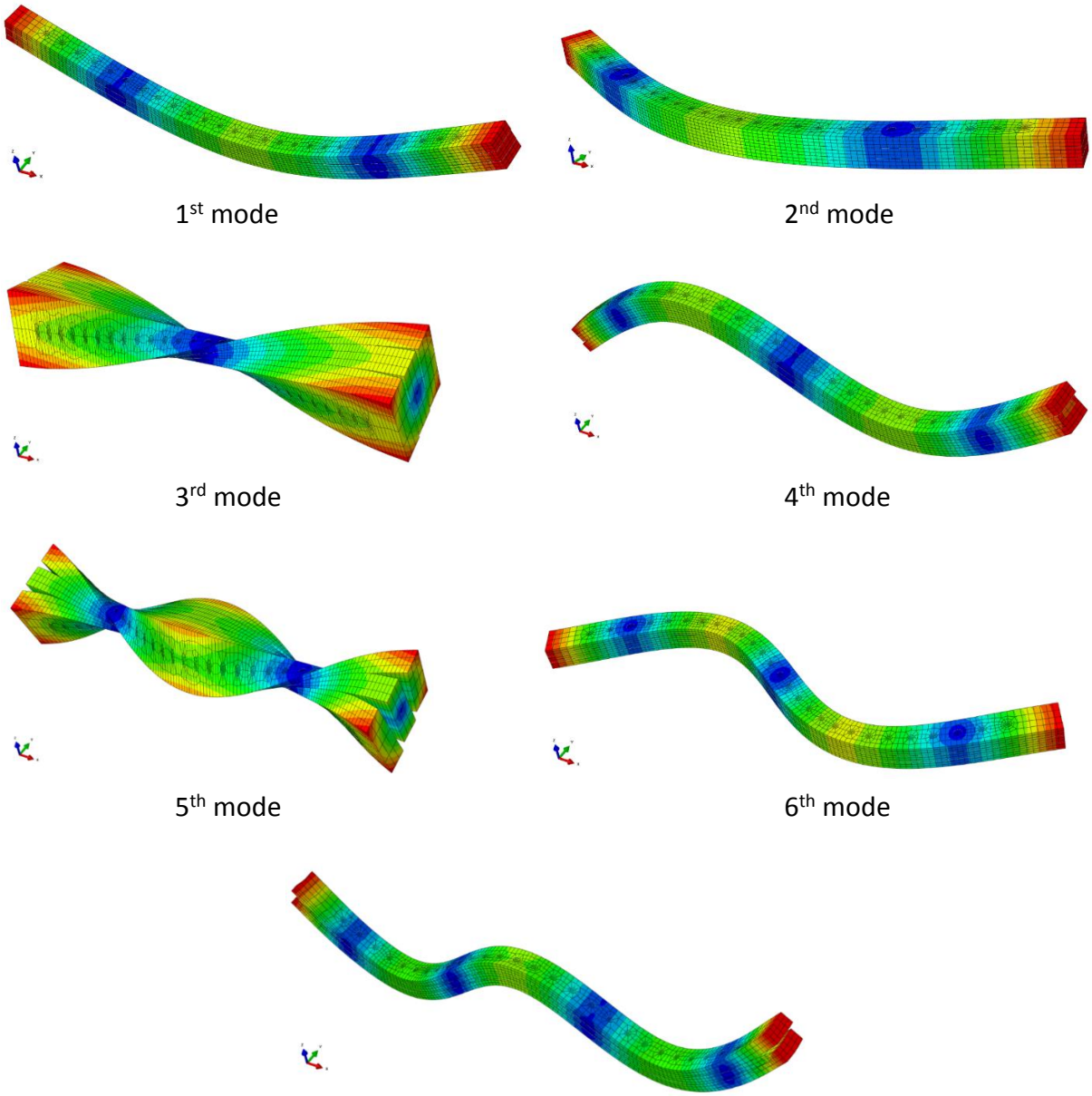

Figure 3.13: The first seven numerical mode shapes of AFLB

3.3.4 Effect of stiffness of CSD on frequencies of AFLB

Although the sensitivity of natural frequencies of AFLB to material properties of dowels is small, the dowels play an important role in AFLB. Therefore, the effect of stiffness of dowel on frequencies of AFLB is studied here. Figure 3.14 shows the variation of frequencies of AFLB when the dowels vary from being flexible to being rigid. The elastic and shear modulus of CSD are reference values. The stiffness of dowel is changed by multiplying all moduli of dowel by a ratio which varies from 10^{-4} to 10^{3}. Poisson's ratios are kept constant.

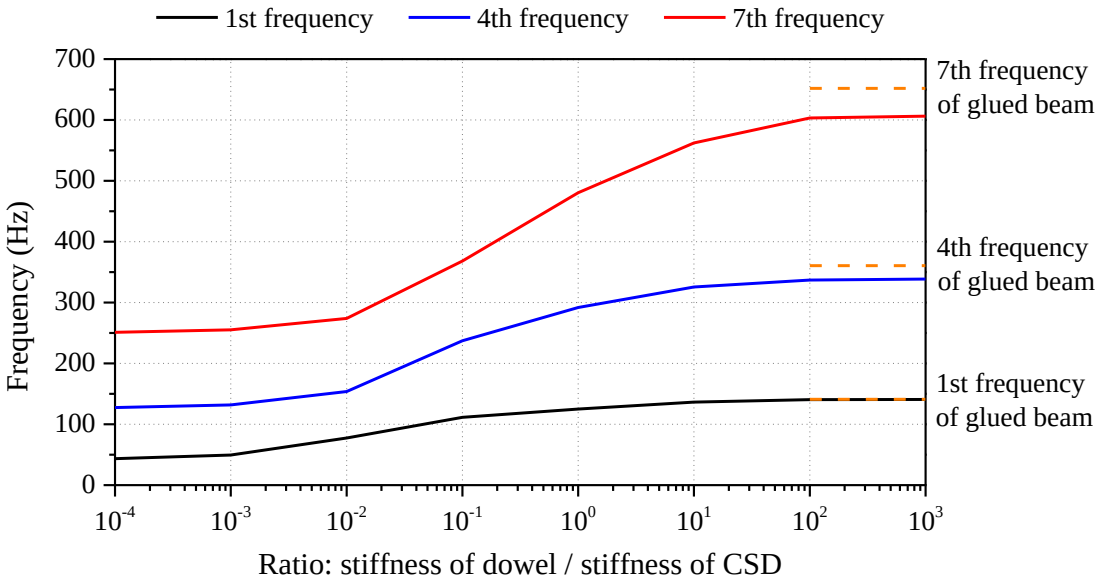

Figure 3.14: Effect of stiffness of dowel on frequencies of AFLB

Dowels act as fasteners; they join layers together. However, they do not work when their stiffness is divided by 1000 or more compared with the stiffness of CSD. The AFLB frequencies are then equal to the frequencies of single layer beam. If the stiffness of dowel increases, the frequencies of AFLB increase. Figure 3.14 shows that the red line (7^{th} frequency of AFLB) has a greater slope than the black line (1^{st} frequency of AFLB). Therefore, the stiffness of dowel has a greater influence on the higher frequencies of AFLB. The frequencies of AFLB are close to that of glued beam when the stiffness of dowel is 100 times higher than that of CSD. In this case, dowels are like rigid studs; they resist relative slip between layers. If relative slip between layers cannot occur, the mechanical behaviour of AFLB is close to the behaviour of glued beam.

3.4 FE model for AFCLT panel

A FE model to simulate the AFCLT panel without groove (Figure 3.15) is built based on the FE model of AFLB. Once the FE model is validated by comparison against experimental results, it can be used to predict the vibrational behavior of a realistic large-scale flooring system made with AFCLT panel, avoiding extensive experimental campaigns.

The FE model are validated with mean frequencies of five AFCLT panels measured experimentally (see Section 2.6). Therefore, all lamina in the FE model can be defined with similar material. Their longitudinal elastic modulus is equal to the mean value from 16 oak single layer beams (Section 3.3). Their density is adjusted so that the total mass of the panel in the model is equal to the mean measured mass of the real panels.

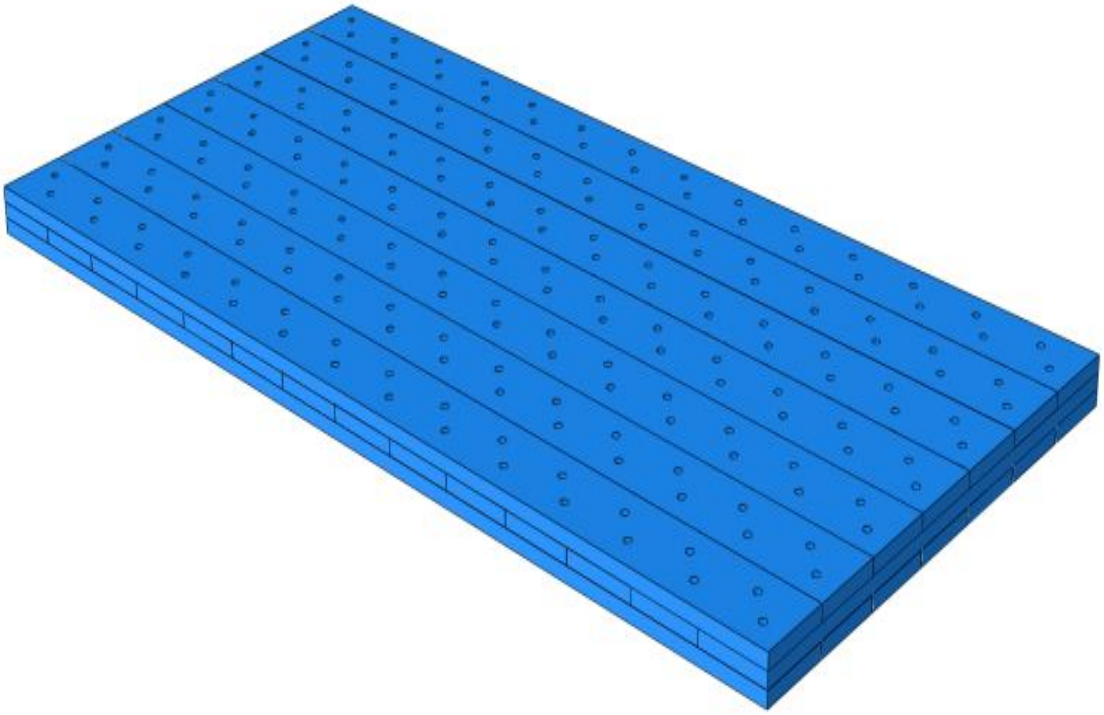

Figure 3.15: CAD model of AFCLT panel without groove

3.4.1 Verification of the model

Figure 3.16 shows the effect of the number of elements on the result for the FE model of AFCLT panel. It can be observed that the frequencies converge with 75280 elements. The converged mesh of the FE model is shown in Figure 3.17.

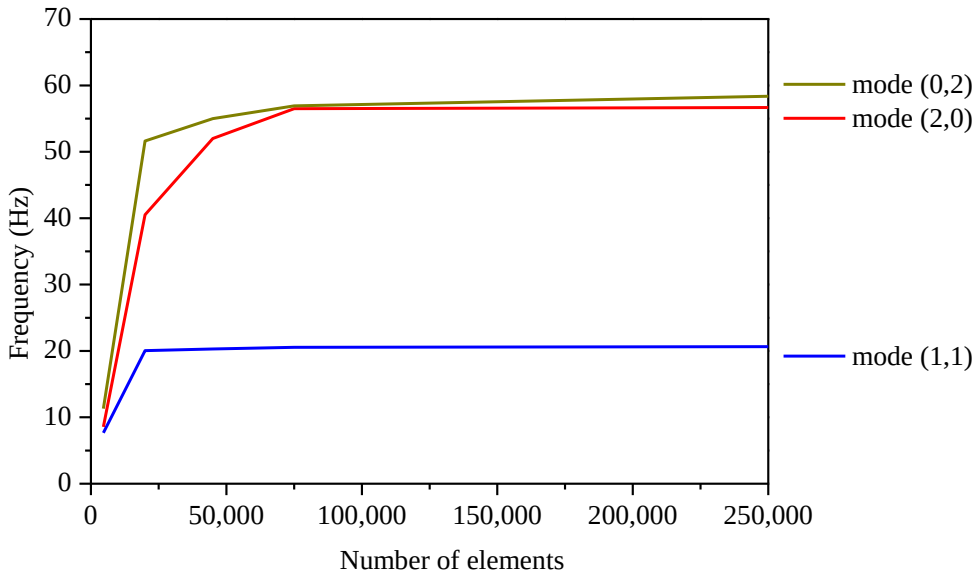

Figure 3.16: Convergence study of the first three frequencies

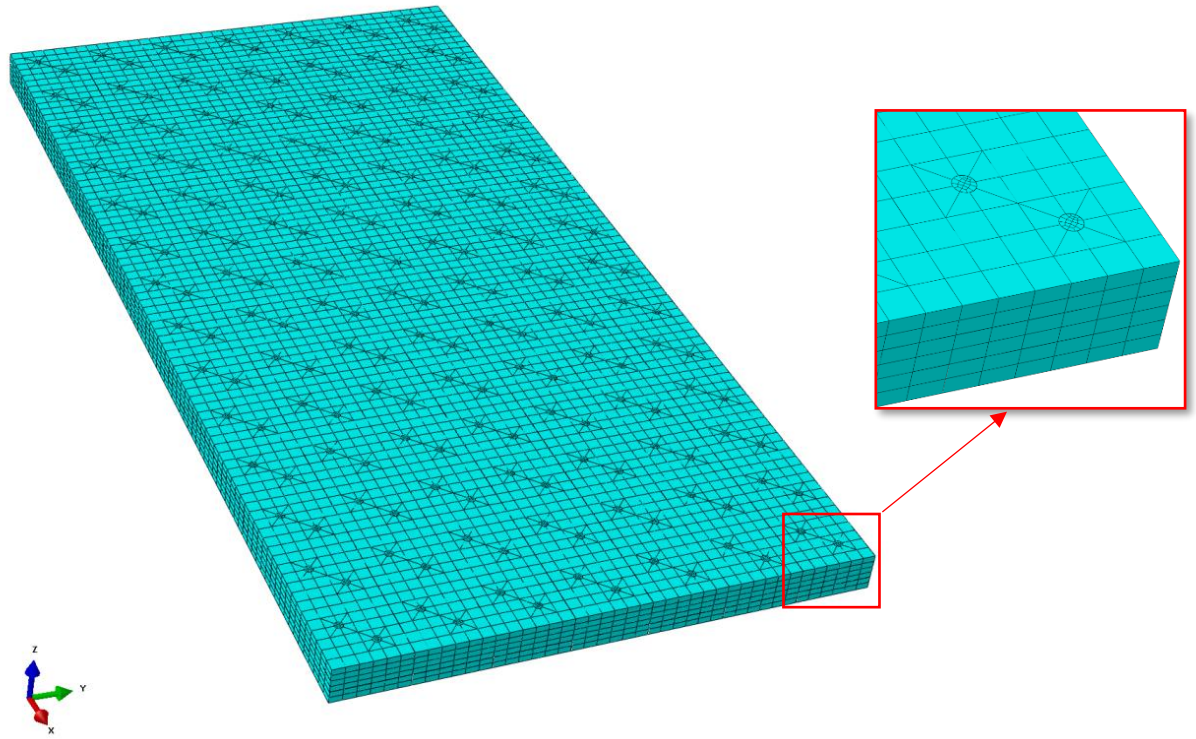

Figure 3.17: Converged mesh of AFCLT panel

3.4.2 Validation of the model

Table 3.11 compares numerical frequencies from the FE model with mean experimental frequencies of five normal AFCLT panel (see Section 2.6). Given the uncertainty of material properties and complexity of the structure, it can be seen a fairly good agreement.

Mode	Numerical frequency	Experimental frequency	Difference	MAC
(1,1)	20.9 Hz	21.9 Hz	-4.6%	0.99
(2,0)	56.5 Hz	54.5 Hz	3.7%	0.97
(0,2)	56.9 Hz	56.3 Hz	1.1%	0.98
(2,1)	66.1 Hz	63.8 Hz	3.6%	0.95
(1,2)	69.4 Hz	68.6 Hz	1.2%	0.95
(2,2)	104.9 Hz	102.0 Hz	2.8%	0.94
(3,0)	116.2 Hz	110.3 Hz	5.4%	0.93
(3,1)	128.4 Hz	119.6 Hz	7.3%	0.94
(3,2)	162.0 Hz	152.2 Hz	6.4%	0.94

Table 3.11: Comparison between numerical and experimental results for AFCLT panel

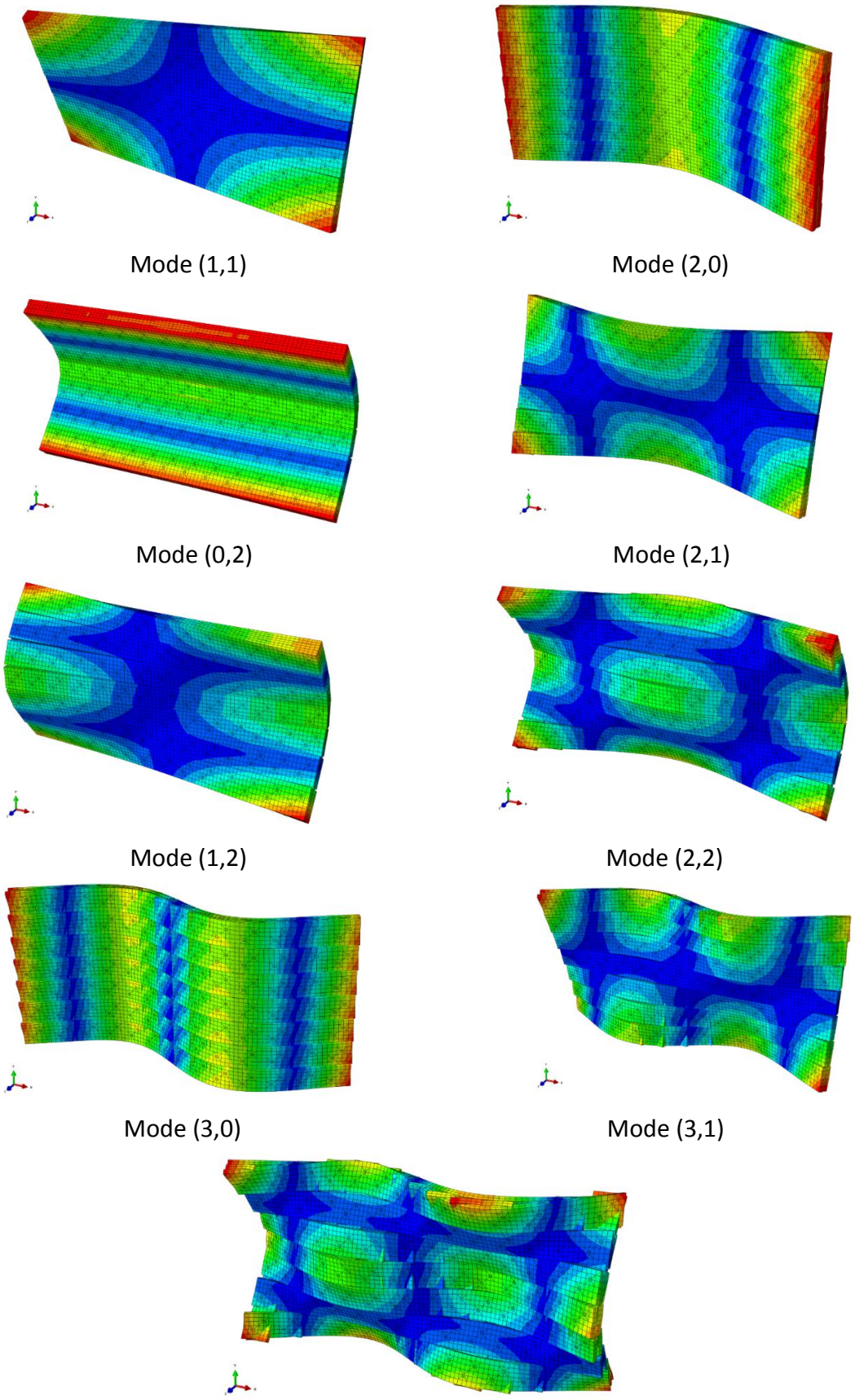

Figure 3.18: Numerical mode shapes of AFCLT panel

Numerical mode shapes presented in Figure 3.18, are similar with that observed from experiment (Table 2.5). Moreover, the MAC values in Table 3.11 are close to 1 indicating a good agreement between experimental and numerical mode shapes.

Frequencies of groove panel are predicted and compared with frequencies of normal panel in Table 3.12. The two types of panels have similar material properties and free-free boundary conditions. Small difference between frequencies of normal and groove panels confirms that groove have negligible effect on the vibrational behavior of AFCLT panel.

Mode	Normal panel	Groove panel	Difference
(1,1)	20.9 Hz	21.0 Hz	0.5%
(2,0)	56.5 Hz	56.4 Hz	-0.2%
(0,2)	56.9 Hz	57.3 Hz	0.7%
(2,1)	66.1 Hz	66.2 Hz	0.2%
(1,2)	69.4 Hz	69.9 Hz	0.7%
(2,2)	104.9 Hz	105.2 Hz	0.3%
(3,0)	116.2 Hz	116.0 Hz	-0.2%
(3,1)	128.4 Hz	128.5 Hz	0.1%
(3,2)	162.0 Hz	162.2 Hz	0.1%

Table 3.12: Comparison of numerical frequencies of normal panel and groove panel

Moreover, the FE model is also used to simulate a linear elastic and static bending test. Table 3.13 compares the experimental and numerical maximum deflection of the AFCLT panel in a three-point bending test. The experimental value is the mean deflection of all panels under 1kN static load according to Eurocode 5. The error is acceptable. Therefore, the predictive capability of the proposed Abaqus finite element models is satisfactory.

	Numerical	Experimental	Difference
Deflection (*w*)	1.01 mm	1.08 mm	-6.5%

Table 3.13: Comparison between numerical and experimental deflection for AFCLT panel

3.5 FE model for full-size AFCLT panel

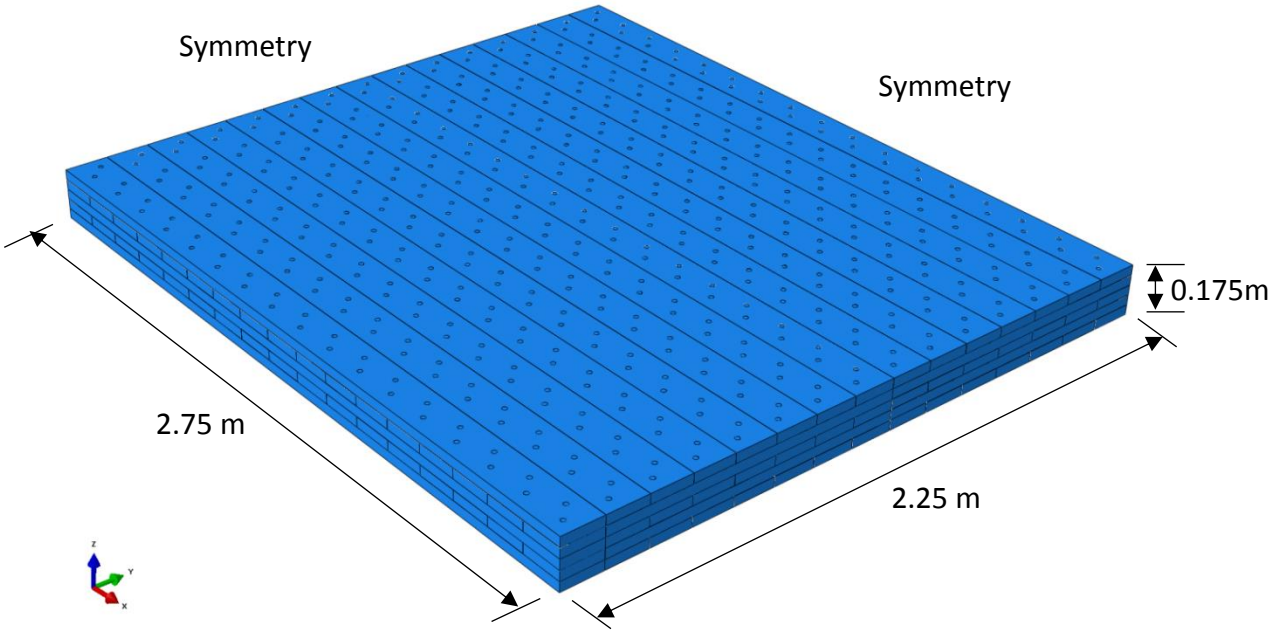

Figure 3.19: CAD model of full-size AFCLT panel

A FE model is built to predict the vibrational behaviour of real flooring system made of AFCLT panel. The comparison between results from the model and three design requirements of Eurocode 5 can give us the vibrational performance of real AFCLT floor. Moreover, the model can be used to study the effect of the parameters on the frequency of AFCLT floor, thereby optimizing the stiffness of the floor.

The panel is 5.5m long, 4.5m wide and 0.175m thick (including 5 layers). Due to the symmetry, the size of panel in the model is equal to one quarter of the real panel (Figure 3.19). The panel is assumed as simply supported along its four sides.

3.5.1 Prediction of frequencies and modal shapes

Figures 3.20 and 3.21 show the first four frequencies and mode shapes of the full-size AFCLT panel obtained with the converged mesh. It can be seen that the difference between AFCLT panel and glued CLT panel with similar dimensions and material is not large, in particular for the first modes. Therefore, the stiffness of AFCLT panel is close to that of a glued panel.

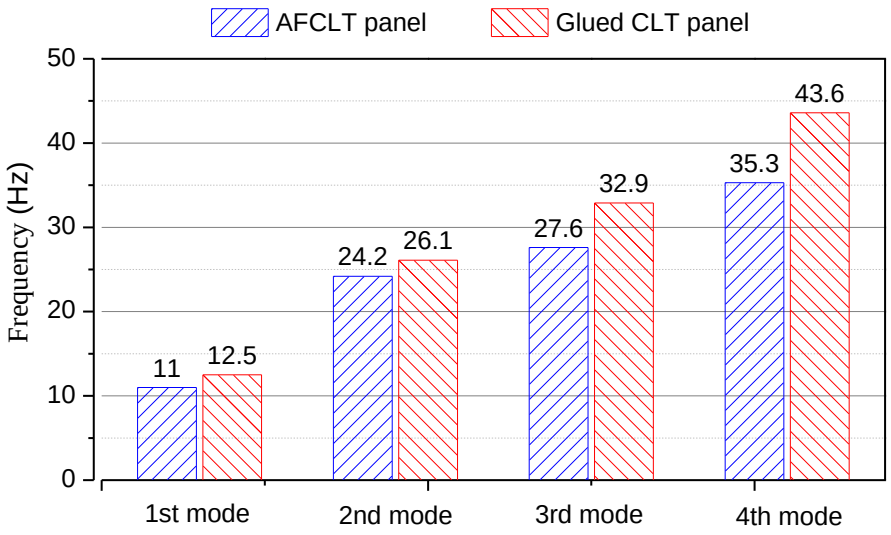

Figure 3.20: Comparison of predicted frequencies between AFCLT panel and glued CLT panel

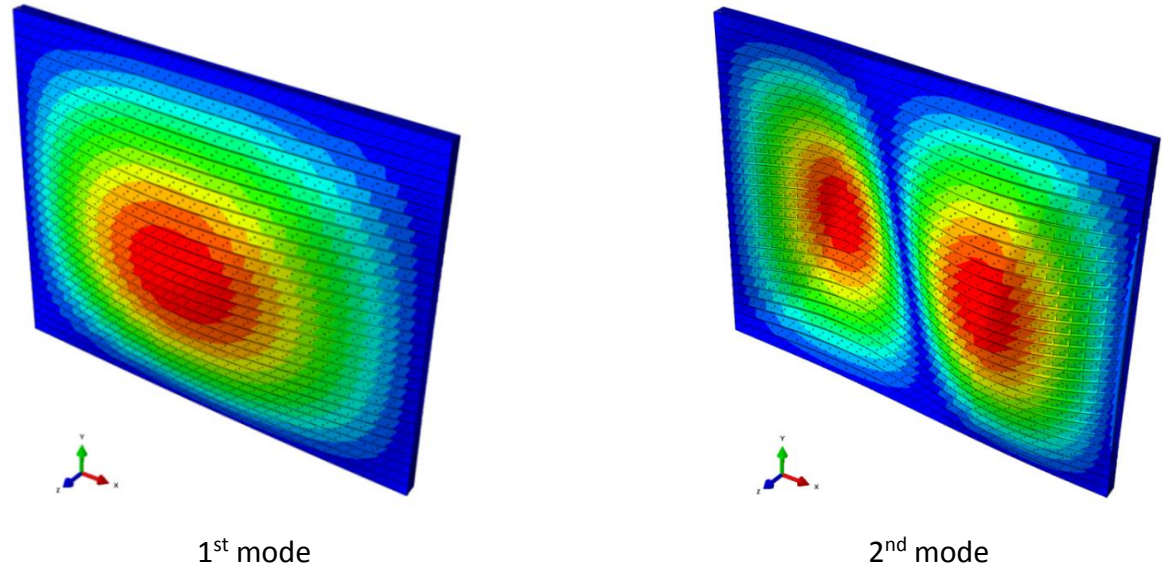

1st mode 2nd mode

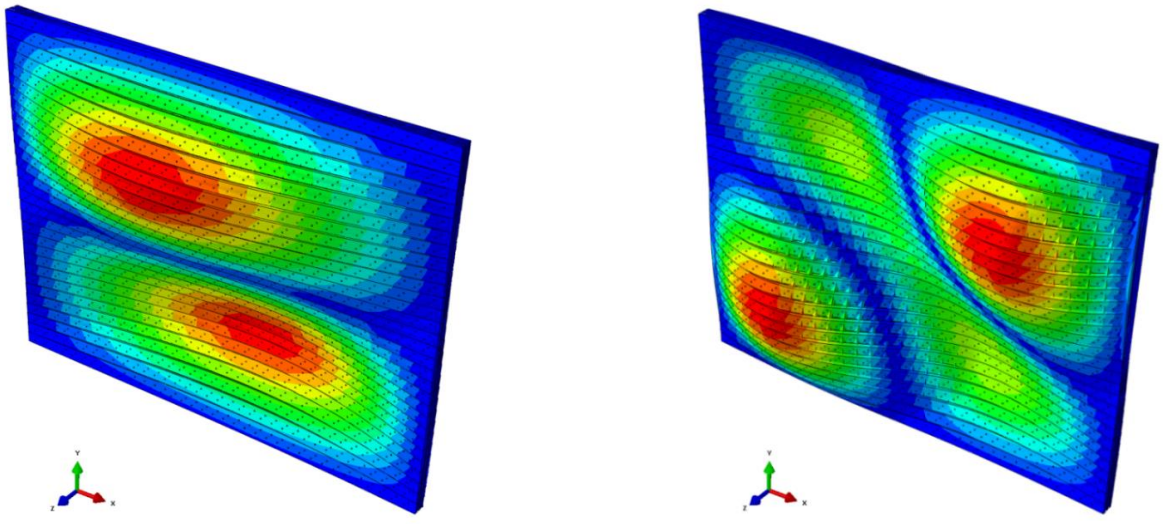

3rd mode 4th mode

Figure 3.21: The first four numerical mode shapes of full-size AFCLT panel

3.5.2 Comparison with EC5 requirements

Furthermore, the vibrational comfort of the AFCLT panels is assessed based on the three main criteria which have been adopted in the Eurocode 5 for the vibrational serviceability design of timber floors:

- Fundamental frequency:

$$f_1 = \frac{\pi}{2L^2}\sqrt{\frac{(EI)_L}{m}} > 8(\mathrm{Hz}) \tag{3.6}$$

- Unit point load deflection (see Figure 3.22):

$$w \leq a(\mathrm{mm/kN}) \tag{3.7}$$

- Unit impulse velocity response (see Figure 3.22):

$$v \leq b^{(f_1\xi-1)}(\mathrm{m/Ns^2}) \tag{3.8}$$

where L is the floor span, $(EI)_L$ is the equivalent bending stiffness of the plate according to an axis perpendicular to the span, m is the mass per unit of area of the panel, a is the design limit deflection of the floor, b is a parameter depending on the design limit deflection a and ξ is the modal damping ratio. Note that the parameter b is deduced, from Figure 3.22, knowing the parameter a representing the deflection of the panel under unit load.

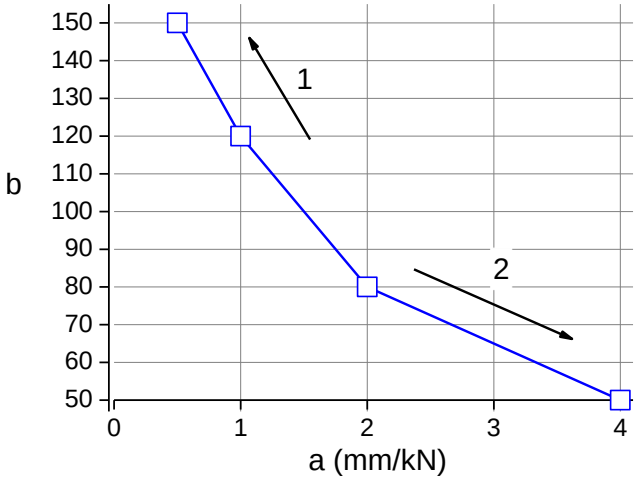

Figure 3.22: Design parameters *a* and *b* recommended by the Eurocode 5

Note that the unit impulse velocity response is not obtained by experimental measurement but calculated using an empirical formula (Equation 3.9) suggested by the Eurocode 5 for rectangular panels with dimensions of *B* x *L*, simply supported along their four edges.

$$v = \frac{4(0.4 + 0.6n_{40})}{mBL + 200}(\mathrm{m/Ns^2}) \tag{3.9}$$

with n_{40} is the number of modes with natural frequencies up to 40 Hz expressed as:

$$n_{40} = \frac{B}{L}\left[\left(\left(\frac{40}{f_1}\right)^2 - 1\right)\frac{(EI)_L}{(EI)_B}\right]^{1/4} \tag{3.10}$$

where $(EI)_B$ is the equivalent plate bending stiffness of the panel according to an axis parallel to the beam direction in Nm^2/m.

The vibration characteristic values of the full-size AFCLT panel are summarized and compared with requirements of Eurocode 5 in Table 3.14.

	Full-size panel	Eurocode 5 requirements
First frequency (f_1)	11.0 Hz	> 8 Hz
Deflection (a)	0.82 mm/kN	0.5 – 4 mm/kN
Parameter (b)	137	50–150
Impulse velocity (v)	0.006 m/(Ns^2)	$\leq b^{(\xi f_1 - 1)}$= 0.012
Number of frequencies ≤40Hz (n_{40})	4	

Table 3.14: Vibrational characteristic values of full-size AFCLT panel according to the Eurocode 5 requirements

From Table 3.14 and Figure 3.23, it can be seen that the full-size panel satisfies all the three criteria suggested by the Eurocode 5 for serviceability vibrational comfort. However, design optimization is necessary to improve the stiffness as well as the first frequency of AFCLT panel.

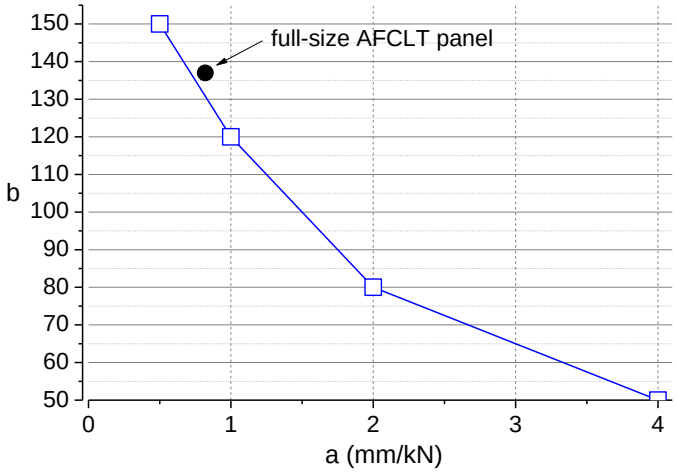

Figure 3.23: Vibration performance of the full-size AFCLT panel

3.5.3 Optimization for the first frequency

A parametric study is performed to maximize the fundamental frequency of AFCLT panel. The parameters summarized in Table 3.15 are timber species used for layers, number of layers (with the same global thickness), number of dowels and inclination of dowels. However, the combination of 4320 dowels and 30° inclination is not possible. Two cases of boundary condition: 2 edges simply supported and 4 edges simply supported, are assessed.

Parameter	Case 1	Case 2
Timber species for layers	Oak	Spruce
Number of layers	5 layers	3 layers
Number of dowels	2160 (Figure 3.19)	4320 (Figure 3.24)
Inclination of dowels	vertical	30° (Figure 3.25)

Table 3.15: Parameters for the design of AFCLT panel

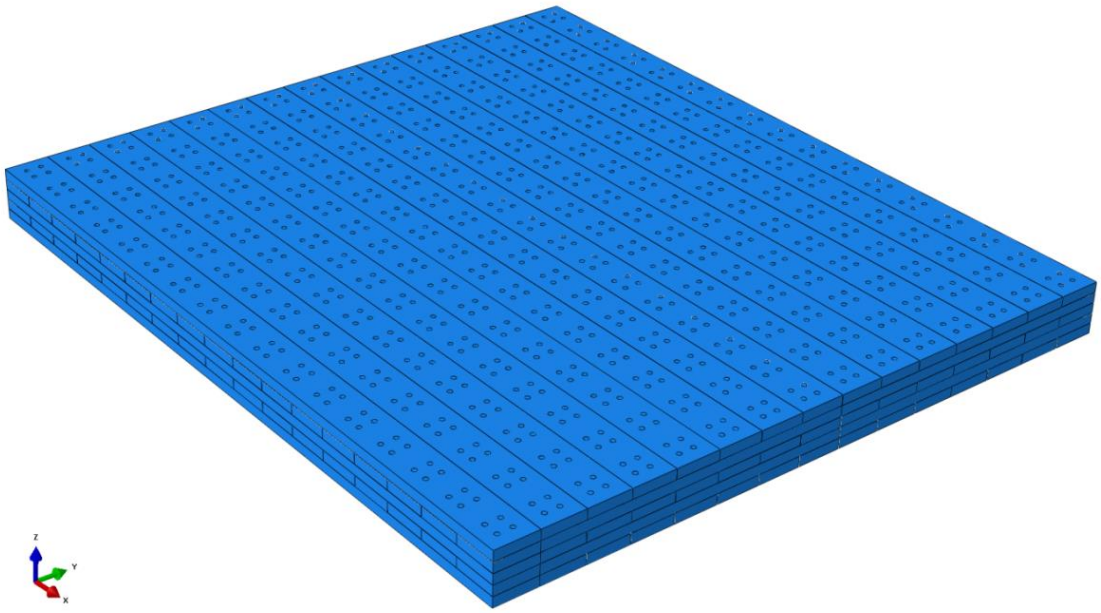

Figure 3.24: Full-size AFCLT panel assembled by 4320 vertical dowels

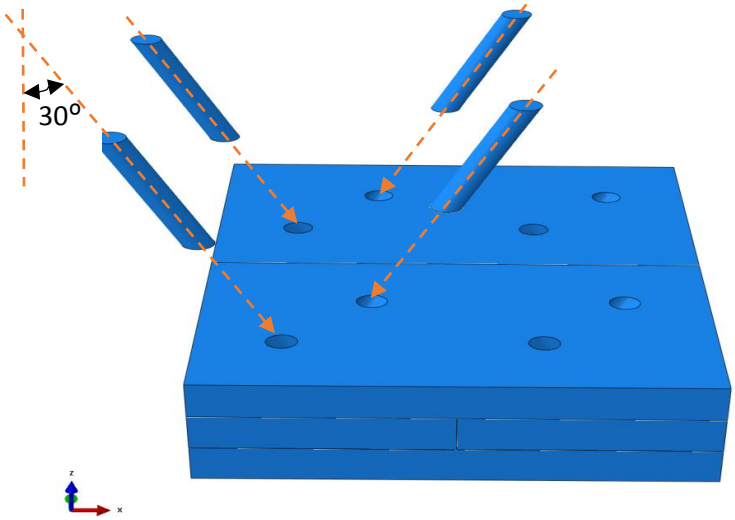

Figure 3.25: AFCLT panel assembled by 30-degree dowels

Figures 3.26 and 3.27 compare the first frequency of full-size AFCLT panel with different configurations of parameters.

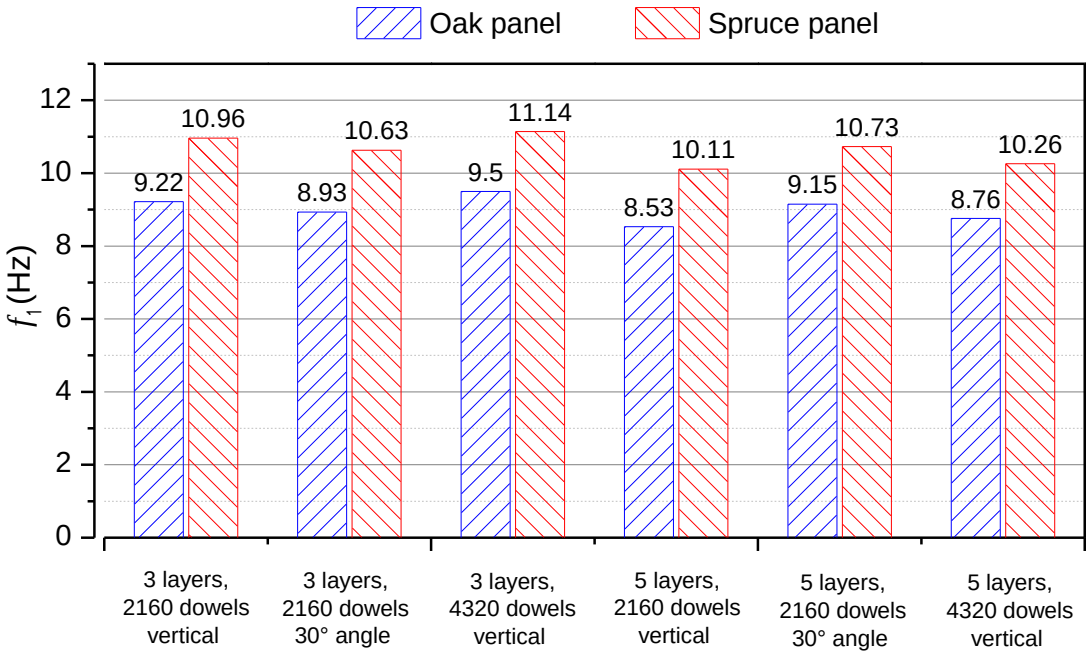

Figure 3.26: First frequency of full-size AFCLT panel with 2 simply supported edges

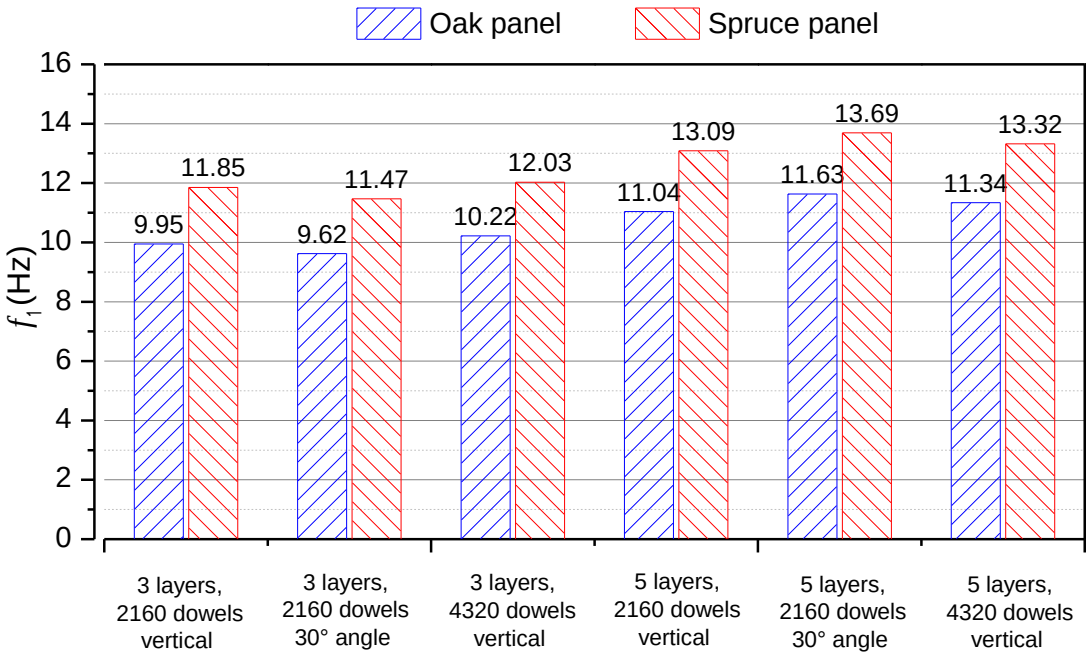

Figure 3.27: First frequency of full-size AFCLT panel with 4 simply supported edges

• In general, 5-layer AFCLT panel is better than 3-layer AFCLT panel in the case of 4 edges simply supported while the 3-layer panel is better than the 5-layer panel in the 2 edges simply supported case. The 5-layer panel with three longitudinal layers and two transverse layers reduces the difference of stiffness between two directions caused by orthotropic properties of timber. Therefore, the five-layer panel is suitable for square flooring system supported on more than 2 sides.

• The frequency of spruce AFCLT panel is higher than the frequency of oak AFCLT panel because of the higher ratio between elastic modulus and density of spruce.

• The frequency of AFCLT panel increases when the number of dowels increases.

• The frequency of AFCLT panel assembled by 30-degree dowels is higher than the frequency of the panel assembled by vertical dowels because of two reasons. First, 30-degree dowel is longer than vertical dowel; therefore, the connection between 30-degree dowels and layers is better. Second reason is the orthotropic properties of dowel. In fact, longitudinal elastic modulus (E_1) of dowel is much larger than the elastic moduli in the other directions (E_2, E_3). However, E_1 have no effect on frequencies of the panel while E_3 have more effect on them in the case of vertical dowel because E_1 is perpendicular to longitudinal and transverse global axis of the panel. The inclination of dowel increases the stiffness of dowel in longitudinal global axis of the panel which in turn increases the global stiffness of the panel (Figure 3.28).

• Finally, five-spruce-layer AFCLT panel assembled by 30-degree dowels and simply supported on 4 edges, has the maximum frequency value.

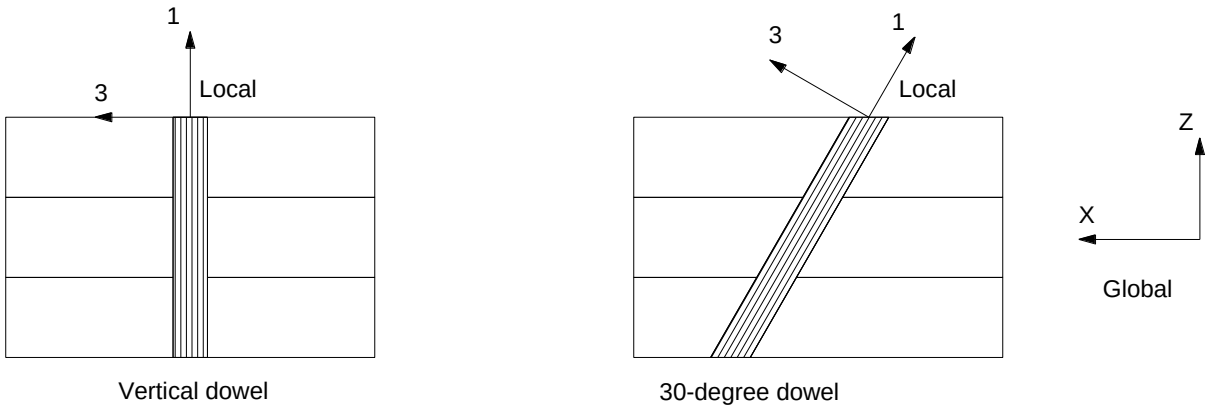

Figure 3.28: Local coordinate system of dowel and global coordinate system of AFCLT panel

3.6 Simplified FE model

There are 471,600 quadratic brick elements with 6,074,208 degrees of freedom (DOFs) in the converged mesh of the model of a quarter of full-size AFCLT panel. Time required for linear mode analysis is 3 hours based on a computer station having the following specifications: Intel (R) Core (TM) i7-6820HQ 2.70 GHz with 32 GB RAM. Therefore, the development of a simplified FE model for AFCLT panel is necessary, in particular if the analysis has to be repeated a certain number of times, namely for further optimization or stochastic analysis. The simplified model must have fewer elements and DOF than the 3D solid FE model to reduce computational time. However, the simplified model must be of acceptable quality. The simplified model must take into account all important physical properties of AFCLT panel as the 3D model does. Moreover, the results obtained with simplified model and 3D solid model must be close. Modal shapes must be approximately the same, with high MAC values. The difference between frequency results of the simplified model and that of the 3D model should be small. We consider here that this difference must be smaller than 5%. One important condition in the verification of a finite element model is convergence. So the results obtained with a simplified model must converge when the mesh is refined. A non-convergent approach is not accepted in this study.

This section presents several simplified FE models for AFLB. First, the vibrational deformation of dowels and layers in the simplified model must be similar with that in the 3D solid model (reference model), as shown in Figure 3.29. A priori the layers can be simulated by either solid or shell elements. For the dowels, the deformation is rather localized at the layers' interfaces. Hence, simplifying the dowels is a challenge. The ability to simulate the dowels using beam elements is presented below.

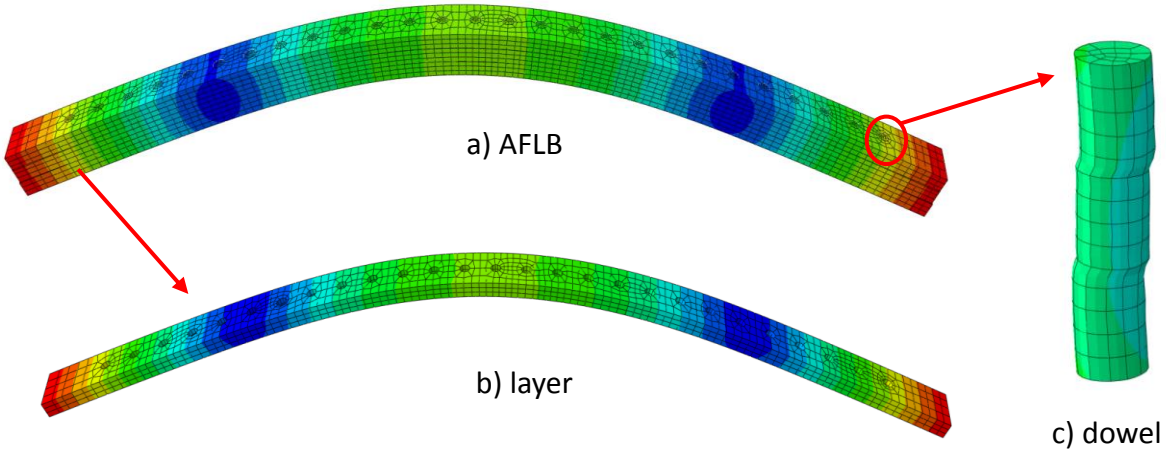

Figure 3.29: Deformation of layer and dowel of the AFLB for the 1st vibrational mode from the reference model

3.6.1 Simplifying dowels by beam elements

The 3D FE model of AFLB has 27 dowels and each dowel is modeled using 252 elements with 3,933 DOFs. Therefore, the number of DOFs of the FE model will be greatly reduced if the dowel is simplified by beam elements (Figure 3.30). However, modeling dowel using beam elements has a limitation: it takes into account bending and transverse shear effects, but it does not consider the possible complex deformation of beam cross-section.

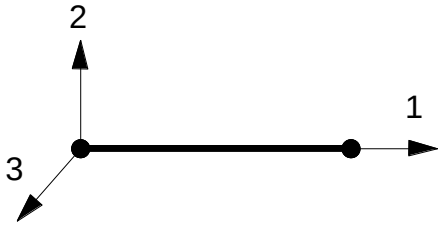

Figure 3.30: Local axes for beam element

The 3D solid model is used to estimate the effect of two problems arising from simplifying dowel by beam elements. First, beam element ignores the flexibility in the transverse direction. Therefore, moduli E_2, E_3 and G_{23} of dowel in the reference model are increased by 100 times to assess the effect of this problem; the results for the AFLB and the AFCLT panel are shown in Table 3.16 and 3.17, respectively.

	Reference model	Increased E_2, E_3 and G_{23} of dowel	Difference
f_1	124.9 Hz	135.5 Hz	8.5%
f_2	142.8 Hz	143.0 Hz	0.1%
f_3	159.5 Hz	170.5 Hz	6.9%
f_4	291.8 Hz	318.8 Hz	9.3%
f_5	328.3 Hz	350.1 Hz	6.6%
f_6	364.2 Hz	369.5 Hz	1.5%
f_7	480.3 Hz	528.3 Hz	10.0%

Table 3.16: Effect of increase of moduli E_2, E_3 and G_{23} of dowel on frequencies of the AFLB

Mode	Reference model	Increased E_2, E_3 and G_{23} of dowel	Difference
(1,1)	20.9 Hz	22.3 Hz	6.7%
(2,0)	56.5 Hz	62.5 Hz	10.6%
(0,2)	56.9 Hz	62.2 Hz	9.3%
(2,1)	66.1 Hz	72.1 Hz	9.1%
(1,2)	69.4 Hz	74.5 Hz	7.3%
(2,2)	104.9 Hz	114.3 Hz	9.0%
(3,0)	116.2 Hz	129.6 Hz	11.5%
(3,1)	128.4 Hz	141.6 Hz	10.3%
(3,2)	162.0 Hz	178.1 Hz	9.9%

Table 3.17: Effect of increase of moduli E_2, E_3 and G_{23} of dowel on frequencies of the AFCLT panel

It can be observed that the effect of dowel's moduli E_2, E_3 and G_{23} on frequencies of the AFLB and the AFCLT panel is moderate. However, the 5% criterion is not met. It means that the standard first order beam theory leads to a moderate error in this case. However, the result is not so bad, showing the prospect of using beam elements to model the dowel. Refining the beam theory can improve the result and it will be a perspective of this research.

Another key issue is the connection between dowel and layer in the FE model. If dowel is modelled by beam elements, it is not easy to constrain beam element to either solid or shell element of layer. The difficulty in beam-to-solid constraint is the difference between the DOFs of beam element and that of solid element. The rotational DOFs of the beam elements cannot naturally interact with DOFs of solid elements. If the layer is modelled by conventional shell elements, the DOFs of the shell element are compatible with beam element but the difficulty is how to model the connection between dowel and layer through the thickness of a given layer. Because in this case, the geometry of the layer is defined by the mid-surface of the layer

and the thickness of layer is defined by section property of shell element, not by a 3D geometry of the layer.

Figure 3.31 shows a simplified FE model that uses beam and shell elements to model dowel and layer, respectively. The holes in the layers are necessary to ensure the mesh meets convergence conditions. Indeed, if the hole is reduced to a point, the connection between the dowel and the hole becomes a point-to-point constraint, which leads to stress concentration at this point and makes the model unstable. Point-to-point approach was also reported to destabilize the FE model for two plates assembled by spot welds (Lardeur *et al.* (2000), (2012b)). In the simplified FE model, the link between all nodes in the hole and all beam nodes within the thickness of layer is rigid except at interfaces between layers (Figure 3.32).

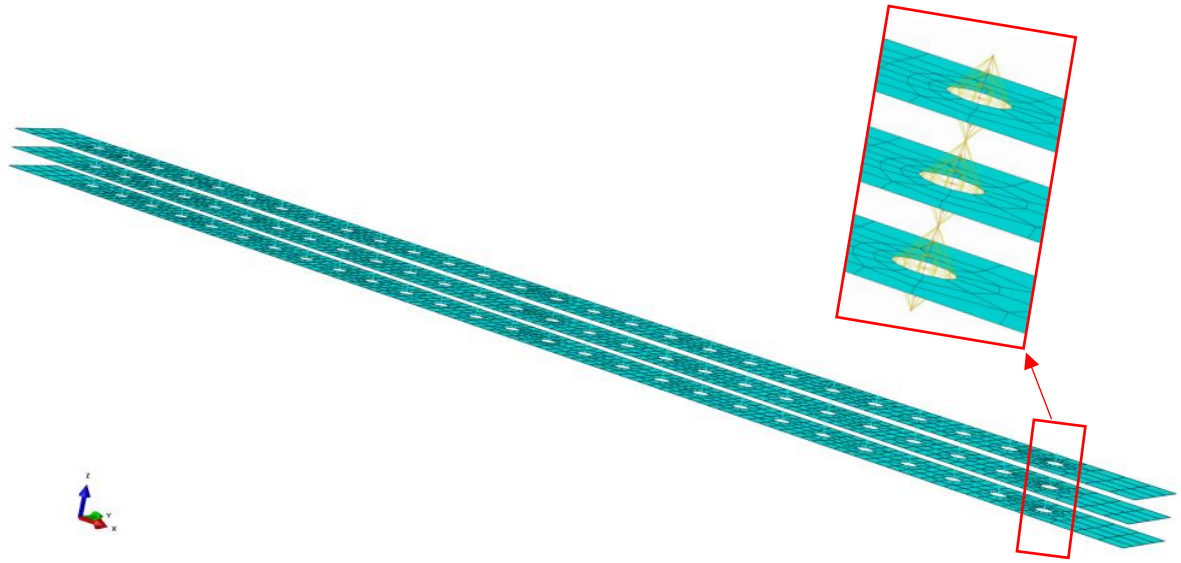

Figure 3.31: Simplified FE model of AFLB using beam and shell elements

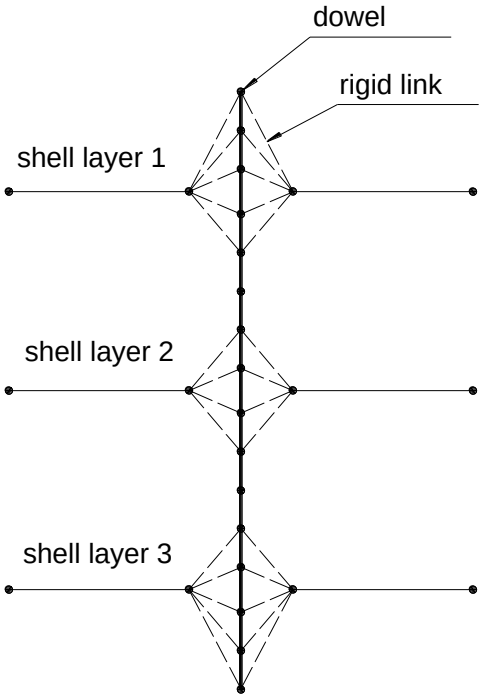

Figure 3.32: Connection detail between layers and dowel

Table 3.18 compares converged frequencies from the simplified FE model and that from the 3D solid model. The simplified FE model is too rigid compared to the reference model due to the rigid link between shell nodes and beam nodes. By using the elastic link (such as a spring or flexible beam element) between the dowel and the layer, the stiffness of the simplified FE model can be tuned to be close to the stiffness of the reference model. However, it is necessary to tune the properties of these springs or beams for each new design, for example when we change the dimension of the multilayered timber structure. Therefore, this approach can't be predictive and has not been chosen for further development.

	Reference model (3D solid model)	Simplified FE model (using beam and shell elements)	Difference
f_1	124.9 Hz	139.0 Hz	11.3%
f_2	142.8 Hz	143.1 Hz	0.2%
f_3	159.5 Hz	175.8 Hz	10.2%
f_4	291.8 Hz	338.5 Hz	16.0%
f_5	328.3 Hz	372.9 Hz	13.6%
f_6	364.2 Hz	370.0 Hz	1.6%
f_7	480.3 Hz	566.1 Hz	17.9%

Table 3.18: Comparison between 3D solid model and simplified FE model uses beam and shell elements

In summary using beam elements to model dowels leads to several difficulties. Consequently, solid element is selected to model dowel in the simplified FE model. The proposed simplified model is presented below.

3.6.2 Simplifying layer by shell elements

Shell elements are suitable to model the layers because these layers have one dimension small compared with the others. Among them, 4-node shell element of Abaqus with reduced integration, called S4R element, is efficient for bending problems (Laulusa *et al.* (2006)). Moreover, the reduced integration of S4R element leads to low computational cost. Therefore, S4R element is chosen for the simplified FE model. Dowel is modelled by twenty-node brick element C3D20R with reduced integration. Specific relations between the degrees of freedom of shell elements and solid elements are necessary, at the interface between the two types of elements. The constraint between layer's elements and dowel's elements is shell-to-solid coupling, which is available in Abaqus/Standard. It couples the motion of shell's nodes around the hole to the motion of nodes on a solid surface lying within a region corresponding to the thickness of shell element. The simplified FE model of AFLB is shown in Figure 3.33.

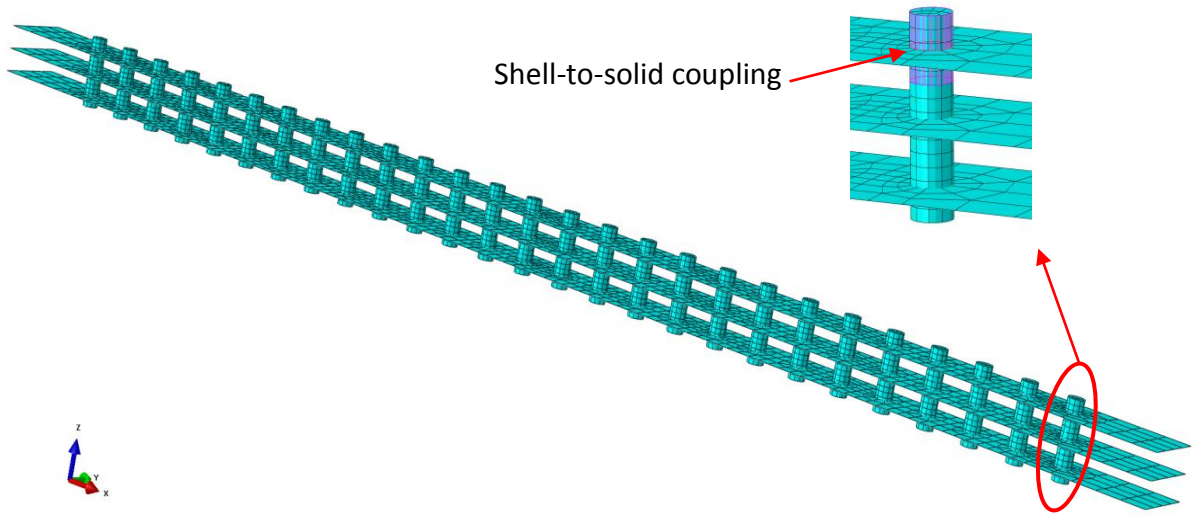

Figure 3.33: Simplified FE model of AFLB using shell elements to model layers

	Reference model	Simplified model	Difference	MAC
f_1	124.9 Hz	122.1 Hz	-2.2%	1
f_2	142.8 Hz	141.8 Hz	-0.7%	1
f_3	159.5 Hz	154.7 Hz	-3.0%	1
f_4	291.8 Hz	280.2 Hz	-4.0%	1
f_5	328.3 Hz	317.2 Hz	-3.4%	1
f_6	364.2 Hz	360.3 Hz	-1.1%	1
f_7	480.3 Hz	458.2 Hz	-4.6%	1

Table 3.19: Comparison between results from the simplified model and the reference model for AFLB

The simplified model of the AFLB provides convergent results with 127,263 DOFs, which is equal to 55% of the number of DOFs of the reference model. Converged frequencies from the simplified FE model of the AFLB are shown in Table 3.19. MAC values and small difference between two models indicate good performance of the simplified model. The frequency error shows that the global stiffness of the AFLB in the simplified model is slightly smaller than that in the reference model. The reason is that the shell-to-solid coupling reduces the stiffness of the dowel. Comparing strain of dowels in the two models in Figure 3.34, it can be seen that the dowel in the simplified model is more flexible. According to Dassault Systèmes Simulia Corp (2014), the local stress and displacement fields in the region of the shell-to-solid interface may be inaccurate. Because the shell-to-solid coupling computes the motion for solid nodes based on the motion of shell node and weight factors. The weight factor is an assumption of the distribution of force and moment from the shell node to each solid node lying within the influence region of shell. This assumption may be inaccurate with the dowel because some solid nodes are located between two layers and are affected by both layers. The imperfection of shell-to-solid coupling was also reported in Guinard *et al.* (2018). Anyway, error of the simplified model is acceptable. A perspective of this research could be to propose a specific shell-to-coupling technique dedicated to this type of structures.

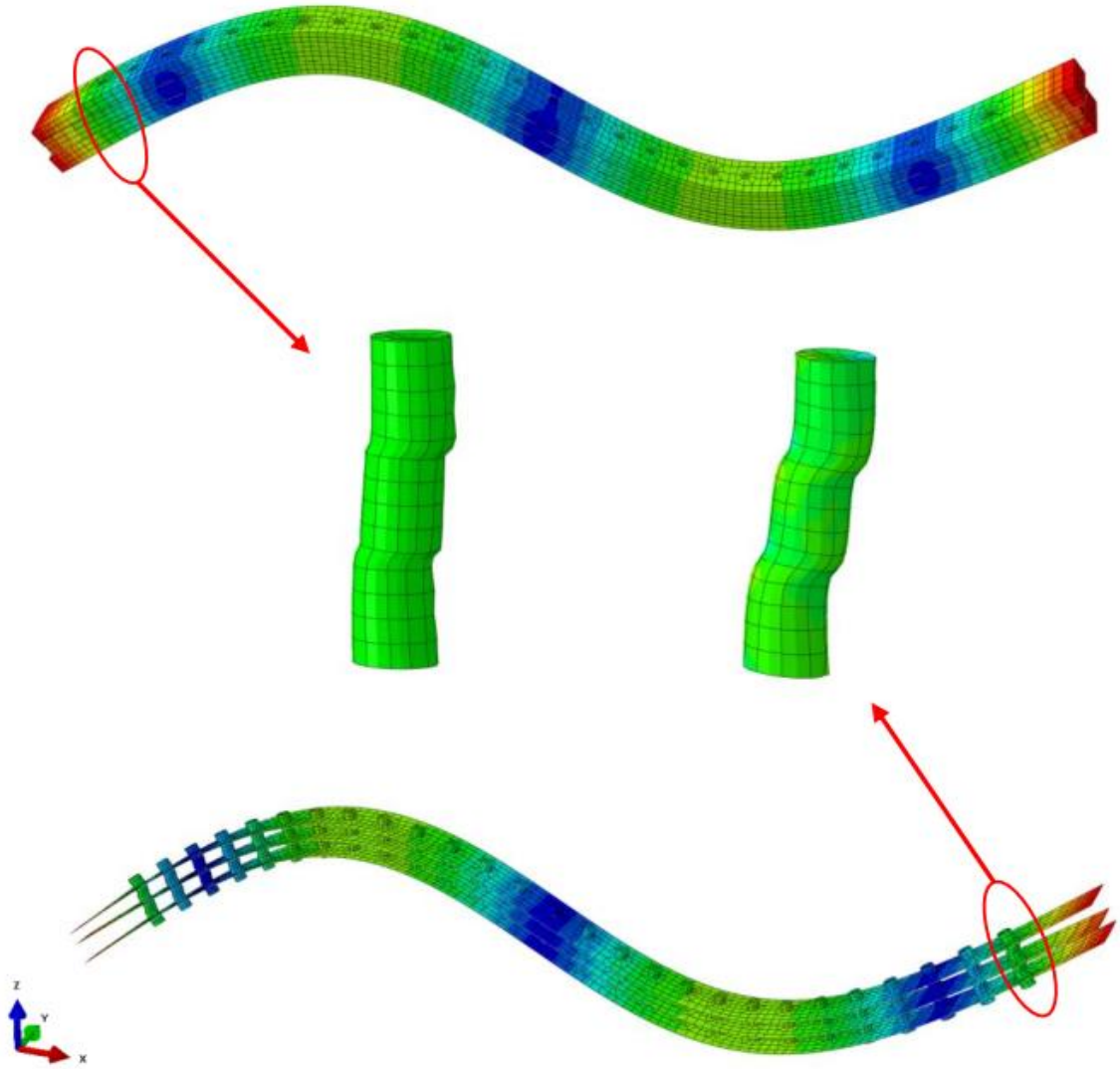

Figure 3.34: Comparison between mode shape from simplified model and mode shape from reference model

3.6.3 Simplifying shape of dowel

The model of dowel has high number of elements because of circular shape of dowel. Therefore, the number of dowel's elements will be reduced if we change dowel's shape from circular to square. The square dowel must have cross-section area as well as second moment of inertia similar with that of the original dowel. Hence, the dimensions of square dowel are 14 mm x 14 mm x 67.5 mm (Figure 3.35).

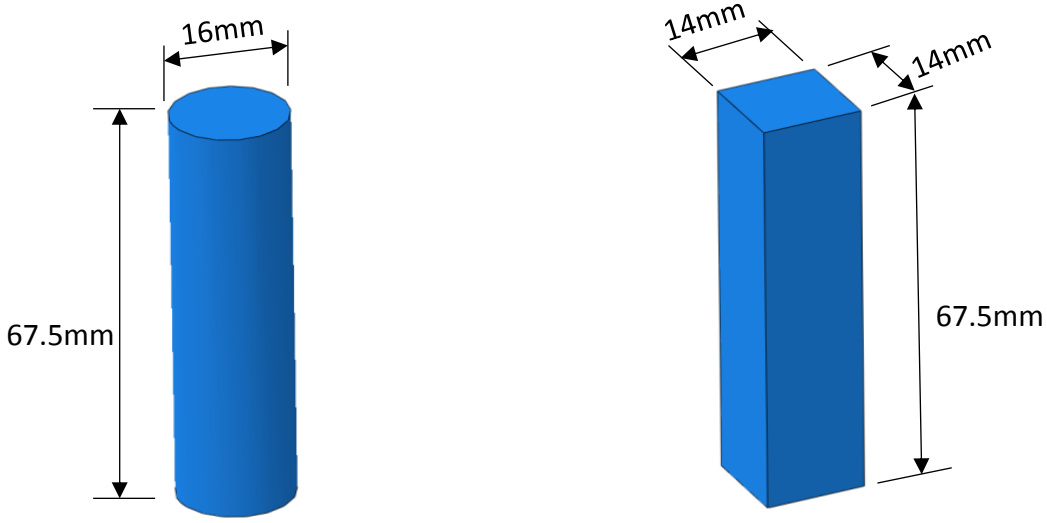

Figure 3.35: Dimensions of original dowel (a) and square dowel (b)

3D model of the AFLB with square dowels is displayed in Figure 3.36. Its converged mesh includes a total of 8856 elements with 165,528 DOFs. It consists of 108 elements per square dowel, compared with 252 elements per circular dowel in the reference model. Convergent results of the 3D model with square dowels are compared with that of the reference model in Table 3.20. The differences on frequencies and MAC values show a negligible effect of dowel shape on global stiffness of the AFLB. Therefore, this simplification can be combined with shell model for the layers to achieve minimum computational cost.

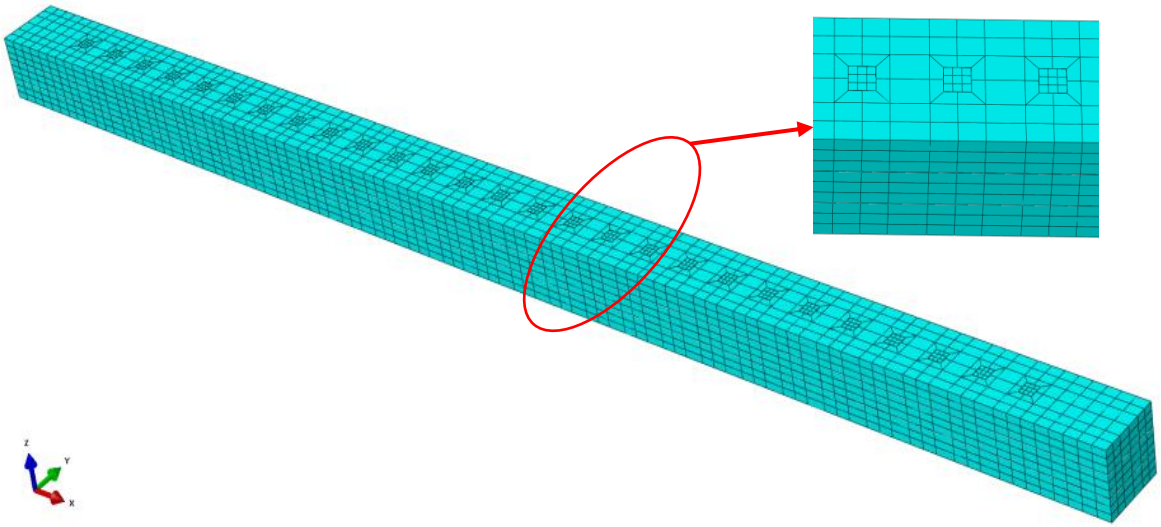

Figure 3.36: 3D model of AFLB with square dowels

	Reference model	3D model with square dowels	Difference	MAC
f_1	124.9 Hz	125.3 Hz	-0.3%	1
f_2	142.8 Hz	142.9 Hz	0.1%	1
f_3	159.5 Hz	159.4 Hz	-0.1%	1
f_4	291.8 Hz	293.0 Hz	-0.4%	1
f_5	328.3 Hz	328.0 Hz	-0.1%	1
f_6	364.2 Hz	364.5 Hz	0.1%	1
f_7	480.3 Hz	482.6 Hz	-0.5%	1

Table 3.20: Comparison between results from the 3D square-dowel model and the reference model for AFLB

Figure 3.37 shows proposed simplified FE model of the AFLB, which uses shell elements to model layers and simplified dowel shape. Shell-to-solid coupling technique is used again in this model. Convergence requires 75,708 DOFs, which is 33% of the number of DOFs of the reference model. Convergent results from this model are compared with that from the reference model in Table 3.21. It can be seen that performance of the proposed simplified FE model is acceptable. However, dowel model still requires a high number of elements for mesh convergence. The number of elements by dowel can be reduced by using solid-beam elements, which combine advantages of both solid and beam elements. A solid-beam element has a three-dimensional geometry like a solid element but uses beam theory. At the moment, the literature about this type of element is very lacking. Frischkorn and Reese (2013), (2015) developed a solid-beam element and used it for medical applications. The development of solid-beam element is an interesting and useful perspective for modeling dowels in multilayered timber structures.

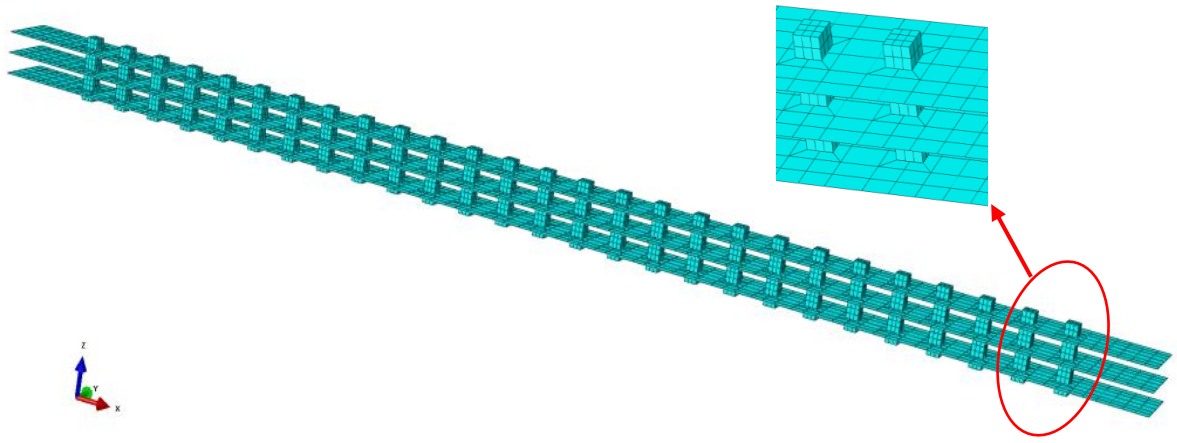

Figure 3.37: Proposed simplified FE model of AFLB

	Reference model	Proposed simplified FE model	Difference	MAC
f_1	124.9 Hz	121.5 Hz	-2.7%	1
f_2	142.8 Hz	141.8 Hz	-0.7%	1
f_3	159.5 Hz	153.8 Hz	-3.6%	1
f_4	291.8 Hz	278.1 Hz	-4.7%	1
f_5	328.3 Hz	316.5 Hz	-3.6%	1
f_6	364.2 Hz	361.2 Hz	-0.8%	1
f_7	480.3 Hz	453.5 Hz	-5.6%	1

Table 3.21: Comparison between results from the proposed simplified FE model and the reference model for AFLB

3.6.4 Computational cost effect

The proposed simplified FE model of full-size AFCLT panel is shown in Figure 3.38. The number of elements in converged mesh and computational cost of the proposed simplified model is compared with that of the reference model in Table 3.22. The convergent results of the two models are compared with each other in Table 3.23. It can be seen that performance and computational cost of the proposed simplified model is good.

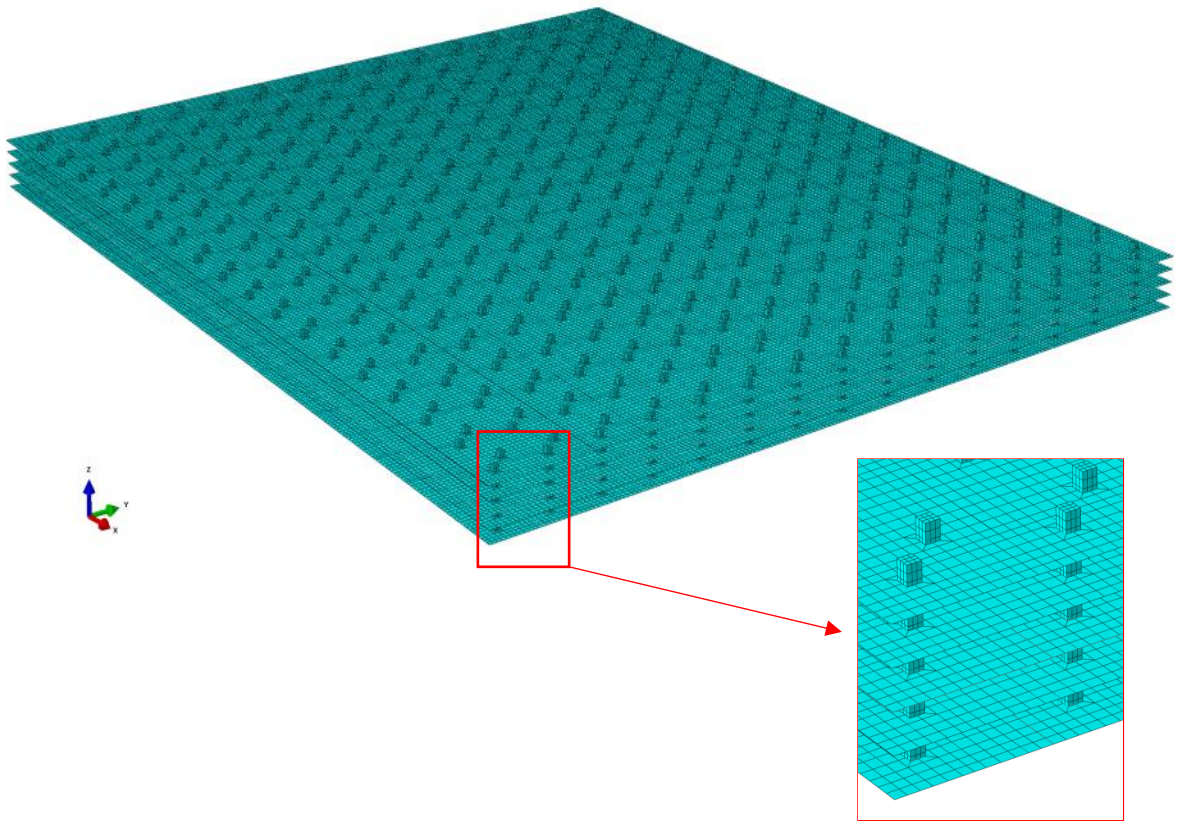

Figure 3.38: Proposed simplified FE model for full-size AFCLT panel

	Reference model	Proposed simplified FE model	Gain
Number of DOFs	6,074,208	2,125,972	65%
Computational cost	10,988 seconds	4,065 seconds	63%

Table 3.22: Comparison of computational cost between the proposed simplified FE model and the reference model for full-size AFCLT panel

	Reference model	Proposed simplified FE model	Difference	MAC
f_1	11.0 Hz	10.6 Hz	-3.6%	1
f_2	24.2 Hz	23.3 Hz	-3.7%	1
f_3	27.6 Hz	26.3 Hz	-4.7%	1
f_4	35.3 Hz	33.5 Hz	-5.1%	1

Table 3.23: Comparison between results from the proposed simplified FE model and the reference model for full-size AFCLT panel

3.7 Academic contribution

A 3D solid FE model was developed to predict vibrational characteristics of the AFLB and the AFCLT panel. Verification and Validation methodology was applied to evaluate the performance of the model. Due to the uncertainty in mechanical properties of wood, a sensitivity analysis was performed to know whether the different parameters have a significant influence on the result obtained from the FE model. A parametric study was performed to optimize the stiffness of the full-size AFCLT panel.

A simplified FE model was proposed to reduce the computational cost. The difficulties of simplifying the dowel were reported, thus suggesting a perspective for solid-beam element.

3.8 Conclusion

3D solid FE model was developed to simulate the single layer beam, the AFLB as well as the AFCLT panel. Verification and Validation methodology was applied to evaluate the performance of the model. A good agreement between numerical and experimental frequencies and mode shapes was observed.

The 3D solid model was then used to predict the vibration performance of the full-size AFCLT panels under simply supported conditions. The predicted results were compared with three vibrational serviceability requirements of the Eurocode 5. The results indicated that vibrational performance of full-size AFCLT panel satisfies all design requirements.

A parametric study was carried out to optimize the connection design of full-size AFCLT panel. The results show that the AFCLT panel assembly with 30-degree dowels has highest stiffness.

Finally, a simplified FE model was developed for the full-size AFCLT panel to reduce computational cost. The layers are modelled by shell S4R elements. The dowels with effective square cross section are modelled by quadratic solid C3D20R elements. The connection between dowel and layer is insured by shell-to-solid coupling. The simplified model provides acceptable performance compared with the reference model. However, dowel model still requires high number of elements for mesh convergence. The solid-beam element can be developed for the dowel model in perspective in order to reduce the FE model size of multilayered timber structures.

Chapter 4:
Variability with MSP

The Modal Stability Procedure (MSP) is developed in this chapter in order to study numerically the variability of natural frequencies of the multilayer timber structures assembled by compressed wood dowels. The MSP is compared with the FE analysis in the nominal case of the single layer beam, the AFLB and the AFCLT panel. Then, the statistic results (mean value, standard deviation, coefficient of variation and distribution) obtained from the MSP are compared with the results from the reference method (direct Monte Carlo simulation) and experimental results. An error estimator is discussed to approximately evaluate the error between the MSP and the direct Monte Carlo simulation with a small number of trials. Variability of the fundamental frequency of the full-size AFCLT panels under different conditions is predicted by the MSP. The design of the full-size AFCLT panels has been improved to meet the requirement of Eurocode 5 thanks to the MSP. Finally, the comparison of computational cost between the MSP and the direct Monte Carlo simulation is presented.

4.1 Introduction

Physical reality is always associated with uncertainty, especially for timber structures. From experimental results (Chapter 2), it can be observed that vibration behavior of the AFLB and the AFCLT panels exhibit high variability. There are many sources which may cause variability of the multilayered timber structures. On the one hand, the mechanical properties, namely the elasticity properties and the density of timber material, which govern the vibration behavior, exhibit high variability. Moreover, the manufacture imperfections may induce an additional source of variability. Therefore, studying the variability of the multilayered timber structures is important, in order to improve the predictive capabilities of the FE models and avoid large experimental campaigns.

The variability can be taken into account by considering that some input parameters are not deterministic. Consequently, the output quantities of the numerical model are not deterministic, either. Several non-deterministic methods have been developed up to now and a short overview is presented below.

4.1.1 Short overview on non-deterministic methods

According to Mace *et al.* (2011), the variability studies can be distinguished in two categories: possibilistic approach and probabilistic approach.

In the possibilistic approach, minimal and maximal values of input parameters are taken into account, in order to identify the minimal and maximal values of the output quantities of interest. For a better reading on the possibilistic methods, the readers can refer to Moens and Vandepitte (2005); Massa *et al.* (2009); Moens and Hanss (2011).

For the probabilistic approach, the input parameters are defined by statistical law (the distribution type, the mean value and the standard deviation). In this case, the statistical characteristics of the output quantities are the targets. The direct Monte Carlo Simulation (MCS) is a robust probabilistic method. In this method, a large number of trials are performed with random input values in order to estimate the statistical characteristics of the output quantities. This method was used to study the response of a timber footbridge with uncertain material properties under the walking load (García *et al.* (2019)).

However, direct MCS requires thousands of trials to obtain convergence. Therefore, the direct MCS is computationally expensive, especially when applied to large size FE models. In this context, a lot of studies has been performed to reduce the number of trials or to improve the computational efficiency of each trial. Among the techniques proposed to reduce the number of trials, one can find Latin hypercube sampling in Helton and Davis (2003), importance sampling in Schuëller *et al.* (1989), reliability approaches in Ditlevsen and Madsen

(1996), meta-models in Pichler *et al.* (2012) and component mode synthesis in Hinke *et al.* (2009). The perturbation method based on the Taylor series expansion is also used for variability calculation. The first order perturbation in finite element models was introduced by Cambou (1975). Then, the second order and the nth order perturbations were proposed to improve the results (Kaminski (2001), (2013)). Other methods are summarized in Schuëller (1997); Elishakoff and Ren (2003); Stefanou (2009); Daouk *et al.* (2015).

In the context of multilayered timber structures, there are many probabilistic studies (Köhler *et al.* (2007); Fink *et al.* (2015); Kandler *et al.* (2015); Kandler and Füssl (2017); Pech *et al.* (2019)). However, a probabilistic method that provides accurate results with an efficient computational cost and that meets the following conditions is required:

- relevant for small or large size models;
- relevant for a small or large number of random variables;
- relevant for a low or high level of variability;
- compatible with any standard finite element software (Nastran, Abaqus, Ansys...);
- compatible with any type of distribution of random variables or random fields.

The Modal Stability Procedure (MSP) has been developed to study the variability of natural frequencies of structures. Many studies (Martini (2008); Arnoult *et al.* (2011); Lardeur *et al.* (2012a); Druesne *et al.* (2014); Hallal (2014); Hamdaoui *et al.* (2015); Druesne *et al.* (2016); Yin *et al.* (2018)) confirmed that the MSP provides good results with cheaper computational cost than the direct MCS, even if the number of random variables or degrees of freedom is large.

4.1.2 Presentation of the Modal Stability Procedure (MSP)

The MSP method is based on a mechanical assumption: the mode shapes are independent of uncertain input parameters. In the general case, the modal shapes may be uncertain. Therefore, the assumption is generally not exactly met. Many studies (Druesne *et al.* (2014), (2016)) compared nominal and perturbed mode shapes by the Modal Assurance Criterion (MAC). For real industrial cases as a car body, this assumption was assessed. It could be observed, in the context of a Monte Carlo simulation, that for some trials, the modal shapes are relatively uncertain. But the mean MAC value is good and therefore the modal stability assumption is quite robust from a statistical point of view. In some particular cases, this assumption is exactly met, leading to an exact method.

Thanks to the modal stability assumption, only one finite element analysis is required to extract the nominal mode shapes and modal strains. Based on these information as well as the MSP assumption, a MSP metamodel of natural frequencies is created. Uncertain material properties are modeled by random variables or random fields. Then a MCS is performed on

the MSP metamodel, allowing the evaluation of perturbed natural frequencies for each trial. The variability (mean value, standard deviation, coefficient of variation and distribution) of natural frequencies can subsequently be obtained. The flowchart of the MSP is given in Figure 4.1.

Our proposal is to exploit the MSP to study the variability of natural frequencies of multilayered timber structures with uncertain material properties. The MSP formulations for bar, beam and shell elements have been described by Martini (2008) and Arnoult *et al.* (2011). Hallal (2014) developed the formulation for 8-node linear solid element. However, the MSP for 20-node solid element does not exist. Therefore, it is necessary to develop MSP for 20-node solid element. The formulation and results obtained are described in this chapter.

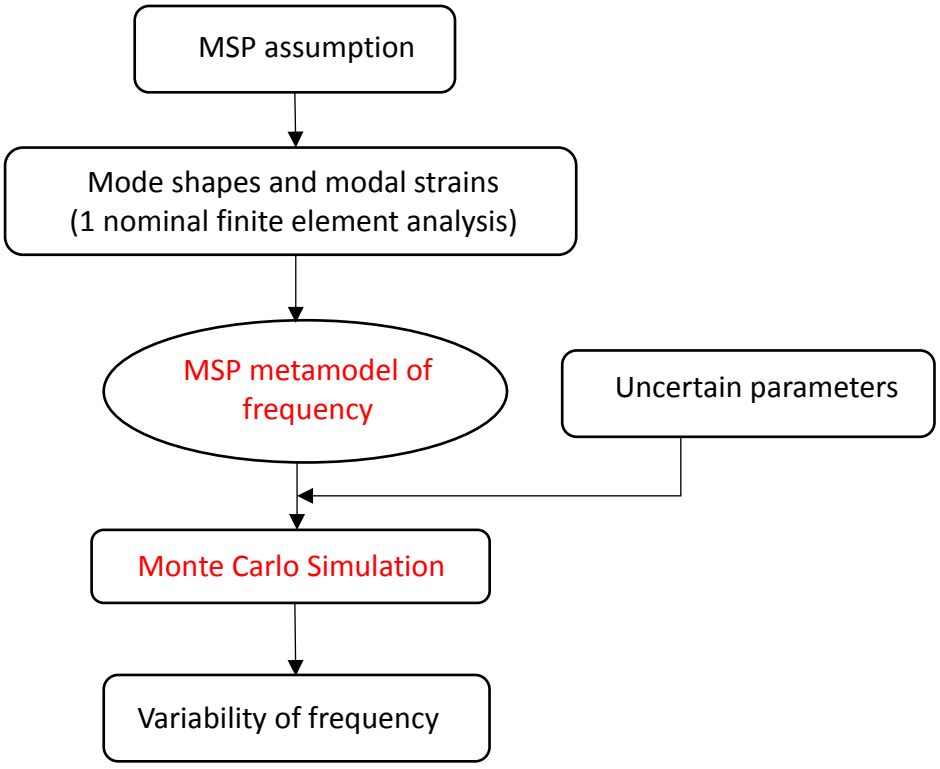

Figure 4.1: Flowchart of the MSP (Yin *et al.* (2018))

4.2 General MSP formulation

The deterministic natural value problem for finite element dynamic analysis is described by the following equation, the subscript "0" defining the nominal case:

$$K_0\Phi_0 = M_0\Phi_0\Lambda_0 \tag{4.1}$$

where K_0 and M_0 are the stiffness and mass matrices, respectively, Λ_0 is the diagonal matrix of the natural values and Φ_0 is the modal matrix. For a single mode i, equation 4.1 becomes:

$$K_0\phi_0^i = \lambda_0^i M_0 \phi_0^i \tag{4.2}$$

where λ and ϕ are respectively the eigenvalue and eigenvector. For the perturbed system due to input uncertainties, the solution is given by:

$$K_p\phi_p^i = \lambda_p^i M_p \phi_p^i \tag{4.3}$$

where the subscript "p" denotes the perturbed case. From the matrix perturbation theory (Yang *et al.* (2001)), the perturbed eigenvector can be written as:

$$\phi_p = \phi_0 + \Delta\phi_p \tag{4.4}$$

Considering the expression of the Rayleigh quotient and Equation 4.4, the perturbed natural angular frequency ω_p can be written as:

$$\omega_p^2 = \lambda_p = \frac{\left(\phi_0 + \Delta\phi_p\right)^T K_p \left(\phi_0 + \Delta\phi_p\right)}{\left(\phi_0 + \Delta\phi_p\right)^T M_p \left(\phi_0 + \Delta\phi_p\right)} \tag{4.5}$$

According to the modal stability assumption $\Delta\phi_p = 0$, one can write:

$$\omega_p^2 = \frac{\phi_0^T K_p \phi_0}{\phi_0^T M_p \phi_0} \tag{4.6}$$

where the presence of variability is kept only on the stiffness matrix K_p and the mass matrix M_p. Extracting perturbed matrices K_p and M_p at each MCS trial is an expensive operation and may be impossible with many standard finite element software. In order to avoid this operation, terms of Equation 4.6 can be expressed as a summation over the n elements of the finite element model as follows:

$$\omega_p^2 = \frac{\sum_{j=1}^{n} \phi_{0j}^T k_{pj} \phi_{0j}}{\sum_{j=1}^{n} \phi_{0j}^T m_{pj} \phi_{0j}} \tag{4.7}$$

where ϕ_{0j}, k_{pj} and m_{pj} are the nominal eigenvector, stiffness matrix and mass matrix for the *j*th element, respectively. Extracting matrices k_{pj} and m_{pj} is also a difficult task with many finite element software. Moreover, parameters of interest of the stiffness matrix are not always easy to isolate. However, the numerator of Equation 4.7 is the expression of the elementary internal strain energy. The elementary internal strain energy π_{int}^{elem} can be expressed as the integration over the elementary volume V_{pj} of the product of the stresses by the deformations:

$$\pi_{int}^{elem} = \frac{1}{2}\phi_{0j}^T k_{pj} \phi_{0j} = \frac{1}{2}\int_{V_{pj}} \sigma_{pj}\varepsilon_{pj} dV \tag{4.8}$$

where V_{pj} is the finite element volume, σ_{pj} is the elementary modal stress vector and ε_{pj} is the elementary modal strain vector. In the elastic domain, the modal stress and strain vectors are related by the generalized Hooke's law:

$$\sigma_{pj} = C_{pj}\varepsilon_{pj} \tag{4.9}$$

where C_{pj} is the constitutive law matrix for the *j*th element. According to Equations 4.8 and 4.9, Equation 4.7 can be transformed into:

$$\omega_p^2 = \frac{\sum_{j=1}^{n} \int_{V_{pj}} \varepsilon_{pj}^T C_{pj} \varepsilon_{pj} dV}{\sum_{j=1}^{n} \phi_{0j}^T m_{pj} \phi_{0j}} \tag{4.10}$$

4.3 Development of MSP formulation for 20-node hexahedral solid element

In Equation 4.10, the numerator is the sum of elementary strain energy over each element while the denominator is the expression of the modal mass terms. It is worth noting that the MSP formulation is independent of the formulation used for the finite element exploited to calculate the nominal mode shapes (here C3D20R of Abaqus). Only the number of nodes must be the same. Consequently, it is relevant to test several formulations, in order to retain the best compromise. In previous studies (Hallal (2014); Druesne *et al.* (2016)) involving 8-node solid element, it was demonstrated that a simple formulation, with constant strains over one given element and a diagonal matrix, are sufficient. To find the best MSP formula for the 20-node solid element, four formulations to calculate the perturbed angular frequency using Equation 4.10 are proposed:

- Formulation 1: the strains are assumed to be constant for each element, diagonal mass matrix is considered;
- Formulation 2: the strains are considered to be variable for the finite element volume, diagonal mass matrix is considered;
- Formulation 3: the strains are assumed to be constant for each element, consistent mass matrix is considered;
- Formulation 4: the strains are considered to be variable for the finite element volume, consistent mass matrix is considered.

In formulation 1, the strains are extracted at the centre of each element and so the strain energy (numerator of Equation 4.10) is easily integrated over each element by multiplying the product of stresses and strains by the volume V_{pj} of the element. The mass matrix of the 20-node solid element is a diagonal matrix with:

$$m_{pj} = \rho_{pj}\left(\frac{V_{pj}}{20}\right) I \tag{4.11}$$

where ρ_{pj} is the perturbed elementary mass density and I is a (60x60) diagonal identity matrix.

In formulation 2, the calculation of mass matrix is similar with that in formulation 1, the elementary strain energy is calculated by numerical integration. To calculate the integral of the terms of Equation 4.10, the reference element is used. Figure 4.2 describes the 20-node hexahedral element in its reference coordinate system V_{ref} and its physical coordinate system V_{phy}. The integral over the element volume is performed numerically using 8 integration points:

$$\int_{V_{pj}} \varepsilon_{pj}^T C_{pj} \varepsilon_{pj} dV = \iiint_{-1}^{1} \varepsilon_{pj}^T C_{pj} \varepsilon_{pj} det(J) d\xi d\eta d\zeta \approx \sum_{k=1}^{8} \varepsilon_{pjk}^T C_{pj} \varepsilon_{pjk} det(J_k) w_k \tag{4.12}$$

where w_k are weighting factors, equal to 1 in the case of 8 integration points. The Jacobian matrix J of the geometric transformation is as follows:

$$J = \begin{bmatrix} \frac{\partial x}{\partial \xi} & \frac{\partial y}{\partial \xi} & \frac{\partial z}{\partial \xi} \\ \frac{\partial x}{\partial \eta} & \frac{\partial y}{\partial \eta} & \frac{\partial z}{\partial \eta} \\ \frac{\partial x}{\partial \zeta} & \frac{\partial y}{\partial \zeta} & \frac{\partial z}{\partial \zeta} \end{bmatrix} \tag{4.13}$$

In the case of linear elasticity for an orthotropic material, the matrix C_{pj} is as follows:

$$C_{pj} = \begin{bmatrix} E_1(1-\nu_{23}\nu_{32})\Upsilon & E_2(\nu_{12}+\nu_{13}\nu_{32})\Upsilon & E_3(\nu_{13}+\nu_{12}\nu_{23})\Upsilon & 0 & 0 & 0 \\ & E_2(1-\nu_{13}\nu_{31})\Upsilon & E_3(\nu_{23}+\nu_{21}\nu_{13})\Upsilon & 0 & 0 & 0 \\ & & E_3(1-\nu_{12}\nu_{21})\Upsilon & 0 & 0 & 0 \\ & & & G_{12} & 0 & 0 \\ & sym & & & G_{13} & 0 \\ & & & & & G_{23} \end{bmatrix} \tag{4.14}$$

where $\Upsilon = \frac{1}{1-\nu_{12}\nu_{21}-\nu_{23}\nu_{32}-\nu_{31}\nu_{13}-2\nu_{21}\nu_{32}\nu_{13}}$, E_i and G_{ij} are the Young's moduli and shear moduli. ν_{ij} are the Poisson's ratios, ν_{ij} and ν_{ji} are related by $\frac{\nu_{ij}}{E_i} = \frac{\nu_{ji}}{E_j}$.

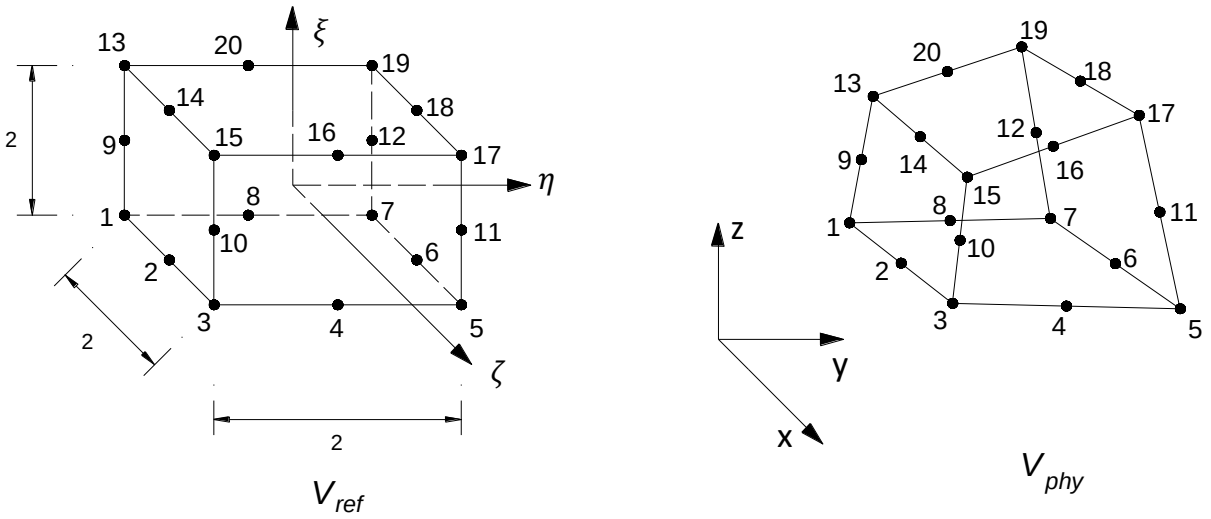

Figure 4.2: Reference and physical coordinate systems of 20-node hexahedral element

In formulation 3, the calculation of strain energy is similar with that in formulation 1, the mass matrix is a consistent matrix with:

$$m_{pj} = \int_{V_{pj}} \rho_{pj}[N]^T[N]dV = \iiint_{-1}^{1} \rho_{pj}[N]^T[N]det(J)d\xi d\eta d\zeta \approx \sum_{k=1}^{8} \rho_{pjk}[N]_k^T[N]_k det(J_k)w_k \tag{4.15}$$

where w_k are weighting factors, equal to 1 in the case of 8 integration points. In the case of 20-node solid element, the matrix of shape functions $[N]$ is as follows:

$$[N] = \begin{bmatrix} N_1 & 0 & 0 & N_2 & 0 & 0 & \cdots & N_{20} & 0 & 0 \\ 0 & N_1 & 0 & 0 & N_2 & 0 & \cdots & 0 & N_{20} & 0 \\ 0 & 0 & N_1 & 0 & 0 & N_2 & \cdots & 0 & 0 & N_{20} \end{bmatrix} \tag{4.16}$$

where the functions N_i are as follows (Dhatt *et al.* (2015)):

- for the vertex nodes:

Node i	1	3	5	7	13	15	17	19
ξ_i	-1	1	1	-1	-1	1	1	-1
η_i	-1	-1	1	1	-1	-1	1	1
ζ_i	-1	-1	-1	-1	1	1	1	1

Table 4.1: Reference coordinates of the vertex nodes

$$N_i = \frac{1}{8}(1+\xi\xi_i)(1+\eta\eta_i)(1+\zeta\zeta_i)(-2+\xi\xi_i+\eta\eta_i+\zeta\zeta_i) \tag{4.17}$$

- for the nodes on the sides parallel to the axis ξ:

Node i	2	6	14	18
ξ_i	0	0	0	0
η_i	-1	1	-1	1
ζ_i	-1	-1	1	1

Table 4.2: Reference coordinates of the nodes on the sides parallel to the axis ξ

$$N_i = \frac{1}{4}(1-\xi^2)(1+\eta\eta_i)(1+\zeta\zeta_i) \tag{4.18}$$

- for the nodes on the sides parallel to the axis η:

Node i	4	8	16	20
ξ_i	1	-1	1	-1
η_i	0	0	0	0
ζ_i	-1	-1	1	1

Table 4.3: Reference coordinates of the nodes on the sides parallel to the axis η

$$N_i = \frac{1}{4}(1+\xi\xi_i)(1-\eta^2)(1+\zeta\zeta_i) \tag{4.19}$$

- for the nodes on the sides parallel to the axis ζ:

Node i	9	10	11	12
ξ_i	-1	1	1	-1
η_i	-1	-1	1	1
ζ_i	0	0	0	0

Table 4.4: Reference coordinates of the nodes on the sides parallel to the axis ζ

$$N_i = \frac{1}{4}(1+\xi\xi_i)(1+\eta\eta_i)(1-\zeta^2) \tag{4.20}$$

In formulation 4, the calculation of strain energy is similar with that in formulation 2 and the calculation of mass matrix is similar with that in formulation 3.

The performance of these four formulations is assessed by a mesh convergence study as well as error between MSP and FE frequencies for one nominal calculation.

4.3.1 MSP mesh convergence

The tests presented in this section are performed in the nominal configuration. This is a necessary step, before using MSP to calculate variability. Mode shapes are calculated thanks to a finite element analysis with Abaqus but frequencies are obtained using equation 4.10.

Figure 4.3 shows the effect of the number of elements on results of MSP for a single layer beam.

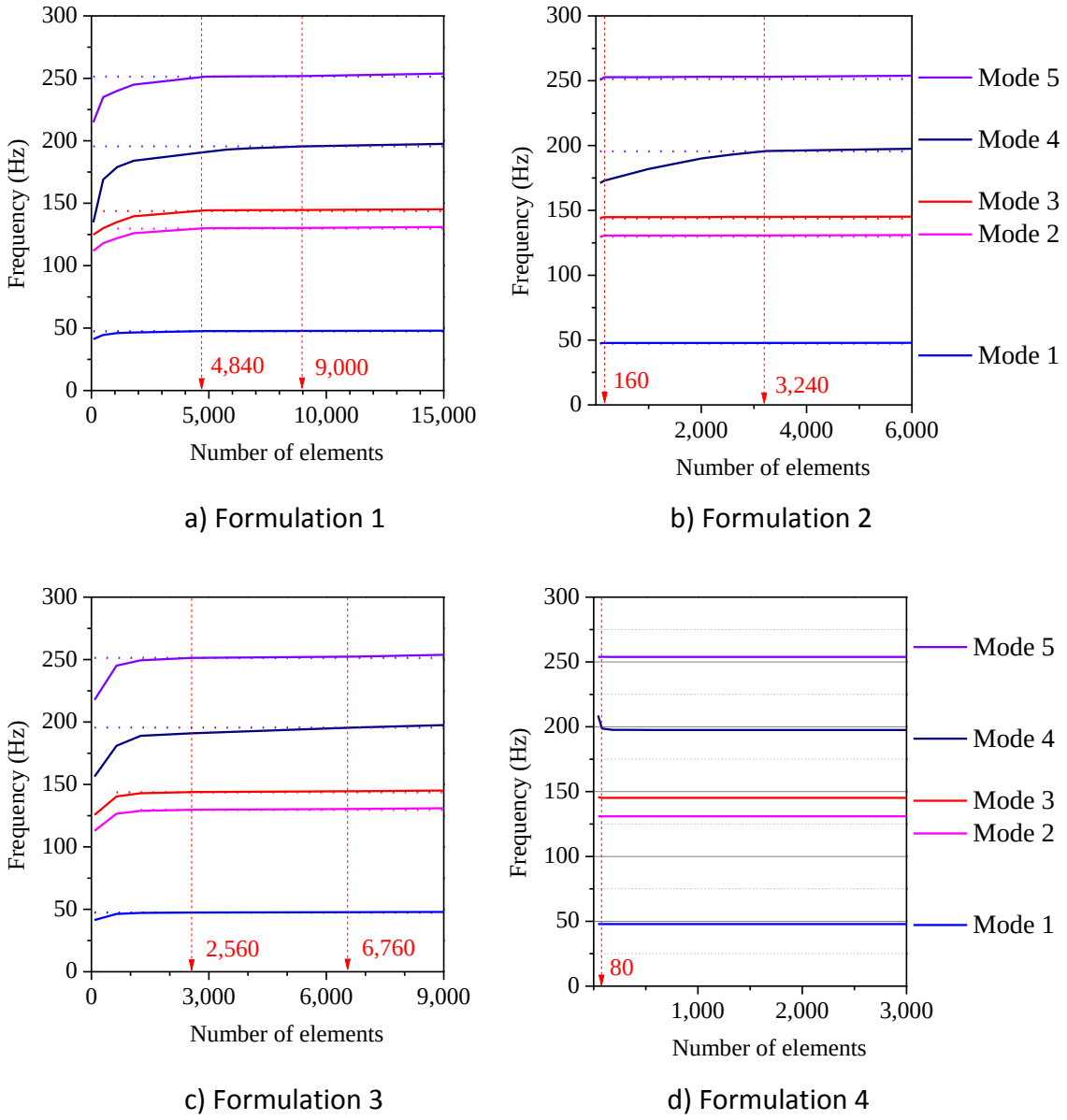

Figure 4.3: Convergence study of MSP nominal frequencies using 4 different formulations

With a convergence criterion of 1%, Figure 4.3 shows that formulation 4 meets the convergence criterion with 80 elements (similar with converged mesh of FE model) while the remaining three formulations require more elements to meet the convergence criterion. Formulation 1 requires 9000 elements while formulation 2 requires 3240 elements and formulation 3 requires 6760 elements. Therefore, both the consistent mass matrix and the variable elementary strains are important for the convergence of the 20-node solid element, especially for the evaluation of torsion frequency (mode 4). In all formulations, the torsion mode (mode 4) requires a higher number of elements than bending modes (modes 1, 2, 3 and 5) to meet the convergence criterion. For example, in formulation 1, the 4th mode requires

9000 elements to be stable, but the 1st, 2nd, 3rd and 5th modes need only 4840 elements. The same trend is observed with the AFLB and the AFCLT panel.

4.3.2 Comparison between MSP and FE model in the nominal case

	FE model	error with FE model			
		Formulation 1	Formulation 2	Formulation 3	Formulation 4
f_1	47.87 Hz	-0.4%	-0.1%	-0.3%	-0.0%
f_2	130.97 Hz	-0.6%	-0.2%	-0.4%	-0.0%
f_3	145.19 Hz	-0.4%	-0.1%	-0.3%	-0.0%
f_4	198.69 Hz	-1.0%	-0.9%	-0.9%	-0.0%
f_5	253.93 Hz	-0.8%	-0.3%	-0.6%	-0.0%

Table 4.5: Comparison of frequencies of single layer beam between FE model and MSP formulations

	FE model	MSP	error
f_1	124.89 Hz	124.88 Hz	0.0%
f_2	142.84 Hz	142.83 Hz	0.0%
f_3	159.50 Hz	159.50 Hz	0.0%
f_4	291.78 Hz	291.76 Hz	0.0%
f_5	328.33 Hz	328.31 Hz	0.0%
f_6	364.24 Hz	364.22 Hz	0.0%
f_7	480.34 Hz	480.29 Hz	0.0%

Table 4.6: Comparison of frequencies of the AFLB between FE model and MSP formulation 4

	FE model	MSP	error
$f_{(1,1)}$	20.92 Hz	20.92 Hz	0.0%
$f_{(2,0)}$	56.45 Hz	56.44 Hz	0.0%
$f_{(0,2)}$	56.94 Hz	56.93 Hz	0.0%
$f_{(2,1)}$	66.10 Hz	66.10 Hz	0.0%
$f_{(1,2)}$	69.44 Hz	69.43 Hz	0.0%
$f_{(2,2)}$	104.89 Hz	104.87 Hz	0.0%
$f_{(3,0)}$	116.24 Hz	116.22 Hz	0.0%
$f_{(3,1)}$	128.41 Hz	128.39 Hz	0.0%
$f_{(3,2)}$	162.02 Hz	161.99 Hz	0.0%

Table 4.7: Comparison of frequencies of the AFCLT panel between FE model and MSP formulation 4

In Table 4.5, the converged frequencies of single layer beam obtained with the four MSP formulations are compared with the frequencies obtained with the FE model. Formulation 4 provides exact results for nominal calculation. The remaining three MSP formulations, however, slightly underestimate the nominal frequencies. However, the error can be reduced when the number of elements is increased. Tables 4.6 and 4.7 confirm that formulation 4 provides very good results for nominal calculation of the AFLB as well as the AFCLT panel. The computational time of one nominal calculation for the AFCLT panel by FE model is 2434 seconds but MSP formulation 4 (using Matlab software) only needs 3.5 seconds. Therefore, formulation 4 is chosen for the MSP to obtain accurate frequencies with small computational cost. On the other hand, the converged frequencies obtained by formulation 2 shows the possibility of using diagonal mass matrix for high order solid element. Indeed, compared to the consistent mass matrix, the diagonal mass matrix can provide quite similar result but requires a higher number of finite elements. Therefore, a perspective of this research can be a modification of the diagonal mass matrix for 20-node solid element in order to improve the mesh convergence.

In summary the MSP formulation 4 has been verified in the nominal case. Very good results have been obtained in comparison with the FE model. The formulation 4 of MSP can now be exploited to calculate variability. At each Monte Carlo trial, Equation 4.21 is used to calculate perturbed natural frequency f_p. The statistical quantities such as mean value, standard deviation, coefficient of variation and distribution can then be evaluated.

$$\omega_p^2 = \left(2\pi f_p\right)^2 = \frac{\sum_{j=1}^{n}\sum_{k=1}^{8} \varepsilon_{pjk}^T C_{pj} \varepsilon_{pjk} det(J_k)}{\sum_{j=1}^{n}\left(\phi_{0j}^T \left(\sum_{k=1}^{8} \rho_{pjk} [N]_k^T [N]_k det(J_k)\right)\phi_{0j}\right)} \tag{4.21}$$

4.4 Uncertain parameters and distribution law

Wood is a natural fibre composite material with uncertainty in mechanical properties such as density, elastic Young's moduli (E_1, E_2 and E_3), Poisson's ratio (ν_{12}, ν_{13} and ν_{23}) and shear moduli (G_{12}, G_{13} and G_{23}). The mean and CoV values of density and E_1 of oak layers from experiments presented in Section 2.4 are chosen to describe input data of MSP and summarised in Table 4.8. The mean and CoV values of properties of compressed wood dowel, which are shown in Table 4.8, are taken from El-Houjeyri *et al.* (2019) and Bouhala *et al.* (2020). For the density the variability level is moderate but it is very large for elasticity moduli. Sensitivity tests from Chapter 3 showed the negligible influence of some properties on the frequencies of timber beam and panel; therefore, these properties were fixed in MSP, which means that possible variability of these properties is neglected. Table 4.9 describes the number of uncertain parameters for single layer beam, AFLB and AFCLT panel. All parameters are considered independent. The number of parameters is limited for the single layer beam

and intermediate for AFLB. On the contrary, this number is very large for the AFCLT panels. The parameter distribution law is assumed to be Gaussian. However, the distribution law is truncated (±3σ) in order to avoid non-physical values (Figure 4.4).

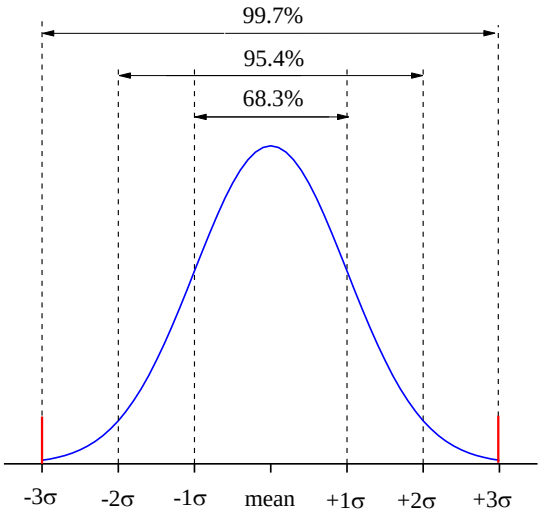

Figure 4.4: Gaussian distribution law

Uncertain parameter	Oak layer				Compressed wood dowel		
	ρ (kg/m^3)	E_1 (GPa)	G_{12} (GPa)	G_{13} (GPa)	ρ (kg/m^3)	E_3 (GPa)	G_{13} (GPa)
Mean	623.9	11.38	1.202	0.922	1133.37	1.082	0.8
CoV	6.5%	13.6%	13.6%	13.6%	4.2%	16.1%	16.1%

Table 4.8: Description of uncertain parameters of oak layer and compressed wood dowel

	Description of the uncertain parameters	Total number of parameters
Single layer beam	ρ, E_1, G_{13}	3
AFLB	(ρ, E_1, G_{12}, G_{13}) x 3 layers (ρ, E_3, G_{13}) x 27 dowels	93
AFCLT panel	(ρ, E_1, G_{12}, G_{13}) x 28 laminae (ρ, E_3, G_{13}) x 196 dowels	700
Full-size AFCLT panel	(ρ, E_1, G_{12}, G_{13}) x 81 laminae (ρ, E_3, G_{13}) x 540 dowels	1944

Table 4.9: Description of the random parameters of single layer beam, AFLB and AFCLT panel

4.5 Assessment of the MSP to calculate variability

4.5.1 Error indicator

The statistical results from MSP method is here compared with that from a reference method for validation purpose. The chosen reference method is the direct MCS using Abaqus for each random trial. The number of random trials for both MCS and MSP methods is 10,000, which is generally necessary and enough to obtain accurate statistical quantities: mean, standard deviation, coefficient of variation and distribution of frequencies (Druesne *et al.* (2014)).

For single layer beam and AFLB, direct MCS with 10,000 trials can reasonably be performed; however, for AFCLT panels the cost of MCS is very high. Therefore, it is necessary to find a way to estimate the error between MSP and direct MCS with small cost. Error indicator was proposed in Yin *et al.* (2018) for this purpose. The flowchart of the error indicator is presented in Figure 4.5. The real error between MSP and direct MCS can be estimated from the error between the two methods with small number of trials using the same input data. For n_t trials, the error between the MSP and the direct MCS is defined by:

$$Err^{n_t} = \frac{R_{MSP}^{n_t} - R_{MCS}^{n_t}}{R_{MCS}^{n_t}} \times 100\% \tag{4.22}$$

where $R_{MSP}^{n_t}$ and $R_{MCS}^{n_t}$ are, respectively, the statistical results (mean value, standard deviation or CoV) obtained by the MSP and the direct MCS with n_t trials.

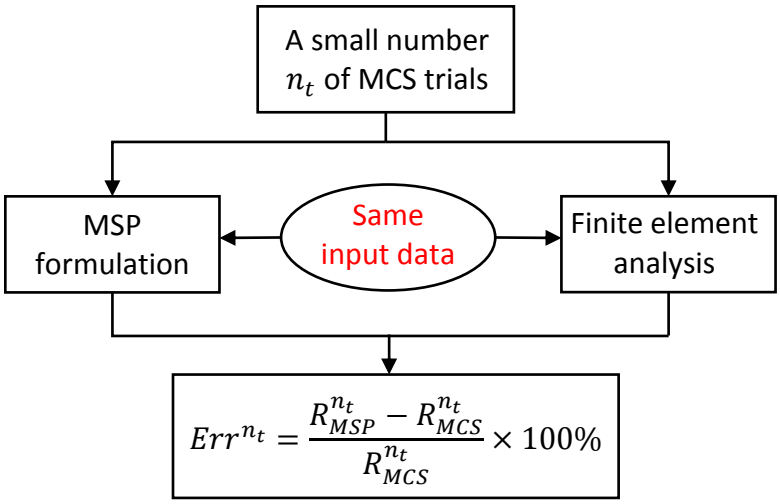

Figure 4.5: Flowchart of the error indicator (Yin *et al.* (2018))

Naturally, the greater the number of trials n_t, the more accurate the estimation error. However, the greater the number of trials n_t, the more expensive cost. Therefore, an optimal value of n_t must be determined. The errors obtained with n_t trials can then be used as an

error indicator. This approach is used here, anyway the influence of the number of trials necessary to obtain an acceptable error estimation has been studied in the context of our timber structures.

4.5.2 Comparison between MSP and direct MCS for single layer beam and AFLB

Figure 4.6 and Table 4.10 compare the results between the MSP and direct MCS (10,000 trials) for single layer beam. It can be observed a very good agreement between MSP and direct MCS. The errors on mean value and standard deviation of the frequencies are close to 0%. These very good results show that in this simple case the MSP assumption is almost met, that is to say the modal shapes are quasi certain. The distributions from MCS and MSP methods are similar, and they are nearly Gaussian ones.

	Mean value			Standard deviation		
	MCS	MSP	Error	MCS	MSP	Error
Frequency 1	46.83	46.83	0.0%	3.47	3.47	0.0%
Frequency 2	128.07	128.07	0.0%	9.41	9.41	0.0%
Frequency 3	143.51	143.60	0.1%	10.68	10.69	0.1%
Frequency 4	194.26	194.29	0.2%	14.76	14.78	0.1%
Frequency 5	248.03	248.06	0.0%	18.95	18.95	0.0%

Table 4.10: Comparison of mean value and standard deviation of frequencies of single layer beams from MSP and direct MCS

	Mean value			Standard deviation		
	MCS	MSP	Error	MCS	MSP	Error
Frequency 1	121.29	122.60	1.0%	5.81	5.62	-3.3%
Frequency 2	139.94	141.53	1.1%	6.65	6.39	-4.1%
Frequency 3	159.51	161.26	1.1%	7.09	6.75	-4.8%
Frequency 4	291.42	295.03	1.2%	11.65	11.06	-5.1%
Frequency 5	328.38	332.32	1.2%	11.82	11.17	-5.5%
Frequency 6	364.85	369.23	1.2%	12.77	12.01	-6.0%
Frequency 7	494.67	500.90	1.3%	17.86	16.73	-6.3%

Table 4.11: Comparison of mean value and standard deviation of frequencies of AFLB from MSP and direct MCS

The comparison between MSP and direct MCS for AFLB are shown in Table 4.11. The number of parameters of AFLB is higher than that of single layer beam leading to a higher error. It should be kept in mind that the variability level of input is high; therefore, the error of MSP is acceptable. One can observe that MSP slightly overestimates the mean frequency, but it underestimates the standard deviation values. The distribution of the first six

frequencies of AFLB is shown in Figure 4.7. As for the single layer beam, the frequencies distributions are close to Gaussian ones, even with higher frequencies. Due to the slight overestimation of the mean frequencies, a systematic limited shift can be observed.

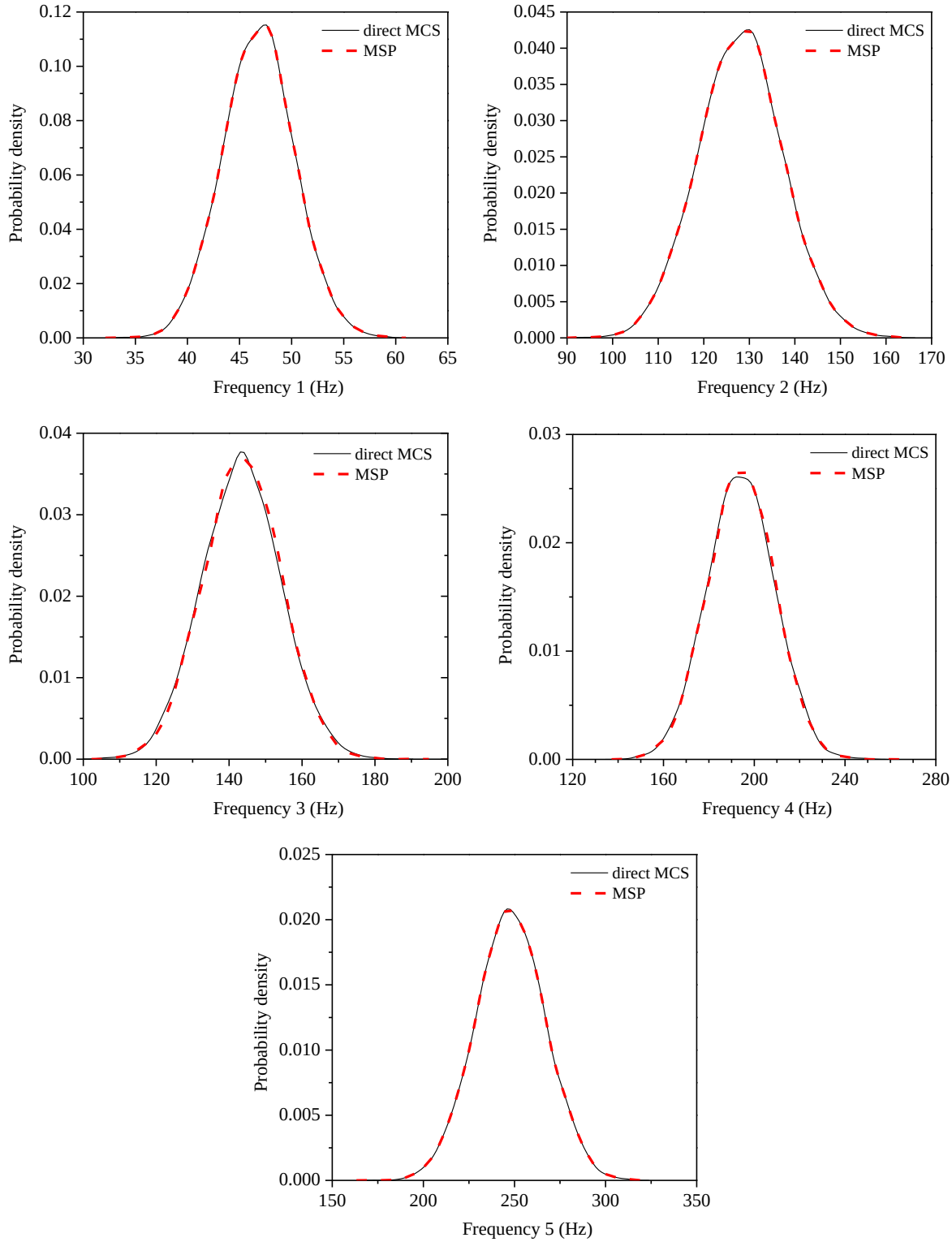

Figure 4.6: Distribution of frequencies of single layer beams

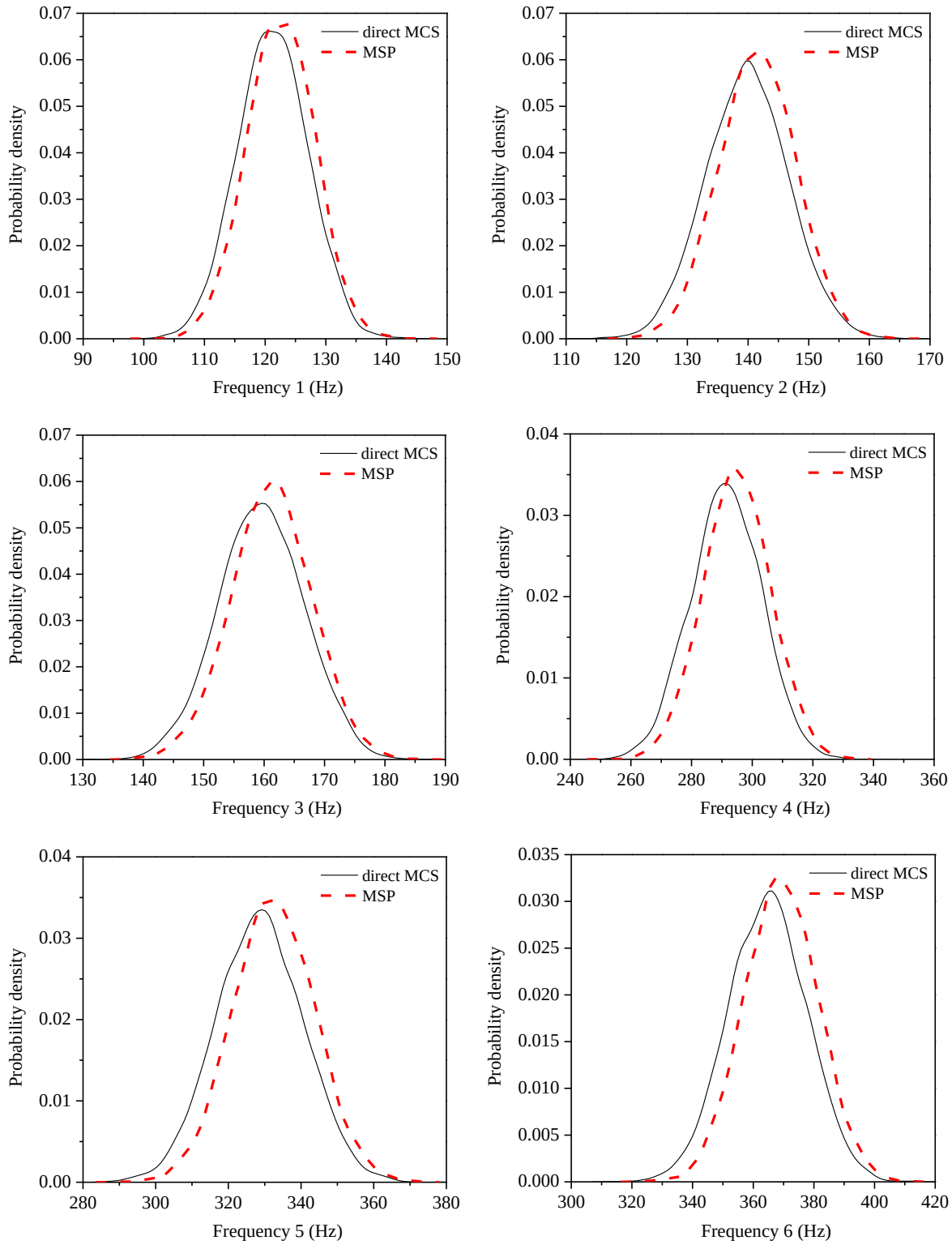

Figure 4.7: Distribution of frequencies of AFLB

In order to select the optimal number of trials for the error indicator, figure 4.8 shows the influence of the number of trials n_t on the error between MSP and direct MCS in case of the 7th frequency of the AFLB. For small number of trials, the error on standard deviation can vary a lot. Therefore, the comparison between two methods was performed 10 times for several values of n_t; the maximum and minimum errors for each case of n_t are shown in Figure

4.8. The errors on the mean frequency are smaller than the errors on standard deviation. The difference Δ must meet the condition given in Equation 4.23. As far as the standard deviation is concerned, the difference Δ between 20 and 10,000 trials is always less than 5%, which is acceptable. Therefore, the errors obtained with 20 trials can be used as an error indicator. For this n_t value, the difference Δ concerning the mean value does not exceed 1%.

$$\Delta = |Err^{n_t} - Err^{10000}| \leq 5\% \tag{4.23}$$

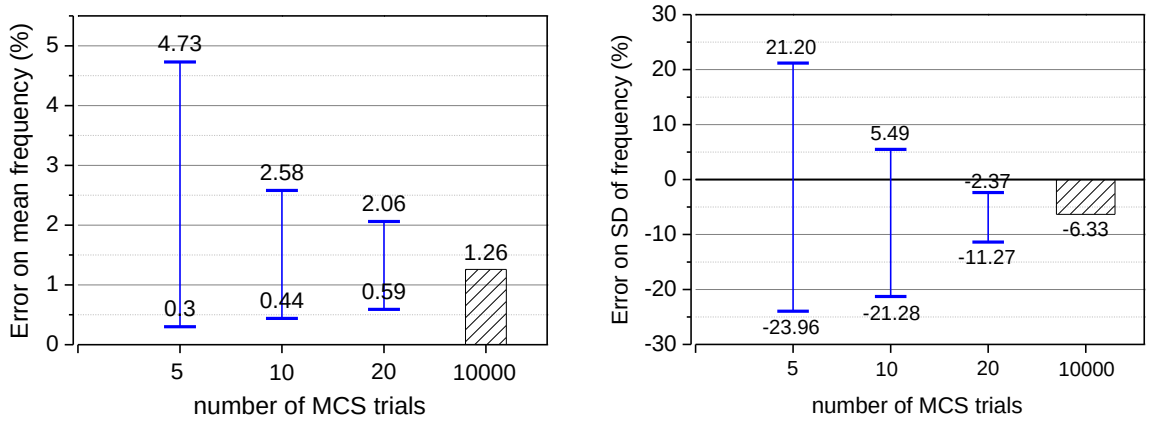

Figure 4.8: Influence of the number of trials n_t on the error between MSP and direct MCS in case of the 7th frequency of the AFLB

4.5.3 Error indicator for AFCLT panels

Tables 4.12 and 4.13 present the estimated errors between MSP and direct MCS for medium and full-size AFCLT panels, respectively. The errors on mean value and standard deviation are first obtained with 20 trials and considered as error indicator. The true error is then estimated from error indicator exploiting the maximal possible difference: 1% for mean and 5% for standard deviation.

Mode	Error indicator on mean frequency		Error indicator on standard deviation	
	20 trials	Estimation of true error (min ; max)	20 trials	Estimation of true error (min ; max)
(1,1)	0.7%	-0.3% ; 1.7%	-5.4%	-0.4% ; -10.4%
(2,0)	1.0%	0.0% ; 2.0%	-6.3%	-1.3% ; -11.3%
(0,2)	0.9%	-0.1% ; 1.9%	-5.9%	-0.9% ; -10.9%
(2,1)	1.1%	0.1% ; 2.1%	-7.6%	-2.6% ; -12.6%
(1,2)	1.1%	0.1% ; 2.1%	-7.2%	-2.2% ; -12.2%
(2,2)	1.2%	0.2% ; 2.2%	-8.1%	-3.1% ; -13.1%

Table 4.12: Estimation error between MSP and MCS for 10,000 trials of AFCLT panel

Mode	Error indicator on mean frequency		Error indicator on standard deviation	
	20 trials	Estimation of true error (min ; max)	20 trials	Estimation of true error (min ; max)
1	1.6%	0.6% ; 2.6%	-9.7%	-4.7% ; -14.7%
2	2.4%	1.4% ; 3.4%	-11.1%	-6.1% ; -16.1%
3	2.6%	1.6% ; 3.6%	-12.2%	-7.2% ; -17.2%
4	3.4%	2.4% ; 4.4%	-14.2%	-9.2% ; -19.2%

Table 4.13: Estimation error between MSP and MCS for 10,000 trials of full-size AFCLT panel

It can be observed that the error on mean frequency between MSP and direct MCS is small. For standard deviation, the maximum error is less than 20%, which is quite acceptable in the case of great number of parameters (700 parameters for the AFCLT panel and 1944 parameters for the full-size AFCLT panel) and high level of input variability (CoV of elastic properties is 13.6% for laminae and 16.1% for dowels). Therefore, the MSP method is very satisfactory to predict the mean value and standard deviation of frequencies of timber structures.

4.6 Influence of uncertain properties of compressed wood dowels

The sensitivity study in Chapter 3 (Table 3.7) shows that properties of compressed wood dowels have small effect on frequencies of AFLB. In this section, the influence of uncertain properties of the dowels on frequencies of AFLB is investigated to confirm this.

Table 4.14 shows the effect of the variability of dowels on the variability of frequencies of AFLB. In order to highlight the effect of dowels, variability of three properties ρ, E_3 and G_{13} of the dowels are taken into account, but all properties of layers are fixed as constants. It can be seen that the variability of frequencies is very small compared with the variability of properties of dowels and compared with variability levels obtained in section 4.5 where variability of layers is taken into account as well. The reason for this phenomenon is that the volume of dowels is very small compared with the volume of layers, leading to small strain energy. Therefore, the contribution of dowels to variability is small. It leads to small effect of dowels on variability of natural frequencies of the AFLB. Similar phenomenon can be observed with the AFCLT panel.

Variability of properties of dowels	Variability of frequencies		
	CoV (f_1)	CoV (f_4)	CoV (f_7)
CoV (ρ) = 4.2% CoV (E_3) = CoV (G_{13}) = 16.1%	0.3%	0.3%	0.4%

Table 4.14: Variability of frequencies of AFLB caused by variability of properties of dowels

4.7 Comparison between MSP and experimental results

The mean value and CoV of frequencies from MSP are here compared with that from experiment. It should be kept in mind that the small number of physical specimens for the experimental campaign may lead to inaccurate results. Indeed, a large number of specimens are theoretically necessary to obtain precise statistical results. However, the comparison between numerical and experimental variability is very important and is one of our objectives.

4.7.1 Comparison for single layer beam

First, the mean frequencies and CoV of 16 single layer beams, obtained by experiment, direct MCS and MSP, are compared in Figure 4.9. The direct MCS and MSP are not performed with random parameters, but with 16 trials using experimental density and elastic modulus of single layer beam as input data. A very good agreement on all mean and CoV values shows good performance of MSP method.

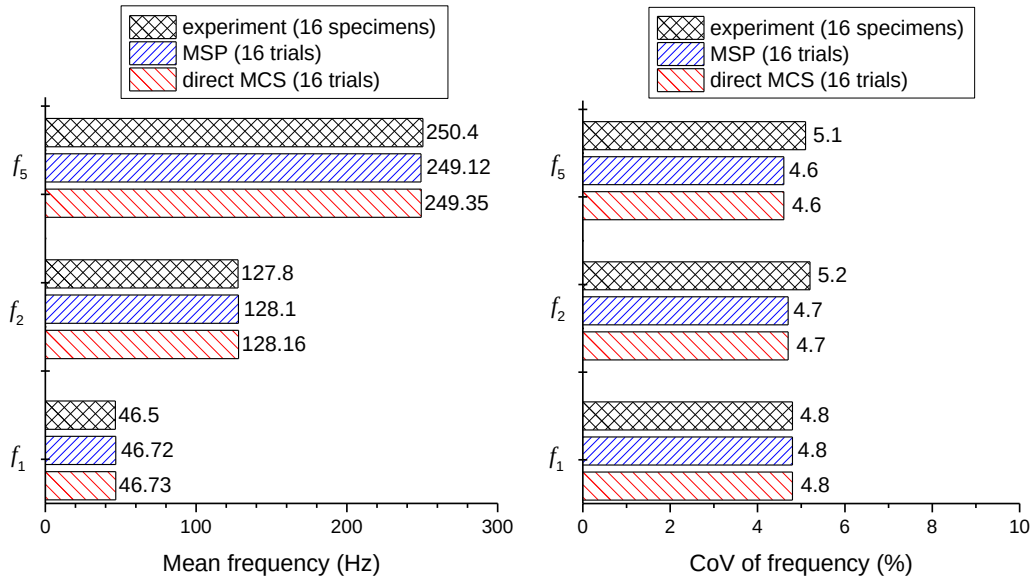

Figure 4.9: Comparison of mean value and CoV of frequencies of oak single layer beam between experiment (with 16 specimens), direct MCS and MSP (16 trials)

Then, the direct MCS and MSP are performed with 10,000 random trials. Figure 4.10 compares the mean value and CoV of frequencies from experiment, MSP and direct MCS. It can be observed a good agreement between experimental and numerical mean frequencies. However, the difference between numerical and experimental CoV values is significant. The reason is that 16 specimens are not sufficient to precisely investigate the CoV value. Experimental assessment of variability level remains a difficulty because the number of specimens is generally limited, just like in this study.

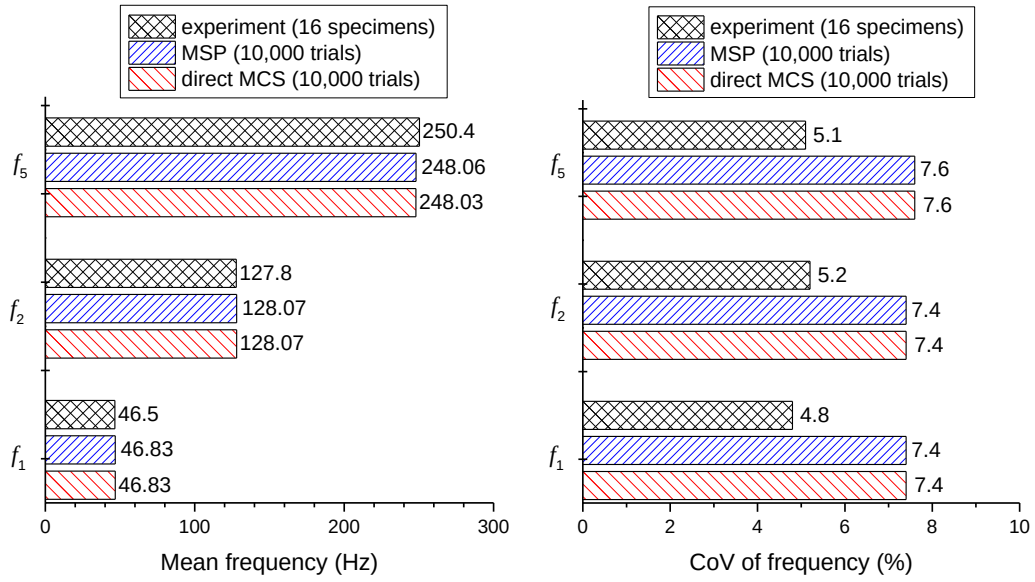

Figure 4.10: Comparison of mean value and CoV of frequencies of oak single layer beam between experiment (with 16 specimens), direct MCS and MSP (10,000 trials)

4.7.2 Comparison for AFLB

The experimental and numerical mean frequencies as well as CoV values of AFLB are compared in Figure 4.11. It can be seen a good agreement for mean frequencies. Order of magnitude of variability observed experimentally is obtained with MSP. The differences between numerical and experimental CoV values are acceptable. Indeed, the comparison between numerical variability and experimental variability is always a difficult task. Both numerical and experimental results may be imprecise. On the one hand, the experimental variability is strongly dependent on the number of specimens. In this case, the experimental variability level is debatable due to the small number of specimens (only 5). On the other hand, the input parameters greatly affect the numerical variability. Therefore, the characteristics of input parameters are very important (such as distribution of parameters, independent parameters or dependent parameters and so on). However, to identify these characteristics of the wood material is a difficulty. Therefore, there are only a few studies comparing the experimental and numerical variability. One can find a comparison between experimental and numerical variability of the thickness of composite parts due to the manufacturing process in Matveev *et al.* (2019). The authors also emphasized the difference due to the small number of specimens. Especially for timber structures, the literature about the comparison between the experimental statistical result and the numerical one is very poor. Kandler and Füssl (2017) investigated the stiffness variability of glued laminated timber beams, obtained by experiment and numerical simulations. The results show that the description of random input parameters is important for the numerical variability and they should be described based on mechanical properties profiles of a large number of timber boards.

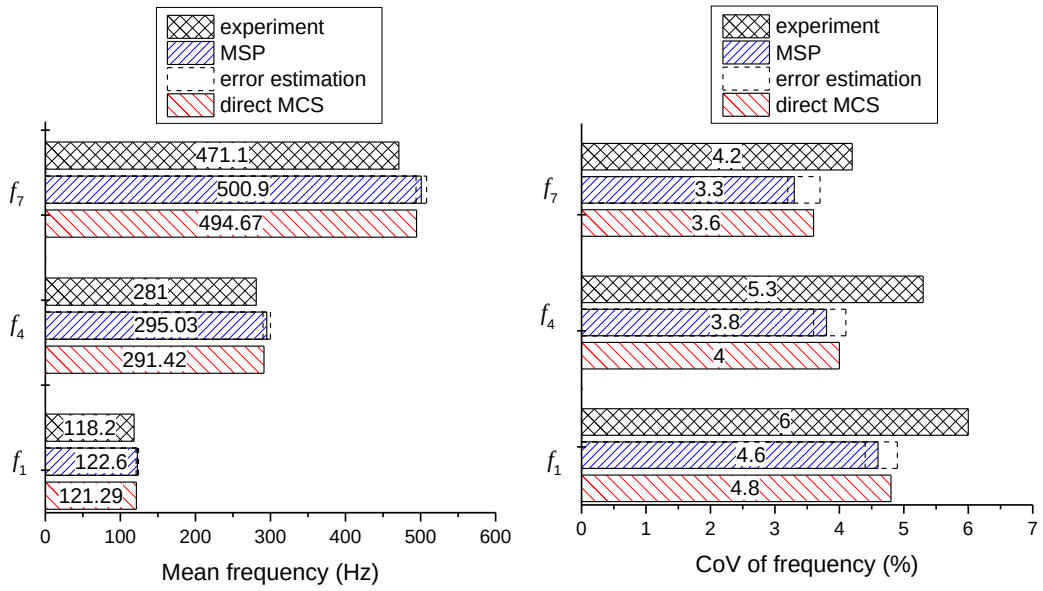

Figure 4.11: Comparison of experimental and numerical mean value and CoV of frequencies of AFLB

Moreover, another phenomenon can be observed. The AFLB, including three timber layers, has numerical CoV values smaller than that of single layer beam because of compensation phenomenon. Indeed, the output variability decreases when the number of input parameters increases. In a simple case, this phenomenon can also be observed in Arnoult *et al.* (2011).

4.7.3 Comparison for AFCLT panel

The distribution of the first six frequencies of AFCLT panel obtained by the MSP method is shown in Figure 4.12. The distribution of other frequencies is quite similar; they are nearly Gaussian distribution. Figure 4.13 compares the mean value and CoV of frequencies of AFCLT panel from experiment and MSP method. All normal and groove panels are taken into account to calculate the experimental mean and CoV values to have better results from a statistical point of view. The error between MSP and direct MCS is estimated. It can be seen that the mean frequencies obtained by the MSP are close to the experimental ones. However, again the difference in CoV values between the MSP and experiment is significant due to the small number of specimens, 10 panels in this case. On the other hand, the numerical variability may be imprecise due to the lack of knowledge about the variability of input parameters as discussed in the previous subsection. Moreover, the complexity of the AFCLT panel may lead to omission of some parameters that are not taken into account in the variability input data.

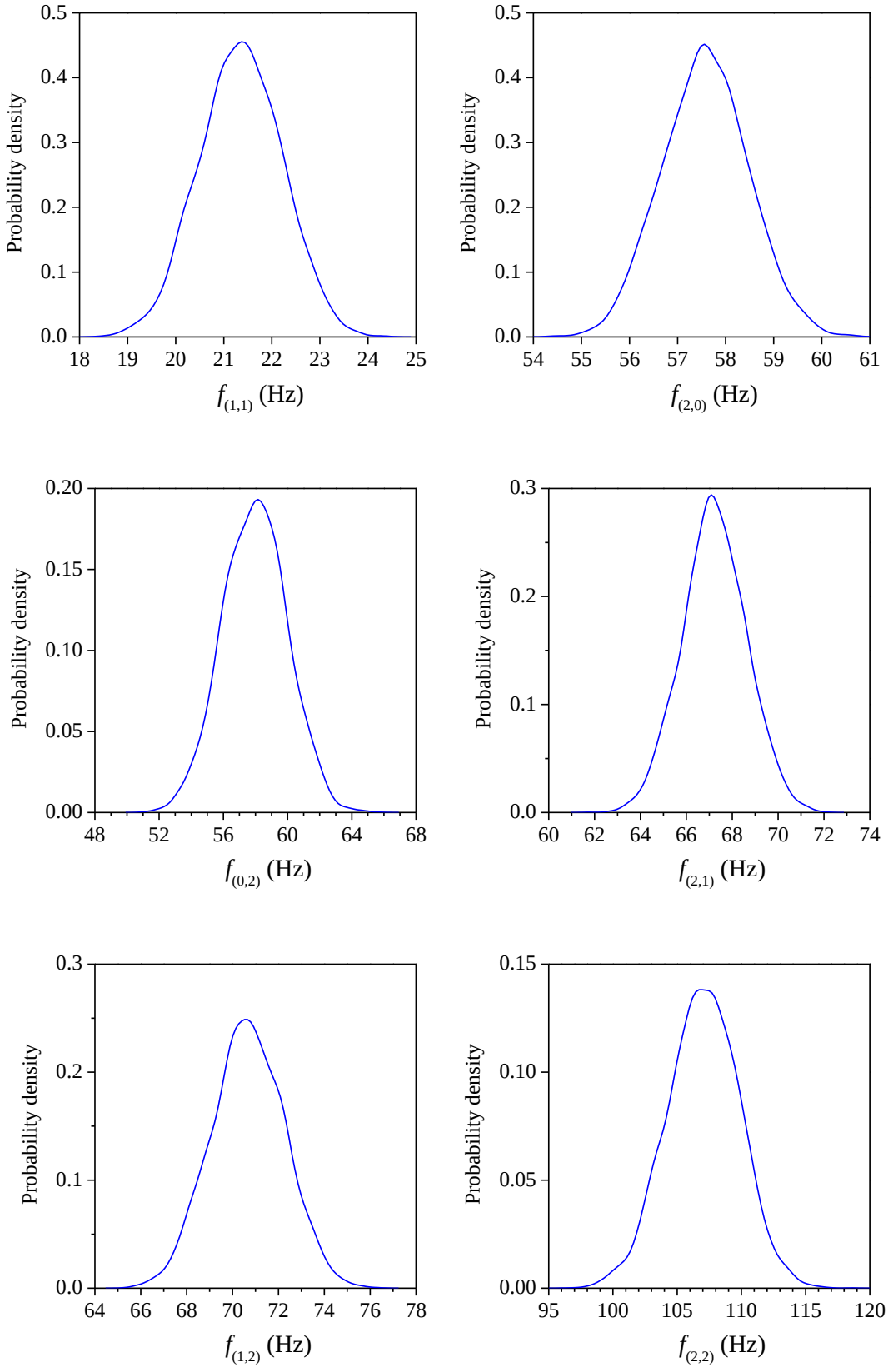

Figure 4.12: Distribution of the first six frequencies of AFCLT panel

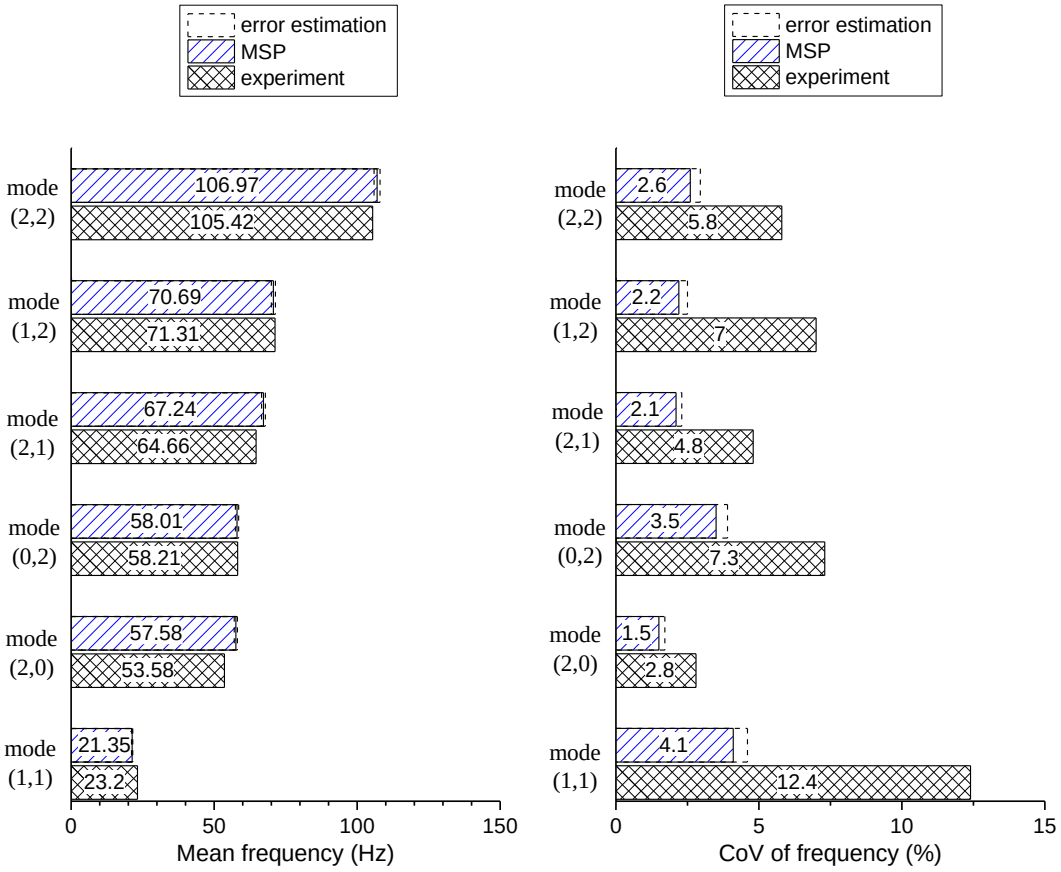

Figure 4.13: Comparison of experimental and numerical mean value and CoV of frequencies of AFCLT panel

4.8 Prediction variability of full-size AFCLT panel

Figure 4.14 shows the mean and standard deviation of the fundamental frequency of eight different types of full-size AFCLT panels obtained by MSP method. The intervals -3σ and +3σ from the mean are added in the figure. The full-size AFCLT panels include 3 or 5 oak layers, assembled by 2160 or 4320 vertical compressed dowels and simply supported at 2 or 4 sides. The MSP error indicator is systematically added. It can be seen that almost all panels have the fundamental frequency higher than 8 Hz. However, a further study is necessary in the future to confirm that the full-size AFCLT panels meet the requirements of Eurocode 5.

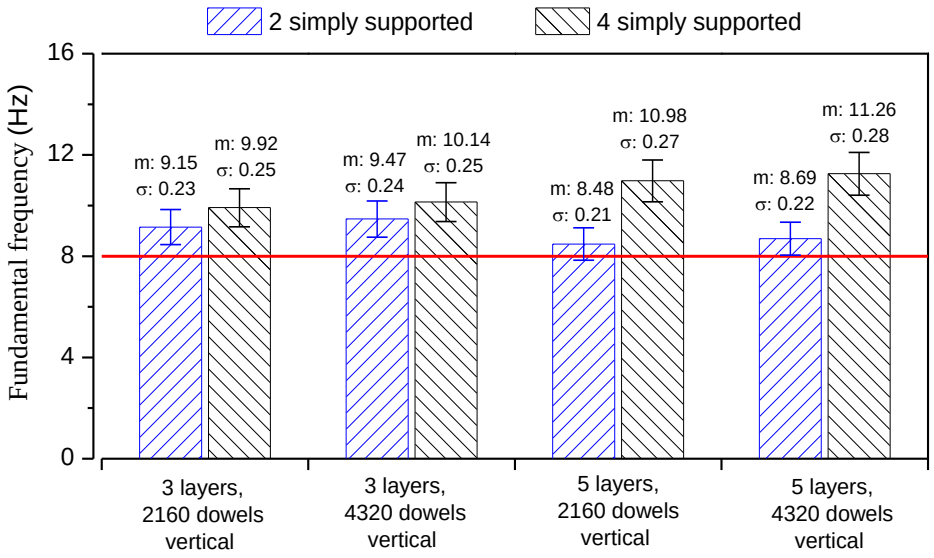

Figure 4.14: Mean and standard deviation of the fundamental frequency of eight full-size AFCLT panels

4.9 Computational cost

	Computational time		Gain MSP/MCS
	Direct MCS	MSP	
Single layer beam	10,000 x 7s = 70,000s	7s + 320s = 327s	214
AFLB	10,000 x 585s = 5,850,000s	585s + 10,470s = 11,055s	529
AFCLT panel	10,000 x 2,434s = 24,340,000s	2,434s + 35,560s = 37,994s	641
Full-size AFCLT panel	10,000 x 10,988s = 109,880,000s	10,988s + 140,810s = 151,798s	724

Table 4.15: Comparison of computational cost between MSP and 10,000 MCS trials

The comparison between computational time of MCS and MSP methods is here presented (Table 4.15). 10,000 direct MCS trials for single layer beam as well as for AFLB trials are performed by Abaqus/Standard. For AFCLT panel and full-size AFCLT panel, it is impossible to carry out 10,000 trials; therefore, the computational time is estimated from the time taken for a nominal analysis in this case. The cost of the MSP includes a single nominal finite element analysis by Abaqus to obtain nominal mode shapes and modal strains, and a postprocessing stage where 10,000 trials are performed by the MSP formula (Equation 4.21). The MSP formula is calculated using Matlab software. All calculation is performed by a computer station with following specifications: Intel (R) Core (TM) i7-6820HQ 2.70 GHz with 32 GB RAM.

It can be seen that the MSP method is not only accurate but also economical from a computational time point of view. Moreover, the gain of MSP compared with MCS increases when the number of elements of the FE model increases.

4.10 Academic contribution

This is the first time that the numerical variability of multilayer timber structures assembled by compressed dowels has been studied. The MSP formula has been developed for the 20-node hexahedral solid element. The mean and CoV values obtained by the MSP formula are compared with the results obtained by a reference method (direct MCS) and the experimental results for the verification and validation purpose. Compared with direct MCS, the MSP formula provides an accurate result in the case of single layer beam, and an acceptable error in the case of large number of random parameters (AFLB, AFCLT panel and full-size AFCLT panel). Therefore, the performance of the MSP formulation is very good. Based on a good understanding of the random input parameters, the MSP formula can provide good results compared to experiment.

4.11 Conclusion

In this chapter, the MSP has been developed to study the variability of natural frequencies of single layer beam, AFLB as well as AFCLT panels. These structures are discretized by 20-node hexahedral solid elements. A formula suitable for the 20-node solid element is therefore developed for the MSP. The consistent mass matrix and numerical integration of the elementary strain energy with 8 integration points are proposed for the MSP formula. Mechanical properties of timber are considered as uncertain parameters and modeled by random variables. The MSP assumes that the mode shapes are independent of uncertain input parameters. Thanks to this assumption, only one finite element analysis is required to extract the nominal mode shapes and modal strains. Then a MCS is performed on the MSP formula and allows to calculate the perturbed natural frequencies for each trial. The mean value, standard deviation, coefficient of variation and distribution of frequencies obtained by MSP are compared with the results obtained by the direct MCS as well as experimental results. The important conclusions are:

- The verification of the MSP formula in a nominal case has been done before variability study. The mesh convergence as well as frequencies obtained from the formula are similar with that obtained from the FE model.
- The mean value, standard deviation, coefficient of variation as well as distribution of natural frequencies of single layer beam obtained from the MSP are similar with the results of the direct MCS. The error between these two methods increases in the case

of AFLB and AFCLT panels because the number of parameters is large. Anyway, the error remains moderate and is acceptable.

- An error indicator using 20 trials is proposed. Therefore, the error level of the statistical results between the MSP and the direct MCS can be quickly estimated.
- The variability of mechanical properties of dowels has a small effect on the variability of frequencies of AFLB and AFCLT panels.
- The mean values of frequencies obtained from the MSP are close to experimental ones. The order of magnitude of variability level is correct. The difference in coefficient of variation between the MSP and experiment is acceptable. One reason of the discrepancy is due to the small number of specimens which leads to approximate experimental variability statistics. Another difficulty is to describe correctly the variability input data.
- The mean and CoV value of the fundamental frequency of eight different types of full-size AFCLT panel is estimated. It shows the prospect of meeting the Eurocode 5 requirement. However, a further study is necessary to confirm.
- The computational cost of the MSP is much lower than the cost of the direct MCS. The gain of the MSP compared to the direct MCS increases when the number of elements in the model increases. The MSP is therefore suitable for the evaluation of variability of an industrial model with a large number of degrees of freedom, a large number of random variables with high variability level.

Chapter 5:
General conclusion and perspectives

5.1 General conclusion

In this thesis, we assessed the vibrational serviceability performance of multilayered timber structures assembled by compressed spruce dowels (CSD), including adhesive free laminated beam (AFLB) and adhesive free CLT panel (AFCLT).

First, natural frequencies of the AFLB and the AFCLT panel under free-free conditions was experimentally assessed. Several types of the AFLB and glued beams with similar dimensions were manufactured for comparison purpose. It was shown that the AFLB assembled by 27 CSDs exhibits the highest frequency among four types of AFLB. The first frequency of the AFLB assembled by 27 CSDs is slightly smaller than that of the glued beams while the difference increases with the higher frequencies. However, the damping ratio of AFLB is higher than that of glued beam. As far as AFCLT panels are concerned, close frequency and damping ratio values were observed for panels with or without grooves. Variability of frequencies and damping ratios were also quantified. The variability level of frequencies is moderate and the variability level of damping ratios is globally high for the AFLB and AFCLT panel.

Second, a 3D solid FE model was developed to simulate the vibration performance of AFLB and AFCLT panel. Verification and Validation methodology was applied to evaluate the performance of the model. The twenty-node hexahedral solid element with reduced integration (C3D20R of Abaqus) was chosen for the model because it is the most efficient for convergence. It can be seen a good agreement between numerical and experimental frequencies and mode shapes. The vibration performance of full-size AFCLT panels with real dimensions and conditions was then predicted. A parametric study was carried out to optimize the connection design of full-size AFCLT panel. The results showed that the AFCLT panel assembly with 30-degree dowels has highest stiffness. In order to reduce computational cost, a simplified FE model was developed. The simplified model provides acceptable performance compared with the reference model.

Third, the variability of natural frequencies of single layer beam, AFLB as well as AFCLT panels was studied numerically based on the MSP. Several variants of MSP formulations were developed for the 20-node hexahedral solid element and the most suitable one was selected for the study. The frequencies from the MSP formula in a nominal case are exactly the same

as those from the FE model. The mean value, standard deviation, coefficient of variation and distribution of frequencies obtained by MSP are compared with the results obtained by the direct MCS. The error is close to zero in the case of single layer beam and small in the case of AFLB. An error indicator was proposed, leading to a quick estimate of the error level of the statistical results between the MSP and the direct MCS. The mean values of frequencies obtained from the MSP are close to experimental ones. The order of magnitude of variability level is correct. The difference in coefficient of variation between the MSP and experiment is acceptable. The comparison of computational cost between the MSP and the direct MCS shows the gain of the MSP.

5.2 Perspectives

Despite several contributions, one can identify in this research work a number of weakness that should be completed and improved in the future.

In short term, a general research to improve the correlation between numerical and experimental variability, in the context of real and complex structures, is necessary. Concerning experimental aspect, obtaining an accurate coefficient of variation (CoV) is a challenge due to the limited number of specimens. In fact, it is impossible to manufacture and test a very large number of specimens, by the contrary of the numerical approach which may lead to 10000 trials. Therefore, the question of what is the minimum number of specimens required must be answered. In addition, the enrichment of the statistical results from a small number of specimens is also an interesting perspective.

Then, the comparison between the numerical and experimental variability of the full-size AFCLT panel should be performed. An experimental campaign with enough number of full-size AFCLT panels is necessary to obtain an accurate experimental variability of the panel. Concerning numerical aspect, the performance of the MSP formulation is very good, but its predictivity is highly dependent on the input parameters which should be accurately identified. Therefore, a large number of timber boards should be tested to better describe the input parameters. Upon completion of the study, it will be possible to conclude about the satisfactoriness of the AFCLT panel with the Eurocode 5 requirements.

In long term, the numerical study about the effect of moisture content on vibration performance of the AFLB (intra variability) should be performed. The swelling of compressed wood dowels and friction connection between the dowel and layer must be simulated in the FE model in this case. The modal analysis will be non-linear. Many studies show that the friction can affect the natural frequencies and damping ratio of structure (Claeys *et al.* (2016); Massa *et al.* (2016); Do *et al.* (2017); Roncen *et al.* (2019)).

In addition, development a simplified FE model for the AFCLT panel using solid-shell elements for the layers and solid-beam elements for the dowels is another good direction. The solid-shell element has a three-dimensional geometry like a solid element but uses shell theory to model the layers while the solid-beam element has a three-dimensional geometry but uses beam theory to model the dowels.

Bibliography

Adhikari, S., Ozarska, B. (2018): Minimizing environmental impacts of timber products through the production process “From Sawmill to Final Products.” *Environmental Systems Research* (**7**)1: 6. DOI:10.1186/s40068-018-0109-x.

Anshari, B., Guan, Z., Komatsu, K., Kitamori, A., Jung, K. (2010): Explore novel ways to strengthen glulam beams by using compressed Japanese cedar. In: *Proceedings of 11th World Conference on Timber Engineering*. Riva del Garda, Italy.

Anshari, B., Guan, Z.W., Kitamori, A., Jung, K., Hassel, I., Komatsu, K. (2011): Mechanical and moisture-dependent swelling properties of compressed Japanese cedar. *Construction and Building Materials* (**25**)4: 1718–1725. DOI:10.1016/j.conbuildmat.2010.11.095.

Arnoult, É., Lardeur, P., Martini, L. (2011): The modal stability procedure for dynamic and linear finite element analysis with variability. *Finite Elements in Analysis and Design* (**47**)1: 30–45. DOI:10.1016/j.finel.2010.07.011.

Baño, V., Arriaga, F., Guaita, M. (2013): Determination of the influence of size and position of knots on load capacity and stress distribution in timber beams of Pinus sylvestris using finite element model. *Biosystems Engineering* (**114**)3: 214–222. DOI:10.1016/j.biosystemseng.2012.12.010.

Blomberg, J. (2006): Mechanical and physical properties of semi-isostatically densified wood. doctoral thesis. Luleå University of Technology

Bouhala, L., Fiorelli, D., Makradi, A., Belouettar, S., Sotayo, A., Bradley, D.F., Guan, Z. (2020): Advanced numerical investigation on adhesive free timber structures. *Composite Structures* (**246**): 112389. DOI:10.1016/j.compstruct.2020.112389.

Bui, T.A., Lardeur, P., Oudjene, M. (2018): Experimental study of vibration uncertainty of multilayered timber beams assembled through wood dowels. In: *International conference on Uncertainty in structural Dynamics*. Leuven, Belgium, pp. 4867–4880.

Cambou, B. (1975): Applications of first order uncertainty analysis in the finite element method in linear elasticity. In: *Proceedings of the 2nd International Conference on Application of Statistics and Probability in Soil and Structural Mechanics*. Aachen, Germany, pp. 67–87.

Cao, Y., Street, J., Li, M., Lim, H. (2019): Evaluation of the effect of knots on rolling shear strength of cross laminated timber (CLT). *Construction and Building Materials* (**222**): 579–587. DOI:10.1016/j.conbuildmat.2019.06.165.

Casagrande, D., Giongo, I., Pederzolli, F., Franciosi, A., Piazza, M. (2018): Analytical, numerical and experimental assessment of vibration performance in timber floors. *Engineering Structures* (**168**): 748–758. DOI:10.1016/j.engstruct.2018.05.020.

Cetrangolo, G., Rodríguez, S., Rodríguez, A., Baño, V. (2015): Influence of boundary conditions on the natural frequencies and damping of timber beams of sweet chestnut. *Construction and Building Materials* (**94**): 613–619. DOI:10.1016/j.conbuildmat.2015.07.047.

Chúláin, C.U., Sikora, K., Harte, A.M. (2016): Influence of connection systems on serviceability response of CLT timber flooring. In: *World Conference on Timber Engineering 2016 (WCTE 2016)*. Vienna, Austria.

Claeys, M., Sinou, J.-J., Lambelin, J.-P., Todeschini, R. (2016): Modal interactions due to friction in the nonlinear vibration response of the "Harmony" test structure: Experiments and simulations. *Journal of Sound and Vibration* (**376**): 131–148. DOI:10.1016/j.jsv.2016.04.008.

Cloutier, A., Fang, C.-H., Mariotti, N., Koubaa, A., Blanchet, P. (2008): Densification of Wood Veneers Under the Effect of Heat, Steam and Pressure. In: *Proceedings of the 51st International Convention of Society of Wood Science and Technology*. Concepción, CHILE.

Daouk, S., Louf, F., Dorival, O., Champaney, L., Audebert, S. (2015): Uncertainties in structural dynamics: overview and comparative analysis of methods. *Mechanics & Industry* (**16**)4: 404. DOI:10.1051/meca/2015010.

Dassault Systèmes Simulia Corp (2014): Abaqus 6.14 user's guide.

Deutsches Institut für Bautechnik (2018): *ETA-13/0785*.

Dhatt, G., Touzot, G., Lefrançois, E. (2015): *Méthode des éléments finis*. Hermes Science Publications.

Dias, A.M.P.G., Kuhlmann, U., Kudla, K., Mönch, S., Dias, A.M.A. (2018): Performance of dowel-type fasteners and notches for hybrid timber structures. *Engineering Structures* (**171**): 40–46. DOI:10.1016/j.engstruct.2018.05.057.

Ditlevsen, O., Madsen, H.O. (1996): *Structural Reliability Methods*. Wiley, Chichester ; New York.

Do, H.Q., Massa, F., Tison, T., Lallemand, B. (2017): A global strategy for the stability analysis of friction induced vibration problem with parameter variations. *Mechanical Systems and Signal Processing* (**84**): 346–364. DOI:10.1016/j.ymssp.2016.07.029.

Druesne, F., Boubaker, M.B., Lardeur, P. (2014): Fast methods based on modal stability procedure to evaluate natural frequency variability for industrial shell-type structures. *Finite Elements in Analysis and Design* (**89**): 93–106. DOI:10.1016/j.finel.2014.05.004.

Druesne, F., Hallal, J., Lardeur, P., Lanfranchi, V. (2016): Modal stability procedure applied to variability in vibration from electromagnetic origin for an electric motor. *Finite Elements in Analysis and Design* (**122**): 61–74. DOI:10.1016/j.finel.2016.09.004.

Ebadi, M.M., Doudak, G., Smith, I. (2018): Vibration responses of glulam beam-and-deck floors. *Engineering Structures* (**156**): 235–242. DOI:10.1016/j.engstruct.2017.11.051.

El-Houjeyri, I., Thi, V.-D., Oudjene, M., Khelifa, M., Rogaume, Y., Sotayo, A., Guan, Z. (2019): Experimental investigations on adhesive free laminated oak timber beams and timber-to-timber joints assembled using thermo-mechanically compressed wood dowels. *Construction and Building Materials* (**222**): 288–299. DOI:10.1016/j.conbuildmat.2019.05.163.

Elishakoff, I., Ren, Y. (2003): *Finite Element Methods for Structures with Large Stochastic Variations*. Oxford University Press.

European Commission (2001): COM(2011) 112 - A Roadmap for moving to a competitive low carbon economy in 2050 — European Environment Agency. Available from: https://www.eea.europa.eu/policy-documents/com-2011-112-a-roadmap (July 5, 2020).

European Committee for Standardization (2004): *EN 1995-1-1 Eurocode 5 Design of timber structures Part 1.1 General Rules General rules and rules for buildings*.

Filippoupolitis, M., Hopkins, C., Völtl, R., Schanda, U., Mahn, J., Krajči, L. (2017): Structural dynamics of a dowelled-joist timber floor in the low-frequency range modelled using finite element simulation. *Engineering Structures* (**148**): 602–620. DOI:10.1016/j.engstruct.2017.07.009.

Fink, G., Frangi, A., Kohler, J. (2015): Probabilistic approach for modelling the load-bearing capacity of glued laminated timber. *Engineering Structures* (**100**): 751–762. DOI:10.1016/j.engstruct.2015.06.015.

Fragiacomo, M., Fortino, S., Tononi, D., Usardi, I., Toratti, T. (2011): Moisture-induced stresses perpendicular to grain in cross-sections of timber members exposed to different climates. *Engineering Structures* (**33**)11: 3071–3078. DOI:10.1016/j.engstruct.2011.06.018.

Frihart, C.R., Hunt, C.G. (2010): Adhesives with wood materials : bond formation and performance. *Wood handbook : wood as an engineering material: chapter 10. Centennial ed. General technical report FPL ; GTR-190. Madison, WI : U.S. Dept. of Agriculture, Forest Service, Forest Products Laboratory, 2010: p. 10.1-10.24.* (**190**): 10.1-10.24.

Frischkorn, J., Reese, S. (2013): A solid-beam finite element and non-linear constitutive modelling. *Computer Methods in Applied Mechanics and Engineering* (**265**): 195–212. DOI:10.1016/j.cma.2013.06.009.

Frischkorn, J., Reese, S. (2015): Solid-beam finite element analysis of Nitinol stents. *Computer Methods in Applied Mechanics and Engineering* (**291**): 42–63. DOI:10.1016/j.cma.2015.03.011.

García, D.A., Rosales, M.B., Sampaio, R. (2019): Dynamic behaviour of a timber footbridge with uncertain material properties under a single deterministic walking load. *Structural Safety* (**77**): 10–17. DOI:10.1016/j.strusafe.2018.11.001.

Glisovic, I., Stevanovic, B. (2010): Vibrational behaviour of timber floors. In: *11th World Conference on Timber Engineering 2010 (WCTE 2010)*. Trentino, Italy.

Grosse, M., Hartnack, R., Lehmann, S., Rautenstrauch, K. (2003): Modellierung von diskontinuierlich verbundenen Holz-Beton-Verbundkonstruktionen / Teil 1: Kurzzeittragverhalten. *Bautechnik* (**80**)8: 534–541. DOI:10.1002/bate.200304120.

Guan, Z., Komatsu, K., Jung, K., Kitamori, A. (2010): Structural characteristics of beam-column connections using compressed wood dowels and plates. In: *11th World Conference on Timber Engineering 2010 (WCTE 2010)*. Trentino, Italy.

Guinard, S., Bouclier, R., Toniolli, M., Passieux, J.-C. (2018): Multiscale analysis of complex aeronautical structures using robust non-intrusive coupling. *Advanced Modeling and Simulation in Engineering Sciences* (**5**)1: 1. DOI:10.1186/s40323-017-0094-z.

Gülzow, A., Richter, K., Steiger, R. (2011): Influence of wood moisture content on bending and shear stiffness of cross laminated timber panels. *European Journal of Wood and Wood Products* (**69**)2: 193–197. DOI:10.1007/s00107-010-0416-z.

Habitat Naturel (2009): Nur Holz, solid panel without glue. Available from: http://www.habitatnaturel.fr/dossiers/11-Le-bois-lamellecroise--CLT/28-Nurholz-panneau-massif-sans-colle/ (July 8, 2020).

Hallal, J. (2014): Études des vibrations d'origine électromagnétique d'une machine électrique : conception optimisée et variabilité du comportement vibratoire. doctoral thesis. University of Technology of Compiègne

Hamdaoui, M., Druesne, F., Daya, E.M. (2015): Variability analysis of frequency dependent visco-elastic three-layered beams. *Composite Structures* (**131**): 238–247. DOI:10.1016/j.compstruct.2015.05.011.

Hassel, I., Berard, P., Komatsu, K. (2008): Development of wooden shear Wall-Improvement of stiffness by utilizing elements of densified wood. *Holzforschung* (**62**)5: 584–590. DOI:10.1515/HF.2008.091.

Helton, J.C., Davis, F.J. (2003): Latin hypercube sampling and the propagation of uncertainty in analyses of complex systems. *Reliability Engineering & System Safety* (**81**)1: 23–69. DOI:10.1016/S0951-8320(03)00058-9.

Henderson, J., Foster, S., Bridgestock, M. (2018): Brettstapel - What are the benefits? Available from: http://www.brettstapel.org/Brettstapel/Why.html (July 7, 2020).

Hinke, L., Dohnal, F., Mace, B.R., Waters, T.P., Ferguson, N.S. (2009): Component mode synthesis as a framework for uncertainty analysis. *Journal of Sound and Vibration* (**324**)1: 161–178. DOI:10.1016/j.jsv.2009.01.056.

Hu, L., Gagnon, S. (2012): Controlling cross-laminated timber (CLT) floor vibrations: fundamentals and method. In: *World Conference on Timber Engineering 2012 (WCTE 2012)*. Auckland, New Zealand.

Huang, H., Gao, Y., Chang, W.-S. (2020): Human-induced vibration of cross-laminated timber (CLT) floor under different boundary conditions. *Engineering Structures* (**204**): 110016. DOI:10.1016/j.engstruct.2019.110016.

Ido, H., Nagao, H., Kato, H., Miura, S. (2013): Strength properties and effect of moisture content on the bending and compressive strength parallel to the grain of sugi (Cryptomeria japonica) round timber. *Journal of Wood Science* (**59**)1: 67–72. DOI:10.1007/s10086-012-1297-z.

International Agency for Research on Cancer (2004): IARC classifies Formaldehyde as carcinogenic to humans. Available from: https://www.iarc.fr/en/media-centre/pr/2004/pr153.html (July 8, 2020).

Jarnerö, K., Brandt, A., Olsson, A. (2015): Vibration properties of a timber floor assessed in laboratory and during construction. *Engineering Structures* (**82**): 44–54. DOI:10.1016/j.engstruct.2014.10.019.

Jelusic, P., Kravanja, S. (2017): Optimal design of timber-concrete composite floors based on the multi-parametric MINLP optimization. *Composite Structures* (**179**): 285–293. DOI:10.1016/j.compstruct.2017.07.062.

Jin, M., Hu, Y., Wang, B. (2015): Compressive and bending behaviours of wood-based two-dimensional lattice truss core sandwich structures. *Composite Structures* (**124**): 337–344. DOI:10.1016/j.compstruct.2015.01.033.

Jodin, F. (1994): *Le bois matériau d'ingénierie*. Arbolor, Nancy Cedex.

Jung, K., Kitamori, A., Komatsu, K. (2008): Evaluation on structural performance of compressed wood as shear dowel. *Holzforschung* (**62**)4: 461–467. DOI:10.1515/HF.2008.073.

Kaminski, M. (2001): Stochastic second-order perturbation approach to the stress-based finite element method. *International Journal of Solids and Structures* (**38**)21: 3831–3852. DOI:10.1016/S0020-7683(00)00234-1.

Kaminski, M. (2013): *The Stochastic Perturbation Method for Computational Mechanics*. Wiley, Chichester, West Sussex, United Kingdom.

Kandler, G., Füssl, J. (2017): A probabilistic approach for the linear behaviour of glued laminated timber. *Engineering Structures* (**148**): 673–685. DOI:10.1016/j.engstruct.2017.07.017.

Kandler, G., Füssl, J., Eberhardsteiner, J. (2015): Stochastic finite element approaches for wood-based products: theoretical framework and review of methods. *Wood Science and Technology* (**49**)5: 1055–1097. DOI:10.1007/s00226-015-0737-5.

Köhler, J., Sørensen, J.D., Faber, M.H. (2007): Probabilistic modeling of timber structures. *Structural Safety* (**29**)4: 255–267. DOI:10.1016/j.strusafe.2006.07.007.

Lardeur, P., Arnoult, É., Martini, L., Knopf-Lenoir, C. (2012):(a): The Certain Generalized Stresses Method for the static finite element analysis of bar and beam trusses with

variability. *Finite Elements in Analysis and Design* (**50**): 231–242. DOI:10.1016/j.finel.2011.09.013.

Lardeur, P., Lacouture, E., Blain, E. (2000): Spot weld modelling techniques and performances of finite element models for the vibrational behaviour of automotive structures. In: *International ISMA25 conference*. Leuven, Belgium, pp. 387–394.

Lardeur, P., Scigliano, R., Scionti, M. (2012):(b): Verification and validation for the vibration study of automotive structures modelled by finite elements: *The Journal of Strain Analysis for Engineering Design*. DOI:10.1177/0309324712466508.

Laulusa, A., Bauchau, O.A., Choi, J.-Y., Tan, V.B.C., Li, L. (2006): Evaluation of some shear deformable shell elements. *International Journal of Solids and Structures* (**43**)17: 5033–5054. DOI:10.1016/j.ijsolstr.2005.08.006.

Li, L., Gong, M., Chui, Y.H., Schneider, M., Li, D. (2013): Measurement of the elastic parameters of densified balsam fir wood in the radial-tangential plane using a digital image correlation (DIC) method. *Journal of Materials Science* (**48**)21: 7728–7735. DOI:10.1007/s10853-013-7593-1.

LMS International (2017): *LMS Test.Lab Solutions Guide*.

Lukacevic, M., Kandler, G., Hu, M., Olsson, A., Füssl, J. (2019): A 3D model for knots and related fiber deviations in sawn timber for prediction of mechanical properties of boards. *Materials & Design* (**166**): 107617. DOI:10.1016/j.matdes.2019.107617.

Mace, B.R., Vandepitte, D.V.H., Lardeur, P. (2011): Uncertainty in structural dynamics. *Finite Elements in Analysis and Design* (**47**)1: 1–3. DOI:10.1016/j.finel.2010.07.021.

Madhoushi, M., Gray, M., Tabarsa, T. (2010): Influence of wood densification on withdrawal strength of fasteners in eastern cottonwood (populus deltoides). In: *11th World Conference on Timber Engineering 2010 (WCTE 2010)*. Trentino, Italy.

Martini, L. (2008): Développement et évaluation de l'hypothèse de stabilité modale pour la variabilité du comportement vibratoire des structures minces modélisées par éléments finis. doctoral thesis. University of Technology of Compiègne

Mascia, N.T., Soriano, J. (2004): Benefits of timber-concrete composite action in rural bridges. *Materials and Structures* (**37**)2: 122–128. DOI:10.1007/BF02486608.

Massa, F., Do, H.Q., Tison, T., Cazier, O. (2016): Uncertain Friction-Induced Vibration Study: Coupling of Fuzzy Logic, Fuzzy Sets, and Interval Theories. *ASCE-ASME J Risk and Uncert in Engrg Sys Part B Mech Engrg* (**2**)1. DOI:10.1115/1.4030469.

Massa, F., Tison, T., Lallemand, B. (2009): Fuzzy modal analysis: Prediction of experimental behaviours. *Journal of Sound and Vibration* (**322**)1: 135–154. DOI:10.1016/j.jsv.2008.10.032.

Matveev, M.Y., Belnoue, J.P.-H., Nixon-Pearson, O.J., Ivanov, D.S., Long, A.C., Hallett, S.R., Jones, I.A. (2019): A numerical study of variability in the manufacturing process of thick

composite parts. *Composite Structures* (**208**): 23–32. DOI:10.1016/j.compstruct.2018.09.092.

Mehra, S., O'Ceallaigh, C., Lakzaeian, F.H.-, Guan, Z., Sotayo, A., Harte, A.M. (2018): Evaluation of the structural behaviour of beam-beam connection systems using compressed wood dowels and plates. In: *World Conference on Timber Engineering 2010 (WCTE 2018)*. Seoul, Republic of Korea.

Meng, X., Li, T., Yang, Q. (2019): Experimental study on the seismic mechanism of a full-scale traditional Chinese timber structure. *Engineering Structures* (**180**): 484–493. DOI:10.1016/j.engstruct.2018.11.055.

Moens, D., Hanss, M. (2011): Non-probabilistic finite element analysis for parametric uncertainty treatment in applied mechanics: Recent advances. *Finite Elements in Analysis and Design* (**47**)1: 4–16. DOI:10.1016/j.finel.2010.07.010.

Moens, D., Vandepitte, D. (2005): A survey of non-probabilistic uncertainty treatment in finite element analysis. *Computer Methods in Applied Mechanics and Engineering* (**194**)12: 1527–1555. DOI:10.1016/j.cma.2004.03.019.

Morsing, N. (1998): Densification of Wood.: The influence of hygrothermal treatment on compression of beech perpendicular to gain. doctoral thesis. Technical University of Denmark

Negreira, J., Trollé, A., Jarnerö, K., Sjökvist, L.-G., Bard, D. (2015): Psycho-vibratory evaluation of timber floors – Towards the determination of design indicators of vibration acceptability and vibration annoyance. *Journal of Sound and Vibration* (**340**): 383–408. DOI:10.1016/j.jsv.2014.12.001.

O'Loinsigh, C., Oudjene, M., Ait-Aider, H., Fanning, P., Pizzi, A., Shotton, E., Meghlat, E.-M. (2012):(a): Experimental study of timber-to-timber composite beam using welded-through wood dowels. *Construction and Building Materials* (**36**): 245–250. DOI:10.1016/j.conbuildmat.2012.04.118.

O'Loinsigh, C., Oudjene, M., Shotton, E., Pizzi, A., Fanning, P. (2012):(b): Mechanical behaviour and 3D stress analysis of multi-layered wooden beams made with welded-through wood dowels. *Composite Structures* (**94**)2: 313–321. DOI:10.1016/j.compstruct.2011.08.029.

Oudjene, M., Tran, V.-D., Khelifa, M. (2017): Cyclic and monotonic responses of double shear single dowelled timber connections made of hardwood species: Experimental investigations. *Construction and Building Materials* (**132**): 188–195. DOI:10.1016/j.conbuildmat.2016.11.127.

Pech, S., Kandler, G., Lukacevic, M., Füssl, J. (2019): Metamodel assisted optimization of glued laminated timber beams by using metaheuristic algorithms. *Engineering Applications of Artificial Intelligence* (**79**): 129–141. DOI:10.1016/j.engappai.2018.12.010.

Peyer, S.M., Wolcott, M.P., Fenoglio, D.J. (2000): Reducing Moisture Swell of Densified Wood With Polycarboxylic Acid Resin. *Wood and Fiber Science* (**32**)4: 520–526.

Pichler, L., Gallina, A., Uhl, T., Bergman, L.A. (2012): A meta-modeling technique for the natural frequencies based on the approximation of the characteristic polynomial. *Computers & Structures* (**102–103**): 108–116. DOI:10.1016/j.compstruc.2012.03.002.

Premrov, M., Dobrila, P. (2012): Experimental analysis of timber–concrete composite beam strengthened with carbon fibres. *Construction and Building Materials* (**37**): 499–506. DOI:10.1016/j.conbuildmat.2012.08.005.

Ramage, M.H., Burridge, H., Busse-Wicher, M., Fereday, G., Reynolds, T., Shah, D.U., Wu, G., Yu, L., Fleming, P., Densley-Tingley, D., Allwood, J., Dupree, P., Linden, P.F., Scherman, O. (2017): The wood from the trees: The use of timber in construction. *Renewable and Sustainable Energy Reviews* (**68**): 333–359. DOI:10.1016/j.rser.2016.09.107.

Riggio, M., Sandak, J., Sandak, A. (2016): Densified wooden nails for new timber assemblies and restoration works: A pilot research. *Construction and Building Materials* (**102**): 1084–1092. DOI:10.1016/j.conbuildmat.2015.06.045.

Rijal, R., Samali, B., Shrestha, R., Crews, K. (2015): Experimental and analytical study on dynamic performance of timber-concrete composite beams. *Construction and Building Materials* (**75**): 46–53. DOI:10.1016/j.conbuildmat.2014.10.020.

Rijal, R., Samali, B., Shrestha, R., Crews, K. (2016): Experimental and analytical study on dynamic performance of timber floor modules (timber beams). *Construction and Building Materials* (**122**): 391–399. DOI:10.1016/j.conbuildmat.2016.06.027.

Roncen, T., Sinou, J.-J., Lambelin, J.-P. (2019): Experiments and simulations of an industrial assembly with different types of nonlinear joints subjected to harmonic vibrations. *Journal of Sound and Vibration* (**458**): 458–478. DOI:10.1016/j.jsv.2019.06.029.

Schuëller, G.I. (1997): A state-of-the-art report on computational stochastic mechanics. *Probabilistic Engineering Mechanics* (**12**)4: 197–321. DOI:10.1016/S0266-8920(97)00003-9.

Schuëller, G.I., Bucher, C.G., Bourgund, U., Ouypornprasert, W. (1989): On efficient computational schemes to calculate structural failure probabilities. *Probabilistic Engineering Mechanics* (**4**)1: 10–18. DOI:10.1016/0266-8920(89)90003-9.

Scigliano, R., Scionti, M., Lardeur, P. (2011): Verification, validation and variability for the vibration study of a car windscreen modeled by finite elements. *Finite Elements in Analysis and Design* (**47**)1: 17–29. DOI:10.1016/j.finel.2010.07.009.

Silva, D.A.L., Lahr, F.A.R., Faria, O.B. de, Chahud, E. (2012): Influence of wood moisture content on the modulus of elasticity in compression parallel to the grain. *Materials Research* (**15**)2: 300–304. DOI:10.1590/S1516-14392012005000025.

Skyba, O., Schwarze, F.W.M.R., Niemz, P. (2009): Physical and mechanical properties of thermo-hygro-mechanically (THM) -densified wood. *Wood Research* (**54**)2: 1–18.

Song, J., Chen, C., *et al.* (2018): Processing bulk natural wood into a high-performance structural material. *Nature* (**554**)7691: 224–228. DOI:10.1038/nature25476.

Sotayo, A., Bradley, D., Bather, M., Sareh, P., Oudjene, M., El-Houjeyri, I., Harte, A.M., Mehra, S., O'Ceallaigh, C., Haller, P., Namari, S., Makradi, A., Belouettar, S., Bouhala, L., Deneufbourg, F., Guan, Z. (2020):(a): Review of state of the art of dowel laminated timber members and densified wood materials as sustainable engineered wood products for construction and building applications. *Developments in the Built Environment* (**1**): 100004. DOI:10.1016/j.dibe.2019.100004.

Sotayo, A., Bradley, D.F., Bather, M., Oudjene, M., El-Houjeyri, I., Guan, Z. (2020):(b): Development and structural behaviour of adhesive free laminated timber beams and cross laminated panels. *Construction and Building Materials* (**259**): 119821. DOI:10.1016/j.conbuildmat.2020.119821.

Stefanou, G. (2009): The stochastic finite element method: Past, present and future. *Computer Methods in Applied Mechanics and Engineering* (**198**)9: 1031–1051. DOI:10.1016/j.cma.2008.11.007.

Structure Craft (2018): Dowel Laminated Timber - The All Wood Panel - Mass Timber Design Guide. Available from: https://structurecraft.com/blog/dowel-laminated-timber-design-guide-and-profile-handbook.

Suárez-Riestra, F., Estévez-Cimadevila, J., Martín-Gutiérrez, E., Otero-Chans, D. (2019): Experimental, analytical and numerical vibration analysis of long-span timber-timber composite floors in self-tensioning and non-tensioning configurations. *Construction and Building Materials* (**218**): 341–350. DOI:10.1016/j.conbuildmat.2019.05.084.

Tapia, C., Aicher, S. (2019): Variation and serial correlation of modulus of elasticity between and within European oak boards (Quercus robur and Q. petraea). *Holzforschung* (**74**)1: 33–46. DOI:10.1515/hf-2019-0038.

Unece (2017): Forest Products Annual Market Review 2016-2017. Available from: https://www.unece.org/fileadmin/DAM/timber/publications/FPAMR2017.pdf.

Ussher, E., Arjomandi, K., Weckendorf, J., Smith, I. (2017):(a): Predicting effects of design variables on modal responses of CLT floors. *Structures* (**11**): 40–48. DOI:10.1016/j.istruc.2017.04.006.

Ussher, E., Arjomandi, K., Weckendorf, J., Smith, I. (2017):(b): Prediction of motion responses of cross-laminated-timber slabs. *Structures* (**11**): 49–61. DOI:10.1016/j.istruc.2017.04.007.

Van der Linden, M.L.R. (1999): Timber-Concrete Composite Floor Systems. doctoral thesis. Delft University of Technology.

Viguier, J., Bourreau, D., Bocquet, J.-F., Pot, G., Bléron, L., Lanvin, J.-D. (2017): Modelling mechanical properties of spruce and Douglas fir timber by means of X-ray and grain angle measurements for strength grading purpose. *European Journal of Wood and Wood Products* (**75**)4: 527–541. DOI:10.1007/s00107-016-1149-4.

Weckendorf, J., Ussher, E., Smith, I. (2016): Dynamic response of CLT plate systems in the context of timber and hybrid construction. *Composite Structures* (**157**): 412–423. DOI:10.1016/j.compstruct.2016.08.033.

Yang, X., Chen, S., Wu, B. (2001): Eigenvalue reanalysis of structures using perturbations and padé approximation. *Mechanical Systems and Signal Processing* (**15**)2: 257–263. DOI:10.1006/mssp.2000.1358.

Yin, Q., Lardeur, P., Druesne, F. (2018): Performances assessment of the Modal Stability Procedure for the probabilistic free vibration analysis of laminated composite structures. *Composite Structures* (**203**): 474–485. DOI:10.1016/j.compstruct.2018.06.112.

Yoshihara, H., Tsunematsu, S. (2007): Bending and shear properties of compressed Sitka spruce. *Wood Science and Technology* (**41**)2: 117–131. DOI:10.1007/s00226-006-0091-8.

Zhang, B., Rasmussen, B., Jorissen, A., Harte, A. (2013): Comparison of vibrational comfort assessment criteria for design of timber floors among the European countries. *Engineering Structures* (**52**): 592–607. DOI:10.1016/j.engstruct.2013.03.028.

Zhang, S., Zhou, J., Niederwestberg, J., Chui, Y.H. (2019): Effect of end support restraints on vibration performance of cross laminated timber floors: An analytical approach. *Engineering Structures* (**189**): 186–194. DOI:10.1016/j.engstruct.2019.03.042.

Abstract

This study presents an experimental and numerical investigation on the vibrational serviceability performance of novel adhesive free engineered wood products (AFEWPs), namely adhesive free laminated timber beams (AFLB) and adhesive free cross-laminated timber panels (AFCLT), assembled through thermo-mechanically compressed wood dowels (CWD). The experimental modal analyses were carried out under free-free conditions using a hammer impact. Natural frequencies, mode shapes, and damping ratio were assessed experimentally. In addition, similar glued timber beams (conventional glulam) were manufactured and tested for comparison purpose. A 3D FE model was developed and validated by comparison against experimental data and then used to predict the vibrational behavior of a realistic flooring system made with AFCLT panel measuring 4.5 m x 5.5 m. A parametric study was performed on the FE model to maximize the floor stiffness. The predicted FE results were discussed with regard to the Eurocode 5 vibrational serviceability design requirements showing acceptable vibrational performance. A simplified FE model was then developed to reduce computational cost.

The variability level of the results for the AFEWPs was also studied and discussed. The numerical variability of frequencies of the AFEWPs was investigated based on the development of the Modal Stability Procedure (MSP). The MSP result was first compared with the FE result in the nominal case. Then, the statistic results (mean value, standard deviation, coefficient of variation and distribution) obtained from the MSP were compared with the results from the classical method (direct Monte Carlo simulation) and experimental results. A quick error estimation between the MSP and the direct Monte Carlo simulation was developed. Finally, the mean and standard deviation of the frequencies of the realistic AFCLT flooring system were predicted by the MSP.

Keywords: timber construction, CLT, wood dowels, wood densification, vibration serviceability, modal analysis, frequency, damping, mode shape, finite element, simplified model, variability, MSP.

Résumé

Cette thèse présente une étude expérimentale et numérique sur les aptitudes en service en ce qui concerne le comportement vibratoire de planchers réalisés en bois d'ingénierie sans colle (AFEWP), à savoir les poutres en bois lamellé sans adhésif (AFLB) et les panneaux en bois lamellé-croisé sans adhésif (AFCLT), assemblés par des tourillons en bois densifié (CWD). Les analyses modales expérimentales ont été réalisées en conditions libres-libre à l'aide d'un marteau instrumenté. Les fréquences naturelles, les modes propres et les coefficients d'amortissement ont été évalués expérimentalement. De plus, des poutres en bois lamellé-collé similaires ont été fabriquées et testées à des fins de comparaison. Un modèle EF 3D a été développé et validé par comparaison avec des données expérimentales, puis utilisé pour prédire le comportement vibratoire d'un système de plancher à grande échelle réalisé avec un panneau AFCLT mesurant 4,5 m x 5,5 m. Une étude paramétrique a été réalisée en utilisant le modèle EF pour identifier les paramètres qui influent sur la rigidité et les fréquences propres du plancher. Les résultats obtenus ont été analysés au regard des critères de conception exigés par Eurocode 5 en ce qui concerne le confort vibratoire des planchers bois. Un modèle EF simplifié a ensuite été développé pour réduire les coûts de calcul.

Le niveau de variabilité des résultats des AFEWP a été également étudié et discuté. La variabilité numérique des fréquences des AFEWP a été étudiée en utilisant la méthode MSP (Modal Stability Procedure). Les résultats de la méthode MSP ont d'abord été comparés aux résultats EF dans le cas nominal. Les résultats statistiques (valeur moyenne, écart type, coefficient de variation et distribution) obtenus par la méthode MSP ont été confrontés aux résultats de simulation directe de Monte Carlo ainsi qu'aux données expérimentales. Une estimation rapide des erreurs entre la méthode MSP et la simulation directe de Monte Carlo a été développée. Enfin, la variabilité (moyenne et écart-type des fréquences) du comportement vibratoire du système de plancher à grande échelle a été étudiée en utilisant la méthode MSP.

Mots-clés : construction bois, CLT, chevilles bois, densification du bois, aptitude au service vibratoire, analyse modale, fréquence, amortissement, déformée modale, éléments finis, modèle simplifié, variabilité, MSP.